東京大学新領域創成科学研究科

人間環境学専攻

博士論文（要約）

Development of hydrophobic membrane-based compact absorption refrigeration system for automotive air-conditioning application

（撥水性分離膜を用いた車載空調用小型吸収冷凍機に関する研究）

洪　成周

Development of hydrophobic membrane-based compact absorption refrigeration system for automotive air-conditioning application

A Dissertation (Abridged)

Submitted to the Faculty

of

The University of Tokyo

by

Sung Joo HONG

In Partial Fulfillment of the

Requirements for the Degree

of

Doctor of Philosophy

March 2018

Human and Engineered Environmental Studies

Graduate School of Frontier Sciences

The University of Tokyo

The University of Tokyo Graduate School

Statement of Dissertation Approval

Approved, Dissertation committee (in alphabetical order):

Chaobin DANG

Associate Professor, Department of Human and Engineered Environmental Studies

The University of Tokyo

Eiji HIHARA

Professor, Department of Human and Engineered Environmental Studies

The University of Tokyo

Naoki SHIKAZONO

Professor, Department of Mechanical Engineering

The University of Tokyo

Tetsuo MUNAKATA

Professor, Department of Human and Engineered Environmental Studies

The University of Tokyo

Yu CHEN

Associate Professor, Department of Human and Engineered Environmental Studies

The University of Tokyo

ACKNOWLEDGMENTS

I am a lucky person to have many great persons around me. I now round off the valuable life in Japan with the expression of my gratitude to those people.

First of all, I do not know how to show my thankfulness to my advisor, Professor DANG Chaobin, who gave me an opportunity to work on the stimulating and attractive research. His guidance, supports, and challenges throughout my Ph.D. course have helped me to ask right research questions and seek novel answers. I really appreciate his efforts to improve my knowledge in this field and his patience in spending time with me as my mentor. I would like to give him my word that I will never forget his favor and will keep corresponding with him not only for the further research work, but also for having good personal relationships. Again, I would like to show my appreciation for his support and patience.

I would also like to appreciate Professor HIHARA Eiji who has been willing to share his precious time and knowledge to complete my Ph.D. course. He always presented a lot of suggestions to improve my research. His charisma made me proud of myself as a member of his group, and his pure enthusiasm for the research has motivated me to complete this work successfully. Especially, his kindness gave me strength to overcome the tough moments every time I went through trouble with the research and personal things. I will never let go of his benignity and also pray for his well-being.

I wish to thank all my friends and colleagues in Hihara-Dang lab. OKAMOTO Hiroaki, I certainly appreciate that he assisted me with his great experience to establish a basis of my Ph.D. course, and more importantly, encouraged me all the time so that I had the confidence to continue this work. I have a friend, HE Jiacheng, who has been together for my whole Ph.D. course. As we joined this lab at the same time, we have helped each other, shared knowledge, and hung out together in joy and in sorrow. We have had a lot of quality time together for the past few years, and I hate to say goodbye to him at this momentin time. CHEN Zouzhou, he was willing to share his valuable experience to solve my problems I faced when I suffered from the experimental work. He was very ardent for playing basketball, and I will remember him as an outgoing and passionate friend about everything he did. LI Jiyang, we were always smiling and saying nice things together, and from his humorous character, I always have fond memories of living in our lab. ITO Makoto, he is the an indispensable person for our lab. He knew everything that I asked,

and always gave me correct solutions. His positive character and adorable appearance also let me have more favorable impression of Japan than I had. YOSHINAGA Yuki, he was my tutor to kindly take care of me at the beginning of my life in Japan. He has the most excellent character, always tried to amuse all the members. Not only as the tutor but also as a friend, he delivered big happiness to all the members as well as to me. HIGASHI Tomohiro, this brilliant man inspired me new ideas with his broaden knowledge. He was a good friend to share personal problems, also a good colleague to discuss our research tasks, and an excellent researcher to stimulate me to think of all the questions. It is no exaggeration to say that his favor was one of the power sources to lead me to a Ph.D. degree. YU Hanryu, she always smiled at every moment, and has an ability to please others all the time. I was also positively affected by her positive personality. INOUE Shunnosuke, he is a very diligent friend who had worked with me on same research theme. He always tried to enjoy the research, work hard, and actively complete the assigned tasks. He helped me a lot especially when I needed Japanese ability, and also he was my friend I had in-depth discussion about our challenges with. CAO Xufa, and XU Jingren, even though we have been together only for several months since they had joined our lab, but I strongly felt your friendship. You two were always kind to me, smiled at me, and treated me with your warm heart. I hope you will improve that your effort you have been doing in our lab will never betray you. Ms. CHIKAMATSU Chizuko, CHIKUMA Yuka, KAWAI Kyoko, YOSHIMI Sachiyo, four grateful secretaries were always let me free from a mass of paperwork more to focus on my research work. ZHU Yu, we have been together for two years, and he was always willing to share his knowledge to confirm my research progress. We also had much fun by chatting about the social, political, and historical issues. SONG Mengjie, he is the last research fellow I met in this lab. His enthusiasm for his research fields led me to having the motivation to work together in the future. His advice was also valuable to choose my job as I leave this lab.

Last but not least, I am eternally grateful to my family. They are the reason how I have come this far, and I will always be owing their unconditional love.

HONG, Sung Joo

2018. 02. 13.

ABSTRACT

This dissertation pursues the development of hydrophobic hollow fiber membrane-based absorption refrigeration system as an automobile application. Even though vapor absorption refrigeration system promises a bright future for vehicle air-conditioning system, several obstacles which have to be solved remain as challenges before the portable application can be achieved. To this purpose the hydrophobic hollow fiber membrane is proposed as a key item for making the absorption system compact and lightweight.

Three main original achievements are as follows:

1. Hollow fiber membrane-based generator was proposed as a new concept of the compact and lightweight generator in a vapor absorption refrigeration system. The proposed generator was experimentally examined to evaluate the effect of various driving conditions on the heat and mass transfer performance. Moreover, using the permeability value obtained by the gas permeation test, an established theoretical model validated the experimental analysis.

2. Hollow fiber membrane-based solution mass exchanger using the typical hollow fiber membrane module was proposed for mass recovery process, enhancing the performance of absorption system. The theoretical analysis clarified the effect of various working conditions on the mass recovery process; however, the negative mass recovery was observed under the certain conditions.

3. A new type of hollow fiber membrane-based solution mass exchanger was proposed. In the proposed traditional mass exchanger, the heat is transferred between two streams of the feed solutions, which has adverse effect on the mass recovery process; however, the new type of mass exchanger does not allow the heat transfer so that the performance of mass recovery is maximized.

This dissertation consists of six chapters. In chapter 1, problems with the existing automotive air conditioning system are first discussed within the framework of the energy and environmental issues. A single effect vapor absorption refrigeration system (VARs), which uses the lithium bromide (LiBr) and water, is then described as an alternative portable air-conditioning system. Challenges which have to be overcome are proposed for compact and lightweight automobile VARs.

This chapter also includes the literature review regarding the measures to improve the heat and mass transfer in the conventional VARs and the attempts for the use of VARs on the vehicles.

Chapter 2 contains the research objectives to develop the automotive compact VARs. To this purpose, a hydrophobic hollow fiber membrane (HFM) is proposed to overcome the limitations that the conventional VARs have had as a portable application. The literature review section involves the membrane distillation processes and the membrane-based heat and mass exchangers in VARs.

Chapter 3 first presents the basic terminologies of membrane parameters. The structure of the (HFM) used in this study is clarified by the SEM images. The gas permeation test is conducted to estimate the gas permeability across the HFM to characterize the mass transfer.

In chapter 4, a hollow fiber membrane-based generator (HFM-G) is introduced to substitute the conventional generator in VARs. Theoretical heat and mass transfer model is firstly illuminated, and the theoretical simulation results are shown to comprehend the mechanism of the HFM adiabatic desorption process. The effect of the HFM-G on the proposed VARs are then intensively represented under various operating conditions. Transient experiments are also shown to examine the heat and mass transfer characteristics of the HFM-G under various working conditions. The comparison results between experimental and theoretical analysis are described for the validation of theoretical models.

This chapter 5 presents two types of hollow fiber membrane-based solution mass exchangers (HFM-SME). Mass recovery process is emphasized by understanding the simultaneous heat and mass transfer. The characteristics of the mass recovery process, which is a form of the traditional HFM module (named "traditional HFM-SME"), are clarified regarding the flow direction of the solutions. The improved type of the HFM-SME (named "new type of HFM-SME) is also suggested with the theoretical analysis as an alternative to the traditional HFM-SME to achieve maximized mass recovery performance.

In chapter 6, this paper is finalized with the conclusion by summarizing research contribution and discussion of the perspective work directions. The iso-thermal type of HFM-based heat and mass exchangers are designed for the future works. It is expected that the proposed iso-thermal types make up for shortcomings that the adiabatic HFM-based heat and mass exchangers have shown.

本論文は、論文提出者が主体となって疎水性中空糸膜を利用した新しいタイプの熱物質交換機の理論と実験的研究を行ったものであり、これにより、自動車用小型吸収式冷凍機の研究開発のための独創性と有用性は十分である。本論文は、博士学位論文として認められる。したがって、論文提出者に博士（環境学）の学位を授与出来ると認める。

TABLE OF CONTENT

CHAPTER 1. Introduction

1.1. Background: Automobile air conditioning system 1
1.2. Alternative Technology: Vapor absorption refrigeration system 2
1.3. Limitations, and challenges 3

CHAPTER 2. Application

2.1. Membrane 11
2.1.1. Distillation process by hydrophobic membrane 12
2.1.2. Distillation process by hydrophilic membrane 13
2.1.3. Consideration of membranes for vapor absorption refrigeration system 14
2.2. Microporous hydrophobic hollow fiber membrane-based heat and mass exchanger 18
2.3. Research Objectives 23

CHAPTER 3. Preparation of hydrophobic hollow fiber membrane

3.1. Terminology of membrane 25
3.2. Breakthrough pressure 26
3.3. Physical structure of hollow fiber membrane 27
3.4. Gas permeation test 29

CHAPTER 4. Hollow fiber membrane-based generator

4.1. Theoretical model 33
4.1.1. Mass transfer 33
4.1.2. Heat transfer 37
4.1.3. Pressure drop 39
4.1.4. Thermodynamics of vapor absorption refrigeration system with hollow fiber membrane based-generator 39
4.1.5. Dühring chart 41
4.1.6. Simulation procedure 42
4.2. Experiment 45
4.2.1. Apparatus and experimental procedure 45
4.2.2. Data reduction 48
4.2.3. Validation of concentration measurement 49
4.3. Results and discussion 50
4.3.1. Theoretical simulation results 50
4.3.1.1. Characteristics of adiabatic desorption mass transfer 50
4.3.1.2. Effect of generating temperature on system performance 51
4.3.1.3. Effect of mass flow rate of weak solution on system performance 52
4.3.1.4. Effect of cooling water temperature on system performance 53
4.3.1.5. Effect of the number of hollow fiber membranes on system performance 54
4.3.1.6. Effect of recirculation ratio on system performance 55
4.3.1.7. Effect of variation in both feed temperature and mass flow rate on adiabatic desorption heat and mass transfer 56
4.3.1.8. Effect of variation in both length and number of hollow fiber membranes on

adiabatic desorption heat and mass transfer 57
4.3.2. Transient experimental results 62
4.3.2.1. Effect of feed solution temperature on heat and mas transfer 62
4.3.2.2. Effect of feed solution mass flux on heat and mass transfer 62
4.3.2.3. Effect of condenser pressure on heat and mass transfer 64
4.3.2.4. Pressure drop via hollow fiber membrane-based generator 64
4.3.2.5. Comparison of experimental heat and mass transfer with theoretical results 66

CHAPTER 5. Hollow fiber membrane-based solution mass exchanger 67

CHAPTER 6. Conclusion, and future work 68

INDEX 69
Nomenclature
Greek symbol
Subscript

REFERENCE 72

1

Introduction

1.1. Background: Automobile air conditioning system

The number of automobiles is approximately a billion all over the world and is projected to double by 2035 [Sharlene A. McEvoy]. Automobile manufacturers have employed vapor compression refrigeration system (VCRs) to control the temperature, humidity, and air circulation within vehicles due to their small size and high performance-to-volume ratio. VCRs, however, has caused the severe problems, such that: massive energy consumption, and the greenhouse effect. The compressor is the heart of VCRs, playing a significant role in operating the cycle by transferring and pressurizing the refrigerant. This compressor is connected to a crankshaft of car engine through the belting system and runs by using the axial energy of the engine [Fig. 1-1]. Thus, automotive air conditioning system (A/C) imposes a burden on the workload of the engine and gives rise to the auxiliary energy consumption. Zulkifli et al. (2015) estimated that the fuel consumption of a vehicle increases up to 20% by the use of this belt-driven compressor-based A/C. Refrigerants in VCRs, e.g., hydrocarbon derivatives (HCFC, HFC) have still been responsible for global warming. CO_2 emission from the transportation sector, for instance, accounts for 18.6% of the total emission in Japan. It is estimated that in summer, the existing air-conditioning units used in automobiles contribute to 7% of fuel consumption (or emission of 8 million ton CO_2) [Japanese Ministry of Land, Infrastructure, Transport and Tourism (2013)].

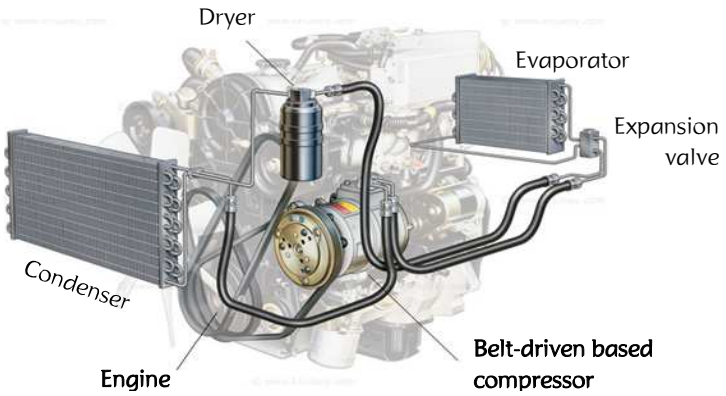

Fig. 1-1. Automobile air-conditioning system, vapor compression refrigeration system (VCRs), depicting a compressor connected to an engine crankshaft [http://www.audiocoustics.co.za/car_air_conditioning_cape_town.htm]

1.2. Alternative technology: Vapor absorption refrigeration system

The vapor absorption refrigeration system (VARs), which uses the environmental working fluids, has a great potential to substitute the traditional automotive air-conditioning systems. VARs is capable of utilizing low-grade thermal energy directly for air conditioning purpose. This heat-actuated absorption system can run without additional energy consumption by using waste heat obtained from the exhaust gas of an internal combustion engine. The absorbent and refrigerant in VARs, a lithium bromide (LiBr) and water pair, are eco-friendly, and therefore, the automobile VARs do not contribute to environmental problems, such as the greenhouse effect or ozone depletion.

Since the single-effect VARs was introduced in 1930, this thermally activated absorption system has been widely used for the industrial applications. Numerous studies were extensively carried out for the exploration and construction of the thermo-physical properties of aqueous LiBr solution [McNeely L.A. (1979), Patterson and H. Perez-Blanco (1988), DiGuilio et al. (1990), Lee et al. (1990), Jeter et al. (1992), Lenard et al. (1992), Kaita (2001)]. Several extensive numerical and experimental works on the single-effect VARs were also conducted [Talbi and Brian (2000), Florides et al. (2003), Şencan et al. (2005), Aphornratana and Sriveerakul (2007), Pongtorn kulpanich A. et al. (2008), Kim and Infante Ferreira. (2008), Kaushik and Akhilesh (2009), Gomri (2010)]. The single effect LiBr-water VARs consists of six components: a generator, an absorber, a condenser, an evaporator, a solution heat exchanger, and a solution pump, as labeled in Fig. 1-2. The LiBr solution is circulated and is pressurized using the solution pump in

the heat-operated generator. The heat energy is directly supplied to a tube bundle installed in the generator so that the refrigerant vapor (i.e., water vapor) is desorbed from the LiBr solution at high pressure. The desorbed water vapor is condensed in the condenser by the cooling process where the heat is rejected out to the surroundings and then is expanded into the evaporator through an expansion valve. The refrigerant, water, is then evaporated at low pressure for the cooling purpose and leaves the evaporator. Meanwhile, the LiBr solution becomes stronger in the generator as the water vapor is desorbed. The strong solution heads for the absorber via the solution heat exchanger. The strong solution is then expanded through an expansion valve and enters the absorber. In the absorber, the evaporated water vapor from the evaporator is absorbed into the strong solution at low pressure, releasing the heat of absorption by the cooling process. The solution heat exchanger induces the higher coefficient of performance (COP) by preheating the weak LiBr solution to reduce the heating load for desorption process in the generator.

1.3. Limitations, and challenges

Certain challenges must be overcome so that VARs can become more attractive for portable applications. VARs has a much more complicated thermodynamic cycle compared to conventional automotive VCRs, which allows them to achieve a high theoretical system performance. However, this higher performance demands a number of heat and mass exchangers and complex control systems. VARs is too heavy to be used in vehicle application as the primary heat and mass exchangers are stainless steel-based structures due to the high corrosiveness of the LiBr solution [Oleinik et al. (2003)]. The massive heat and mass exchangers in VARs are responsible for the high cost and volume required to attain the required cooling capacity. LiBr-water absorption system runs at a static vacuum pressure associated with the large specific volume of water vapor, causing the large volume of the system. The generator and absorber are both major components that determine the system performance. The heat and mass transfer to volume ratio in the conventional generator is quite weak. In general, a heating tube bundle is installed in the conventional generator and is immersed in the LiBr solution, where the heat transfer occurs by boiling the solution (Fig. 1-3*a*). The inefficient use of space against the heat transfer surface leads to the inefficient desorption of water vapor. Desorption takes place only at the liquid-vapor interface, which also impedes mass transfer. Additionally, the liquid phase of the LiBr solution has

a considerably large mass resistance. The absorption of water vapor takes place in the conventional falling film absorber, but the gravity-driven hydrodynamic formation of the LiBr falling film resists the water vapor absorption through a thick falling film produced over the cooling tube (Fig. 1-3b, and Fig. 1-3c) [Behfar et al. (2014)]. VARs has not been an attractive alternative for portable air conditioning systems as the unconstrained LiBr solution (i.e., liquid-vapor interface) exists in both the generator and absorber. For example, the LiBr solution is likely to overflow into the condenser when the vehicle drives on hills and is then intermixed with the liquid refrigerant, causing the system to malfunction (Fig. 1-3d). While the vehicle is in motion, the slope and vibration also hinder the uniform distribution of the sprayed solution over the cooling tube in the absorber, leading to unstable system performance [Killion and Garimella (2004)].

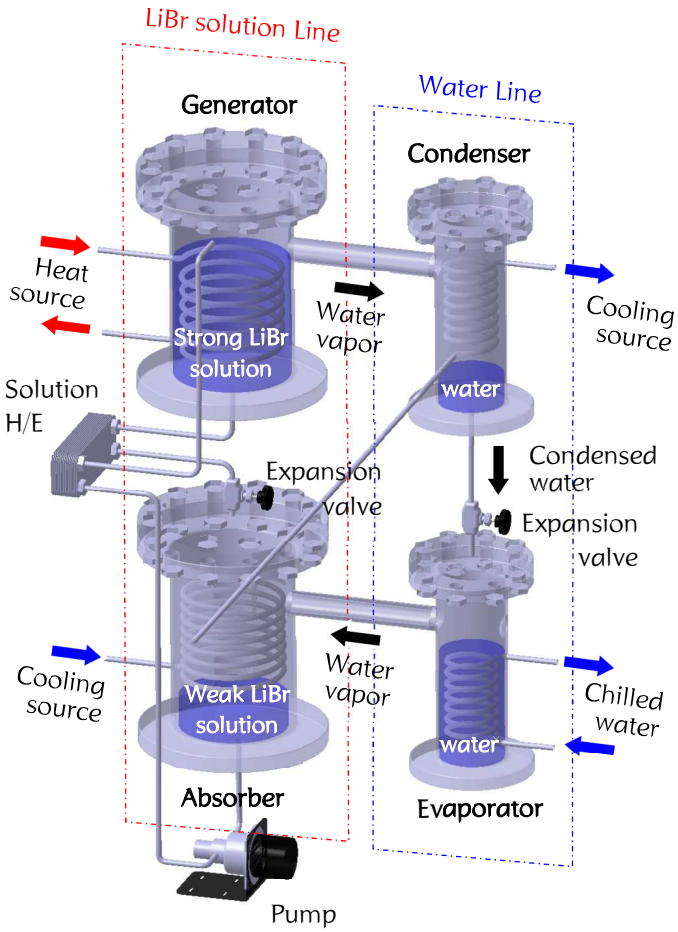

Fig. 1-2. Single effect LiBr-water absorption refrigeration system

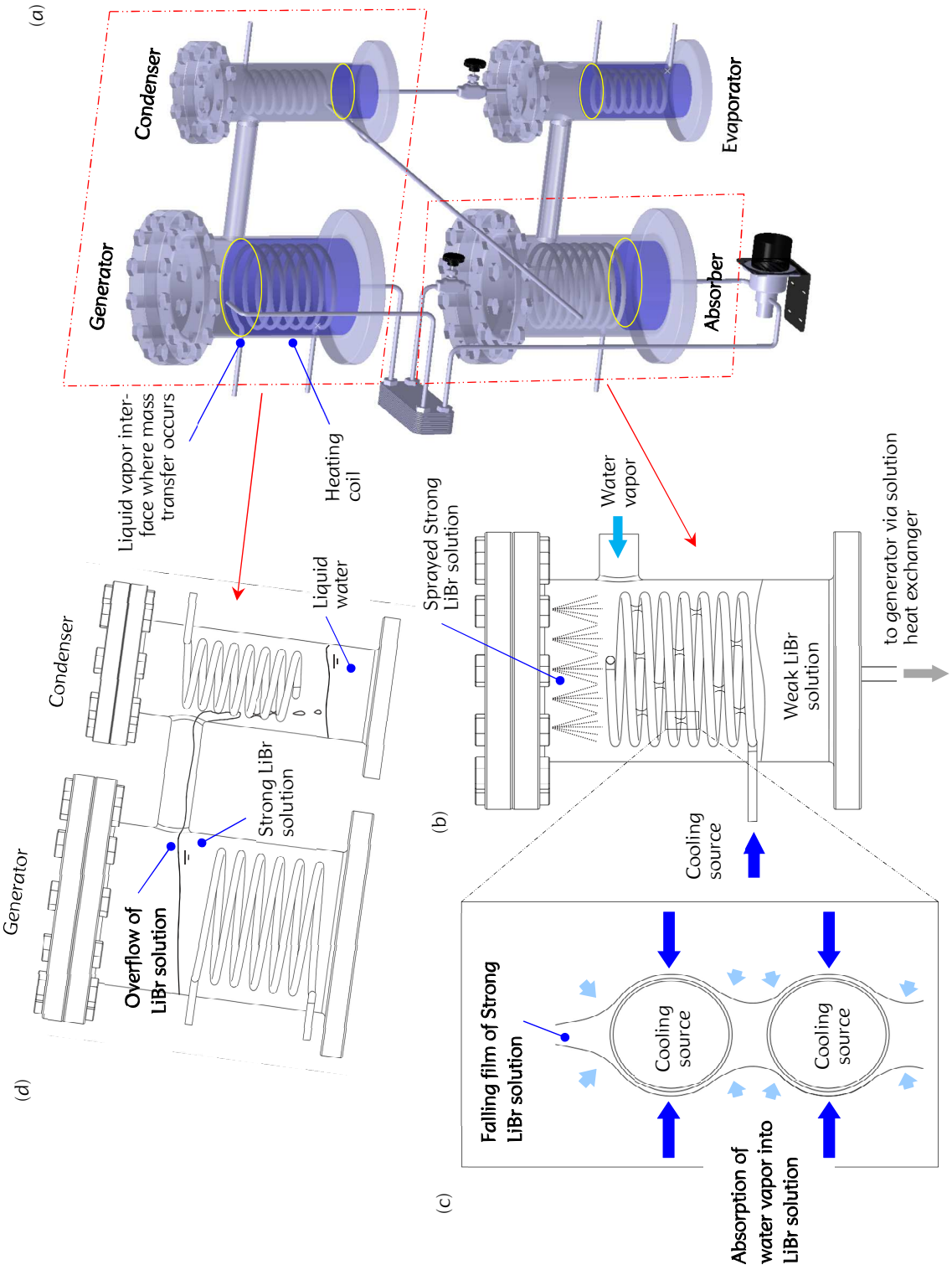

Fig. 1-3. Schematic of (a) conventional single effect VARs, (b) falling film absorber, depicting sprayed strong LiBr solution on cooling tubes, (c) hydrodynamic of LiBr solution over cooling tube, and (d) the declined generator and condenser on the slope

VARs promises a bright future for vehicle air conditioning system due to the use of waste heat and an eco-friendly refrigerant; however, low heat and mass transfer has prohibited VARs from compact and lightweight scaled system applications, and the existence of the free surface of the working fluids remains as another challenge before portable applications can be attained. Thus, the current study pursues the development of new type of VARs with the following requirements.

- Enhancement of heat and mass transfer of the heat and mass exchangers in VARs for the compact and lightweight system.
- Elimination of the free surface of working fluids in the heat and mass exchangers.

It is no exaggeration to mention that the enhancement of the heat and mass transfer of the heat and mass exchangers is one of the key stages to make VARs minimize enough for the automotive application. Many attempts have for a long time been made to exploit the additives, which is known as the most cost-efficient mechanism of improving the absorption performance. The thick LiBr solution film over the cooling tube impedes the heat and mass transfer in the absorption process (Fig. 1-3c). The additives, higher alcohols, induce the lower surface tension of the LiBr solution so that the thinner solution film is sprayed over the tube (i.e., enhanced wettability). The heat transfer becomes significantly boosted in the absorber, and as a result, the efficiency of the mass transfer is highly improved. Since Kashiwagi et al. (1985) begun to the experimental work for more fundamental and quantitative understanding of the relationship between the additives and Marangoni instability, the extensive experimental and theoretical works have been conducted. Hozawa et al. (1991) reported that the increase in the concentration of LiBr solution leads to the increase in surface tension, but on the other hand, causes the decrease in the surface tension when the additive is added. Hihara and Saito (1993) explained the mechanism of interfacial turbulence, Marangoni instability, and reported the considerable enhancement of absorption rate by the additive by improving the distribution of the LiBr solution over the cooling surface (Fig. 1-4a, and 1-4b). The static surface tension data [Yao et al. (1991), Kim et al. (1994), Ishida and Yasuhiko (1996), Yuan and Herold (2001), Kulankara and Herold (2002)] and dynamic data [Kim and Janule (1994), Kren (1999)] of the LiBr solution with various additives were established and the numerical works were well performed using the established data. Daiguji et al. (1997) conducted both the numerical and experimental works to investigate the prediction of the occurrence of Marangoni instability and the mass transfer enhancement, and well described Marangoni convection by the salting effect. Glebov and Setterwall (2002)

conducted two series of experimental works to look into the effect of 2-methyl-1-pentanol on the enhancement ratio, comparing the cooling effect with and without the additive. In the first experimental series which injected the additive into LiBr solution, they found 20 % of the increase in the enhancement ratio at the optimum additive concentration; the enhancement ratio became 32.3 % in the second experimental series that the additive is introduced to the refrigerant (i.e. evaporator). Their observation supported that the additive is volatile that travels around the cycle and even small amount of additives in vapor phase helps the heat and mass transfer in the absorber more successfully than the case of additive-in-solution. Rivera and Cerezo (2005) reported the impact of the additives, 1-octanol, and 2-ethyl-1-hexanol, on 2 kW of single effect VARs in which the absorber temperature is in range of 70 to 110 ˚C. They found that adding 1-octanol hardly influences the enhancement of system performance; however, 40 % of enhancement is observed by adding 2-ethyl-1-hexanol at the optimum operating condition.

Wettability of the LiBr solution film over the cooling tube is a significant measure for the enhancement of heat and mass transfer. Mechanical surface treatments, such as shape or roughness control of cooling tube surface, have been considered. The enhancement of absorption rate by coupling wires with the tube surface was reported by several works [Thomas (1967), Schroeder et al. (1980)]. Many attempts had been established using various configurations, such that: constant curvature surface, grooved and wire-wound tube [Benzeguir and Setterwall (1991)], porous surface [Yang and Jou (1995)], and tubular surface with pin-shaped fin, grooves, and twisted fins [Patnaik et al. (1994)]. Kim J. K. et al. (2003) and Park et al. (2004) numerically and experimentally investigated the effect of the roughness of cooling tube surface on the absorption rate with two types of micro-scale helically grooved tubes and a bare tube. They confirmed that the increase in roughness promotes the wettability (i.e., heat transfer rate), further also enhances the absorption flux.

The microchannel-based heat and mass exchangers, which have high heat transfer coefficient even in laminar flow regime, was proposed. Since Garimella (1999) proposed his prototype microchannel-based absorber in which short length of microchannel tubes are located in multiple square arrays, he and his group investigated the absorption characteristics [J. M. Meacham and S. Garimella (2002), J. M. Meacham and S. Garimella (2003)]. They discovered the problems regarding the solution distribution and the wettability on the prototype absorber and after that

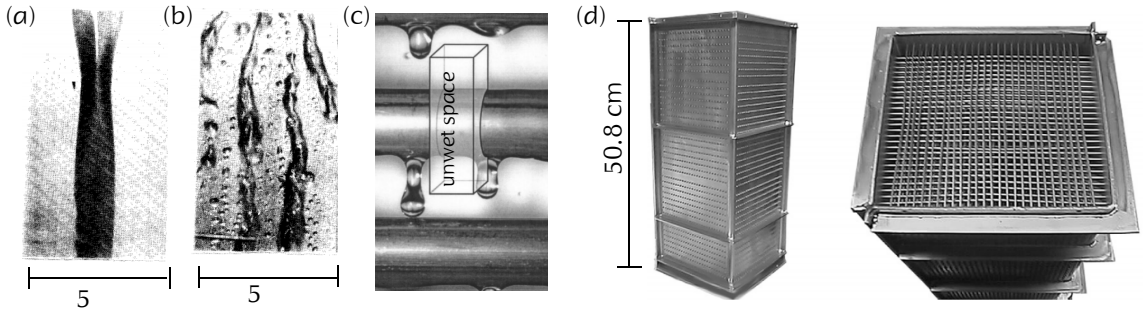

Fig. 1-4. (a) Falling film of LiBr solution without surfactant for $\theta = 90^{\circ}$ and a film Reynolds number of 180, and (b) with surfactant also for $\theta = 90^{\circ}$ and a film Reynolds number of 180 [Hihara and Saito (1993)]. (c) Photograph of hydrodynamic of LiBr solution over cooling tubes, showing ill-space for heat and mass transfer [Killion, J. D., and Garimella, S. (2004)]. (d) Microchannel based absorber [Garimellg et al. (2011)]

proposed an improved absorber configuration, which has only 30 % of surface area of the prototype absorber (Fig. 1-4d) [J. M. Meacham and S. Garimella (2004), S. Garimellg et al. (2011)]. J. M. Meacham and S. Garimella (2004) initiated the visualization test of the solution flow along the array of microchannel tubes and also begun the experiments for the heat transfer performance. 15 kW of absorption capacity was accomplished in a 16.2 × 15.7 × 15.0 cm of the absorber with 0.456 m^2 of surface area. They attained the significant enhancement of the absorption rate by the well-distributed solution. Garimellg et al. (2011) and Determan et al. (2011) made a minor modification of the absorber they proposed to convert it to desorption process. The microchannel-based generator has a solution drip tray brazing 14.0 cm length of 648 microchannel tubes. Their analytical and experimental observation revealed that 17.5 kW of desorption capacity was transferred at overall heat transfer coefficients between 388 and 617 W/m^2K. Their heat and mass exchangers were successfully minimized compared to the conventional components, and it is expected that this miniaturization technology is universally applicable not only to absorber and generator but also to condenser and evaporator. Goel and Goswami (2005) and Goel and Goswami (2007) proposed the microchannel-based falling film absorber with the flow guidance medium by screen mesh/fabric. They first presented the concept of conventional microchannel based absorber that has 3.175 mm outer diameter and 0.4 mm wall thickness of stainless steel tubes and suggested a novel design with the screen mesh/fabric. The screen mesh/fabric is installed in contact with the horizontal cooling tubes, and guides the gravity-driven solution flow, and enables the solution flow rate retarded. Their numerical and exper-

imental results pointed out that the heat load of the proposed mesh-enhanced absorber is improved about 17 to 26 % compared to the conventional microchannel based absorber. This phenomenon supported that the screen guidance improves the liquid hold-up, wetting characteristics, and fin-effect of the mesh/fabric.

Several studies were carried out to apply VARs to the vehicles. Koehler et al. (1997) designed a prototype of VARs powered by the exhaust gas from a truck engine. They estimated the available heat in the exhaust gas and considered it as an energy source for the operation of VARs. They found the significant variations in the available heat depending on the driving conditions: uphill, flat, and down-hill road sections. It was found that the system performance became degraded on the slope and it was hard to obtain the optimal design of the generator due to the sudden variation of the available heat according to the driving conditions. The COP of this prototype was approximately 0.27, which is quite lower than that of the conventional VARs; however, their simulation results showed that the COP is expected to be doubled by the optimization of the system. Horuz (1999) conducted an experimental investigation mainly to observe the effect of engine output power on the flow rate and temperature of the exhaust gas. They considered several obstacles to the application of VARs in the road transport vehicles: the facts that an auxiliary energy source is necessary when the vehicle is stationary or is stuck in a very slow moving traffic, that the effect of increased back pressure on engine performance has to be considered, and that the scale of VARs has to be significantly reduced to suit the vehicles. Talom and Beyene (2009) presented a mathematical model and conducted an experimental study on 10.55 kW VARs operated using the exhaust gas from a 2.8 L V6 internal combustion engine. The experiments were mainly conducted to evaluate the system performance. The variations in chilled water temperature (CWT; i.e., evaporation temperature) at various rotational speeds (revolutions per minute, RPM) of the engine were noted. The CWT increased gradually when the engine was operated below 1800 RPM, but at 2400 RPM, it rose slightly for 5 - 6 min initially and then drastically decreased to 12 °C. At higher speeds such as 2800 RPM, the CWT decreased to 12 °C in about half the time required in the previous case. They concluded that a delay of 10 mins between the engine and the chiller start-up is recommended for safety. Manzela et al. (2010) performed an experimental study on an ammonia-water pair absorption cycle, commercial 215-l refrigerator, by using the exhaust gas from an internal combustion engine for 25, 50, 75 %, and wide-open throttle valve. The steady state temperature and maximum cooling capacity were

achieved about three hours after starting the engine. The maximum COP attained was 0.049 for 25 % open throttle; for the other cases of open throttles, the COP was extremely low, approximately 0.012 - 0.014, which are about five times less than the COP achieved in the study of Koehler et al. (1997). Manzela et al. (2010) firmly asserted that the optimal design of the cycle is necessary for vehicle application.

2

Application

2.1. Membrane

Membrane, including a hollow fiber membrane and flat sheet membrane, is typically a thin film, manufactured from polymers, metals, or ceramics, and recently has been utilized for gas or water distillation from the liquid or gaseous feed stream. The membrane is defined as a selective barrier that enables a particular component to pass through but blocks the passage of others. The membrane is mainly categorized as hydrophobic and hydrophilic membranes concerning attractive or repulsive response to water (i.e., wettability). Characteristic of surface properties of liquid and solid determines the wettability. Due to an unbalance in molecular forces generated when a liquid droplet and a solid surface are in direct contact with each other, a contact angle between them is observed (Fig. 2-1). Hydrophobicity literally means the water-fearing and has little or no tendency to absorb water. In contrast, hydrophilicity literally signifies the water-loving and has the attractive response to water. A solid material which has a low surface tension value has the hydrophobic characteristic with the specified liquid while a high surface tension of the solid material results in the hydrophilicity. The membrane is also categorized, regarding the existence of pores, as two types concerning its structure: porous and dense membrane. The porous membrane has micro- or nano-scale interconnected pores that characterize both the mass transfer and the selectivity of molecules. The dense membrane, however, is non-porous media and is

used for the elimination of tiny molecules. The dense membrane has high selectivity, but has extremely low mass transfer performance because the molecules go through more mass resistances: diffusing to the membrane surface, dissolving into the dense membrane surface, diffusing through the solid membrane wall, and absorbing into or desorbing from the interface of downstream [Asfand and Bourrouis (2015)].

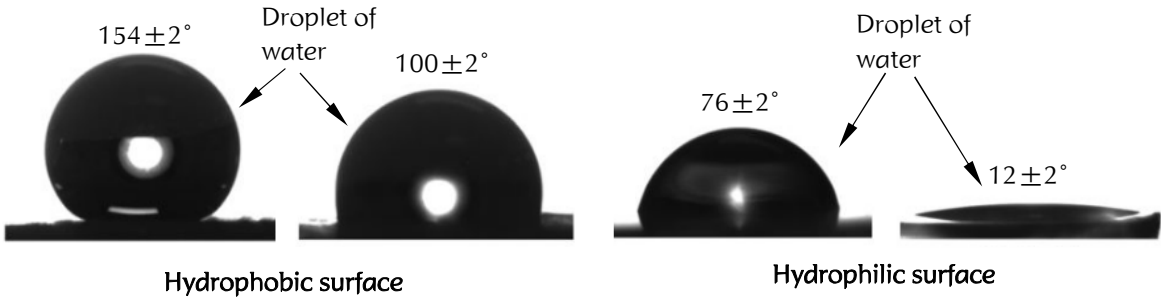

Fig. 2-1. Photographs presenting the contact angle of a water droplet on hydrophobic, or hydrophilic surface [Brown and Bharat (2016)]

2.1.1. Distillation process by hydrophobic membrane

The Hydrophobic membrane distillation is in general thermally-driven separation process where a liquid solution (or water) flows in direct contact with the hydrophobic membrane surface. The hydrophobic membrane surface confines the liquid flow, but molecules of water vapor pass through across the membrane layer. Only heat, low-grade energy, is necessary for the operation of water vapor distillation, and this thermally driven process has a high distillation efficiency due to the principle of liquid-vapor equilibrium. The hydrophobic membrane distillation is generally categorized as four configurations, such that (a) vacuum membrane distillation (VMD), (b) direct contact membrane distillation (DCMD), (c) air gap membrane distillation (AGMD), and (c) sweeping gas membrane distillation (SGMD) (Fig. 2-2). VMD introduces a vacuum in the permeate side, and the heat is applied to the liquid to increase the vapor pressure of the feed fluid. As long as the permeate side (i.e., vacuum side) is kept at the pressure below the equilibrium vapor pressure of the heated liquid, the evaporation of water takes place and the water vapor passes through the pores, resulting in the fact that both the higher temperature of the feed and the lower vacuum degree at the permeate side are essential factors to enhance the mass transfer. In DCMD configuration, two liquid fluids flow in direct contact with both sides of the membrane. The water vapor is transported through the membrane pores as long as the vapor pressures of two solutions

are different. The evaporation occurs due to the difference in the vapor pressure between two fluids, and the evaporated water vapor is again condensed into the fluid at the permeate side. Not only is the heat transferred, but the mass is transferred between two feed fluids and thus this configuration substitutes for traditional heat exchangers in some industrial fields. AGMD has a similar distillation process as VMD, but the operating pressure is not at the vacuum condition. The temperature of cooling plate controls the degree of pressure at the permeate side, but the stagnant air exists between the membrane and the cooling plate. Therefore, the vapor passes through the stagnant air and is condensed over the cooling plate. AGMD is disadvantageous for the distillation efficiency due to an additional mass resistance (i.e., the air). SGMD uses an inert gas to sweep the distilled vapor at the permeate side to the place where the condensation takes place, the outside of membrane module.

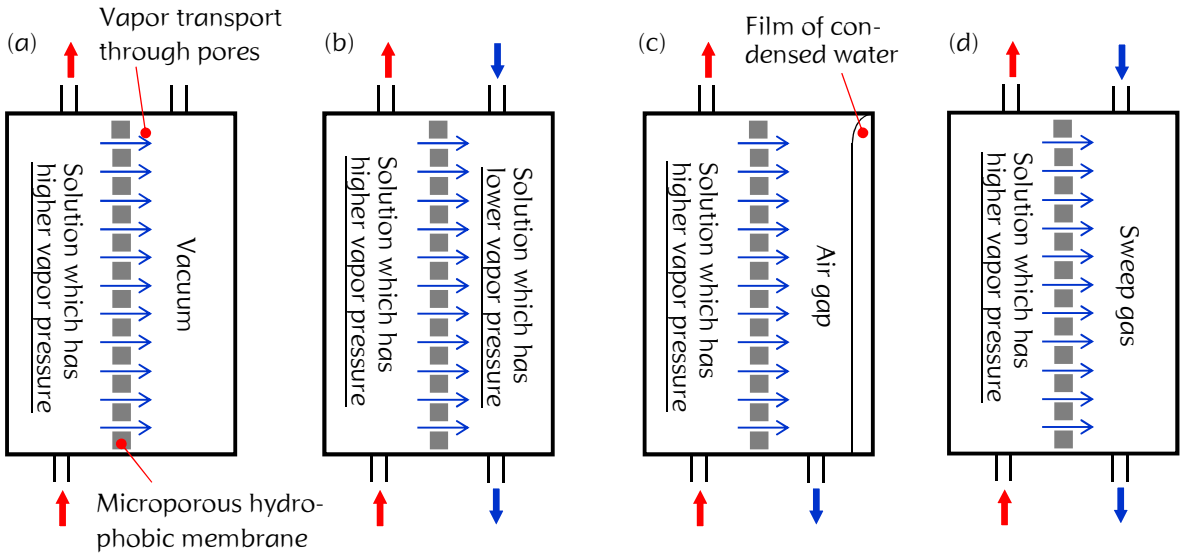

Fig. 2-2. Schematic illustrating the mechanism of (a) vacuum membrane distillation (VMD), (b) direct contact membrane distillation (DCMD), (c) air gap membrane distillation (AGMD), and (d) sweeping gas membrane distillation (SGMD)

2.1.2. Distillation process by Hydrophilic membrane

A hydrophilic membrane has a high surface tension, and readily absorb the water across the membrane layer. As opposed to the distillation process by the hydrophobic membrane, a hydrophilic osmotic distillation is a pressure driven process with pore sizes in the range from 100 molecular weight to several microns. Since the liquid phase of water is penetrated across the hydrophilic membrane layer, the pore sizes need to be appropriately selected to sort out the filtrated

substances (Fig. 2-3). Osmosis is a natural phenomenon for equilibrium defined as the transference of pure water through a semi-permeable membrane from a low to the highly concentrated solution (Fig. 2-4a). The movement of pure water takes place until the osmotic equilibrium is established. A difference in height is called the osmotic pressure, $\Delta\pi$, and thus the pure water is distilled as the feed solution is pressurized over the osmotic pressure (Fig. 2-4b).

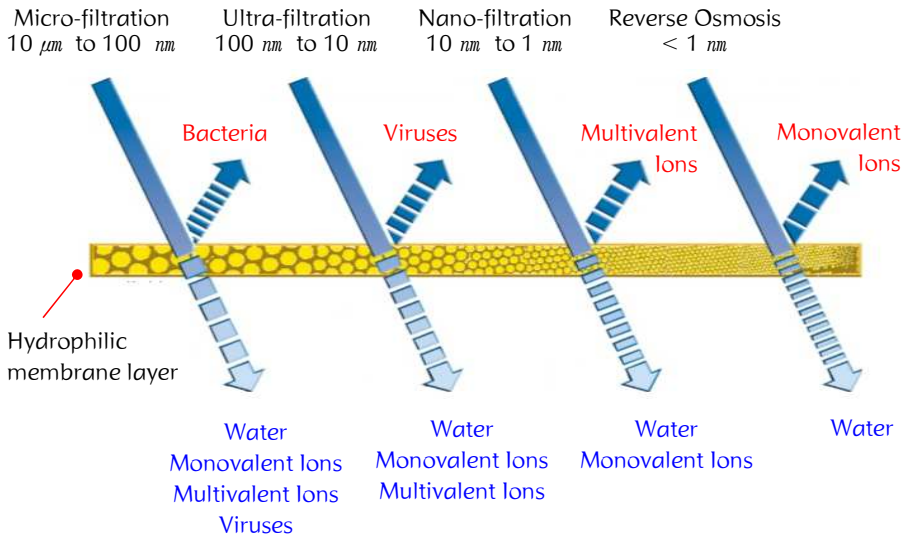

Fig. 2-3. Schematic showing the filtered materials and the permeated materials concerning pore size of hydrophilic membrane [http://www.unechabros.com/Ultra_Filtration_Plant.html]

2.1.3. Consideration of membranes for vapor absorption refrigeration system

The hydrophobic membrane distillation is the thermal-driven process. The temperature difference (also concentration difference) across the membrane layer leads to vapor pressure gradient, giving the water vapor transport through the membrane pores. Mass flux by the hydrophobic membrane distillation is simply expressed with the vapor pressure difference between both sides of membrane:

$$J_v = B_m (p_{v,f} - p_{v,p}) \tag{2-1}$$

where J_v is the mass flux of water vapor across the hydrophobic membrane. B_m is the membrane distillation coefficient by the hydrophobic membrane distillation. $p_{v,f}$ and $p_{v,p}$ are the vapor pressure at the feed and permeate side, respectively. As a result, a higher vapor pressure at the feed produces a higher mass flux across the hydrophobic membrane for the given vapor pressure at the permeate side.

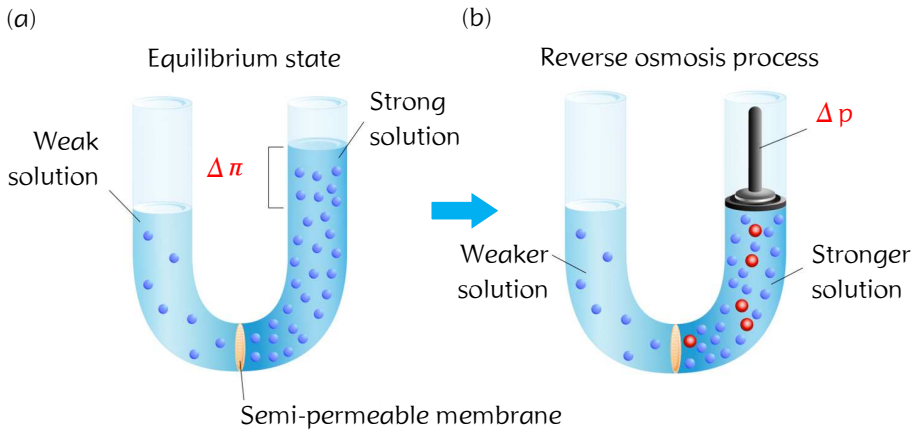

Fig. 2-4. Schematic presenting (a) osmosis pressure through a semi-permeable membrane by concentration difference in equilibrium state, (b) external pressure to overcome the osmosis pressure (reverse osmosis pressure) to produce water [http://www.kandrwaterservice.com]

On the other hand, the hydrophilic osmotic distillation is the pressure driven process where the hydrostatic pressure difference across the membrane layer is the driving force of mass transfer as below:

$$J_l = B_o(\Delta p - \Delta\pi) \tag{2-2}$$

with

$$\Delta\pi = M_c RT \tag{2-3}$$

where J_l is the mass flux of liquid water across the hydrophilic membrane. B_o the membrane distillation coefficient by the hydrophilic membrane distillation. Δp and $\Delta\pi$ are the external pressure to the feed side and the osmosis pressure, respectively. M_c is the molar concentration of the solution. R and T are the gas constant and the temperature, respectively. A more massive external pressure gives rise to a higher mass transfer across the membrane.

Consequently, the membrane distillation process enables the separation of water from the LiBr solution. Considering the use of the hydrophobic or the hydrophilic membrane for the heat and mass exchangers in VARs, characteristics of the water separation from the LiBr solution is distinguished as listed below and also organized in Table 2-1.

- Lithium (Li) and bromine (Br) are deionized and dissolved into water. Only water is volatile, but the LiBr is never volatile under the operating conditions of VARs. The hydrophobic membrane distillation process gives the complete extraction of water from a stream of LiBr solution

mechanically confined by the hydrophobic surface. On the other hands, the hydrophilic osmosis distillation generates the salt passage rate across the membrane, leading to the fact that the distilled water contains the deionized Li^+ and Br^-.

- The hydrophobic membrane does not allow the penetration of liquid phase of the LiBr solution and confines the flow of the solution. The free surface of the LiBr solution, thus, is eliminated that the harsh driving conditions (e.g., the slope, or the vibration) have no adverse effect on the operation. The hydrophilic membrane, however, distills the water by allowing the passage of liquid phase of water in which the free surface of liquid still exists.

- The hydrophobic membrane distillation is highly cost-effective as applied to the automotive application owing to the use of waste heat whereas the hydrophilic osmosis distillation needs an auxiliary energy source for making a tremendous external pressure to overcome the osmotic pressure.

- The hydrophobic membrane constrains the flow of the LiBr solution by large capillary action. Relatively large pores can be utilized to not only increase the mass transfer performance but also reduce the energy cost to attain the required performance. The hydrophilic osmosis distillation, however, requires extremely tiny pore sizes to filtrate dissolved Li^+ and Br^- ions. Therefore, the extremely high pressure is necessary for water separation.

- The use of large pore size suffers less from fouling effect in the hydrophobic membrane distillation whereas the hydrophilic osmotic distillation is more likely sensitive to the fouling due to the small pores.

- The trapped air within hydrophobic membrane pores introduces the further mass transfer resistance of water vapor [Alkhudhiri et al. (2012)]. LiBr-water VARs, however, runs at a static vacuum pressure and thus no such mass transfer resistance is considered in the hydrophobic membrane-based heat and mass exchanger.

Consequently, the microporous hydrophobic membrane is highly recommended as a new type of membrane-based heat and mass exchangers. As described in chapter 1.3, the major conventional heat and mass exchangers, particularly the generator and the absorber, are too bulky as the automotive application because of (a) the low heat and mass transfer due to the limited interfacial area for heat and mass transfer, and (b) the existence of the solution free

surface. Since the hydrophobic membrane restrains and also controls the flow of the LiBr solution, a film thickness of the LiBr solution can be able to be considerably decreased. As a result, the interfacial area for heat and mass transfer is significantly improved for the given flow rate, resulting in the enhanced heat and mass transfer. Also, there is no longer the free surface of the LiBr solution in the hydrophobic membrane based-heat and mass exchangers by confining the flow of the LiBr solution, and therefore, it is highly expected that the system has no adverse effects from the slope or the unexpected vibration while driving. Table 2-2 summarizes the limitations of the conventional VARs for the portable application and the advantages of the hydrophobic membrane-based heat and mass exchangers.

Table 2-1. Comparison between hydrophobic membrane distillation and hydrophilic osmotic distillation when applied for vapor absorption refrigeration system

	Hydrophobic membrane distillation	Hydrophilic osmosis distillation
Purity of distilled water	100 % by the evaporation process	Less than 100 % due to the salt passage rate
Energy source	Low-grade waste heat from a car engine	Pressure from the auxiliary energy source
Operating cost	Relatively low by using waste heat from a car engine	Relatively high for high pressurization
Applicable pore size	Large	Extremely small

Table 2-2. Comparison between the conventional heat and mass exchangers and the hydrophobic membrane-based heat and mass exchangers in VARs.

Conventional heat and mass exchanger	Membrane-based heat and mass exchanger
Low heat and mass transfer due to limited interfacial area	Enhanced heat and mass transfer by reduction of the solution film thickness
Malfunction of system while driving due to the free surface of the solution	Elimination of free surface of solution by confining the solution flow by hydrophobicity
Heavy due to stainless steel-based structure	Lightweight due to the non-metallic polymeric membrane

2.2. Microporous hydrophobic membrane-based heat and mass exchanger

The membrane is mainly categorized as a hollow fiber, and a flat sheet membrane according to its configuration or shape. A microporous hydrophobic membrane has been widely investigated in various industrial fields: water purification [Nakatsuka et al. (1996), Banat and Simandl (1996), Laganà et al. (2000), Urtiaga et al. (2001), Lee and Bruce (2002), Wang et al (2008)], waste water treatment [Kazuo Yamamoto et al. (1989), Wu et al. (1991), Calabro et al. (1991), Shimizu et al. (1996), Busch et al. (2007)], desalination [Li et al. (2003), Yang et al. (2009), Wang et al. (2010), Lee et al. (2011), Wang et al. (2011)], and food industries [Kirk et al. (1983), De Barros et al. (2003)]. In recent years, the microporous hydrophobic membranes have been applied to compact and lightweight heat and mass exchangers in VARs, as listed in Table 2-3. The hollow fiber membrane (HFM), which has submillimeter scale diameters, or the flat sheet membrane (FSM) with an array of micro-channels considerably reduces the film thickness of the LiBr solution, and thus, the heat and mass transfer can be highly enhanced by the enlarged mass transfer interfacial area. As listed in Table 2-3, both the HFM and FSM are deliberated as either the generator or absorber; all of the related studies have asserted that the hydrophobic membrane-based heat and mass exchangers achieved highly enhanced heat and mass transfer per volume ratio, leading an overall reduction in size.

The microporous hydrophobic HFM-based heat and mass exchanger is shaped like a shell and tube heat exchanger and is primarily composed of a bundle of HFMs, two bonded sections for fixing the ends of the HFM bundle, and a housing to enclose and support the HFM bundle (Fig. 2-5a). The lumen and shell side of the HFM-based heat and mass exchanger are ideally separated by placing the bonded sections together with the ends of the housing. To clarify the heat and mass transfer characteristics of the HFM-based heat and mass exchanger, several analytical and experimental studies were conducted. Megual et al. (2004) proposed a numerical model to evaluate heat transfer coefficients of the feed boundary layer of the HFMs and experimentally validated the model using water as a working fluid. They reported that the performance of the HFM, measured regarding water mass flux across the membrane layer, became significantly high with an increase in the solution feed temperature at the module inlet, as described by an Arrhenius type of dependence. Lovineh et al. (2013) presented a simultaneous heat and mass transfer model for sea water in VMD to determine the effects of operating conditions and membrane parameters on the performance of water mass flux across the HFM layers, and

concluded that the mass flux of water increases with an increase in the velocity of working fluid, pore size, and porosity of the membrane, and also increases with a decrease in the working fluid concentration, and thickness of membrane. An increase in the temperature of the inlet solution has a positive effect on the water mass flux but negatively affects the temperature polarization effect. The authors also pointed out that the increase in feed velocity could counter the negative effect caused by the increase in the inlet temperature. An HFM-based heat and mass exchanger has high-potentials, particularly when applied to the portable application with several strong points: reliability, compactness, lightness, low cost, high separation efficiency, large interfacial area to volume ratio, fewer mechanical part demand, and the use of plastic based structure alleviating the corrosion problem [Asfand and Bourrouis (2015)]. In the HFM-based heat and mass exchanger, the feed LiBr solution enters several hundreds of, or thousands of HFM capillaries and the water vapor is transported across the HFM layers (Fig. 2-6). As a result, the total area for the heat and mass transfer becomes significantly enlarged whereas the conventional heat and mass exchangers have the limited interfacial area per unit volume (Fig. 1-3). For example, as the hot LiBr solution enters the HFM-based heat and mass exchanger, water vapor is desorbed across the HFM layers as long as the shell side is maintained at the pressure below the equilibrium vapor pressure of the feed. A large temperature drop takes place due to the consumption of heat for the latent heat of vaporization, and as a result, the vapor pressure decreases in the

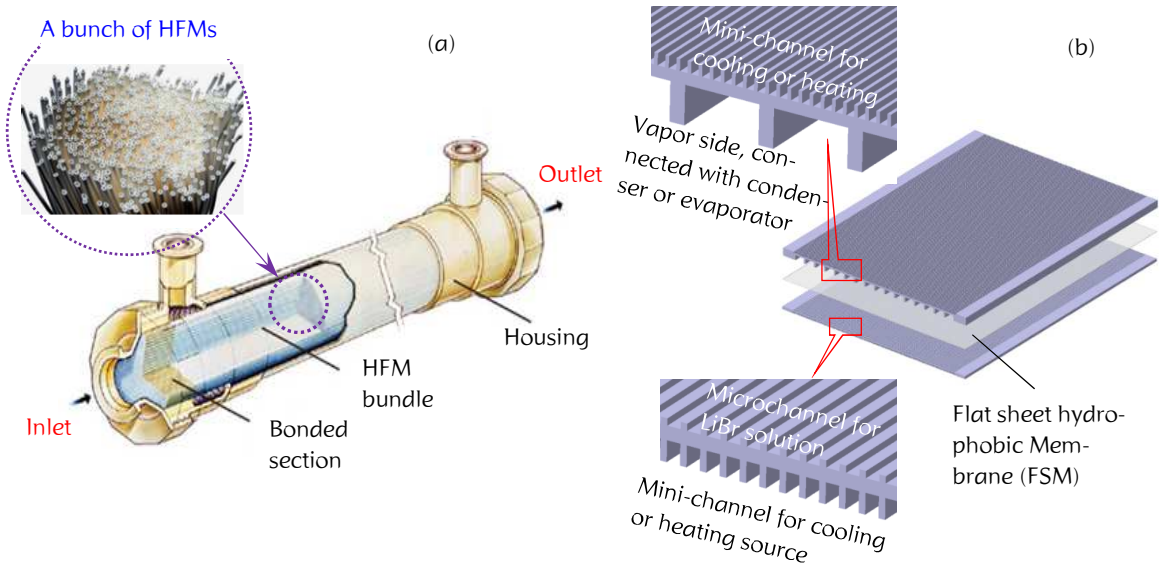

Fig. 2-5. Structure of (a) a hollow fiber membrane module, and (b) a flat sheet membrane with microchannels [http://www.pall.de/main/home.page]

flow direction (i.e., the adiabatic desorption process). In the same way, the adiabatic absorption process occurs in the HFM-based heat and mass exchanger as the vapor pressure of the feed solution is lower than the pressure at the shell side. The solution temperature increases in the flow direction due to the heat of absorption as water vapor is absorbed into the stream of LiBr solution. Chen et al. (2006) proposed an HFM-based absorber designed for VARs which uses an ammonia-water pair. They designed a non-adiabatic HFM-based absorber, which is composed of both microporous and non-porous HFMs for the flow of water vapor and cooling fluid, respectively. The proposed HFM-based absorber had a liquid-vapor mass transfer interfacial area that was 4.3 times larger than the traditional falling film-type absorber. They noted that the COP of VARs combined with the proposed absorber increased by 14.8 %, and the overall system exergy loss was reduced by 26.7 %. Schaal et al. (2005) conducted an experimental study on an HFM-based absorber for the ammonia-water pair. They found a linear relationship between an increase in the absorption and an increase in the change of the ammonia mole fraction. From their observation, the size of the HFM-based absorber became ten times smaller than that of the conventional plate absorber. Wang et al. (2009) tested a polyvinylidene fluoride (PVDF) HFM module to investigate the desorption characteristics under several operating conditions, including feed solution temperature, feed solution flow rate, and pressure at the shell side. They found that the feed solution temperature was a major requirement to enhance the desorption rate exponentially; a higher feed solution flux and lower pressure at the shell side also brought about higher desorption mass flux performance. Hong et al. (2016) presented a detailed theoretical heat and mass transfer mechanism on the HFM-based generator and also analyzed the single-effect VARs combined with the HFM-based generator to characterize the system performance under practical operating conditions. It was concluded that the exhaust gas contained the available heat required to increase the generating temperature, and it effectively reduced the circulation ratio, which is responsible for the size and weight of the system. An increase in the number of HFMs per unit volume increases the system performance by extracting more amounts of water vapor and also decreases the circulation ratio and pressure drop of the solution. Further, the proposed VARs theoretically has a lower COP than the conventional system due to the lower heat recovery performance associated with the temperature drop via the adiabatic desorption process. However, it was noteworthy that a recirculation process of the solution through the HFM-based generator gave rise to both a reduction in the temperature drop and an increase in the desorption mass transfer, resulting in a similar COP to that of a conventional VARs. The HFM-based heat

and mass exchanger were considered as an auxiliary solution mass exchanger in VARs for the mass recovery process [Hong et al. (2016)]. The heat and mass transfer simultaneously take place as both the strong hot and weak warm LiBr solutions enter the HFM-based solution mass exchanger. In this process, the water vapor is transferred from the strong to the weak solution by the vapor pressure difference between two feed solutions. Thus, the mass of water is recovered so that the strong solution becomes stronger and the weak solution becomes weaker. The COP was enhanced by adding the auxiliary HFM-based solution mass exchanger by the reduction of the heating load to the generator.

The FSM accompanied with the micro-channels is shown in Fig. 2-5b. A metallic plate which includes an array of micro-channels on one side and an array of mini-channels on the other side is set with the FSM. The LiBr solution flows through the micro-channels, and the heating or cooling source flows in the mini-channel to make potential for the desorption or the absorption of water vapor. Another metallic plate is also placed in direct contact with the FSM for the condensation or evaporation process. The LiBr solution is fed into the microchannel and is mechanically constrained by the FSM. This narrowly confined solution flow significantly increases the mass transfer area for given flow rate of the feed solution. As the absorber configuration, for example, the non-adiabatic absorption of water vapor across the FSM takes place as the cooling source is applied to the LiBr solution because the vapor pressure of the solution is lower than the evaporation pressure. On the other hand, when the heating source is applied, the desorption process occurs as the vapor pressure of the feed solution becomes higher than the vapor pressure at the opposite side of the FSM. Riffat et al. (2004) investigated a prototype VARs in which a pervaporation membrane replaced the conventional generator. They completed the absorption cycle with 10 ºC evaporation temperature, 80 ºC generating temperature, and 30 ºC condensation temperature. However, the COP of the proposed cycle was lower than the conventional VARs and was further reduced as the circulation ratio increased (i.e., the ratio of the amount of desorbed water vapor to the feed flow rate of the solution increased). They used two types of membranes, a porous silicon membrane, and a non-porous dense membrane. The distillation performance of the silicon membrane was much higher, approximately four to six times that of the dense membrane. However, the permeation rate of the silicon membrane decreased with running time due to the blockage of pores. Thorud et al. (2006) reported the experimental results of

the water vapor desorption rate from the LiBr solution flowing through two kinds of microchannels, each 170 and 745 μm in height. They reported the desorption rate regarding the microchannel height, solution inlet concentration, and the pressure difference across the membrane. It was observed that the heat transfer resistance was reduced with thinner microchannels, and consequently, the desorption rate of the water vapor increased. Note that internal channel boiling does not impede the desorption rate as long as the solution does not reach critical heat flux. The maximum heat flux attained was 12.7 kW/m^2, which was higher than the values achieved by the conventional falling film generator. Isfahani et al. (2013) built a flat sheet membrane-based VARs and examined both the desorption and absorption characteristics regarding the height of the microchannel. They found that thinner microchannels enhanced the heat transfer in the solution thermal boundary layer, causing an increase in absorption across the membrane. They also noted two modes of desorption: a direct diffusion mode where desorption occurs from the single phase of the LiBr solution and a boiling diffusion mode where the vapor phase exists in the LiBr solution. The boiling diffusion mode significantly intensified the desorption rate compared to the direct diffusion mode, and the increase in the velocity of the solution also improved the desorption rate. Compared to the conventional components in VARs, they asserted that the proposed flat sheet membrane-based heat and mass exchangers have several strong points, such as the ease of adjusting and optimizing the solution film thickness, solution flow rate, and heating area.

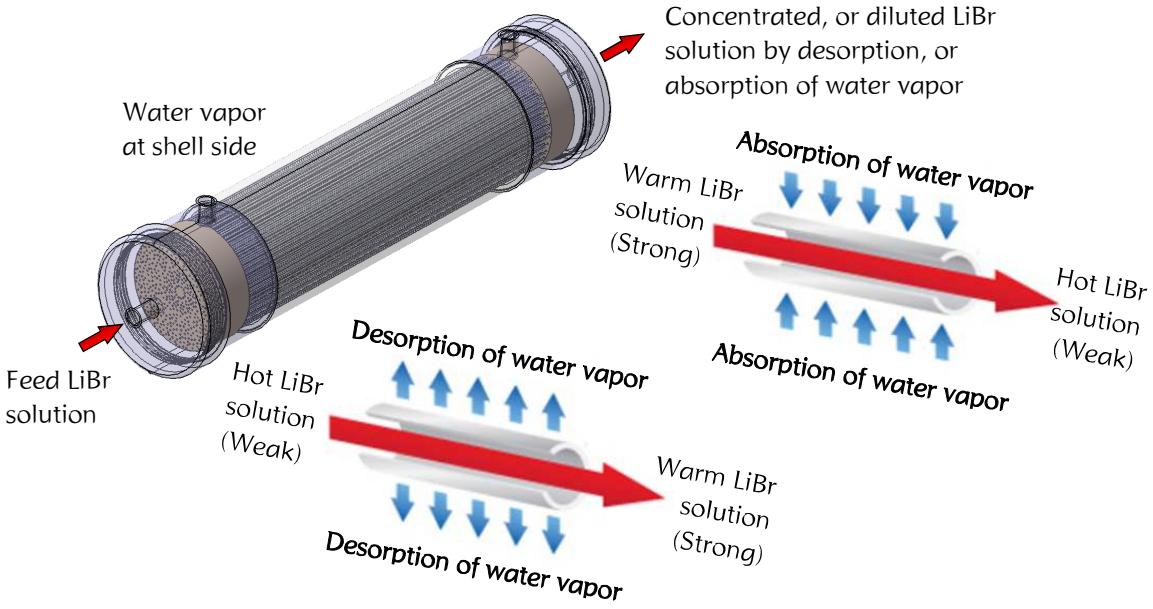

Fig. 2-6. HFM module depicting the adiabatic sorption process across a string of HFM

2.3. Research objectives

An automobile engine provides a high-temperature heat source enough to operate VARs. As an application of membrane technology to VARs, the HFM can be used as the heat and mass exchangers since LiBr solution is mechanically constrained by the hydrophobic layers to prevent the vibrations and slopes while driving from affecting VARs. Enhanced heat and mass transfer can be achieved with the extremely enlarged heat and mass transfer area by controlling the path of LiBr solution (i.e., reducing the film thickness of LiBr solution). Further, it is also expected that the HFM-based heat and mass exchanger is much lighter than the conventional components in VARs because the former is made of polymeric membrane fibers and plastic housing whereas the latter consists of stainless steel components.

Overall, the HFM-based heat and mass exchanger is expected enough to play roles of the heat and mass exchangers in VARs, particularly the generator, absorber, and solution mass exchanger. Development of compact HFM-based VARs requires the comprehensive understanding of the heat and mass transfer on the HFM distillation process. The enhanced heat and mass transfer remain the ongoing challenge for the realization of compact and lightweight VARs as the portable application. The outline for the current study is illuminated as below;

- Investigation of the existing attempts for the realization of compact and lightweight VARs, and further discovery of breakthrough as the automobile application.
- Comprehensive understating of the heat and mass transfer for the feasible design of the HFM-based heat and mass exchangers.
- Theoretical analysis of heat and mass transfer in the HFM-based heat and mass exchanger to look into the effect of the practical driving conditions on the performance characteristics of HFM-based VARs.
- Experimental analysis on the HFM-based based heat and mass exchanger to validate the theoretical heat and mass transfer model.

Table 2-3. Summary of hydrophobic membrane-based heat and mass exchanger used in VARs

Reference	Membrane	Purpose	Working fluid	Pore size [μm]	Porosity [%]	Thickness [μm]	Dimension* [μm]	Study
Thorud et al. (2006)	Flat sheet	Desorber	LiBr-water	N/A	N/A	N/A	170, 745	Experimental
Chen et al. (2006)	Hollow fiber	Absorber	NH_3-water	0.03	40	30	240	Numerical
Kim et al. (2008)	Flat sheet	Desorber	LiBr-water	N/A	N/A	N/A	300	Numerical
Wang et al. (2009)	Hollow fiber	Desorber	LiBr-water	0.16	85	150	800	Experimental
Ali et al.(2009)	Flat sheet	Absorber	LiBr-water	0.2 to 1.0	N/A	60 to 175	4,000	Experimental
Yu et al. (2012)	Flat sheet	Absorber	LiBr-water	6	60	20	50	Numerical
Isfahani et al. (2013)	Flat sheet	Absorber	LiBr-water	1.0	80	N/A	100, 160	Experimental
Isfahani et al. (2014)	Flat sheet	Desorber	LiBr-water	0.45	N/A	50	N/A	Experimental
Venegas et al. (2016)	Flat sheet	Absorber	LiBr-water	1.0	0.8	60	150	Numerical
Hong et al (2016)	Hollow fiber	Desorber	LiBr-water	0.16	85	150	800	Numerical

* Hollow fiber membrane: Inner diameter, Flat sheet membrane: Height of microchannel

3

Preparation of hydrophobic hollow fiber membrane

3.1. Terminology of membrane

In 1986, the "Workshop on Membrane Distillation" was held in Rome, and one of the subjects was to clarify the nomenclature in the field of membrane distillation. There are unacquainted terminologies that are essential to be comprehended for further theoretical analysis.

- Pore size (d_p): The first approximation of mass flux across the membrane. A term, nominal pore size, is also used due to uneven distribution of pores along the membrane [Smolders and Franken (1989)]. Several techniques generally evaluate pore size: visual examination using scanning electron microscopy (SEM) [Chakrabarty et al. (2008)], gas permeation test using the correlation for the coefficient of membrane permeability [Yasuda and Tsai (1974)], or bubble-point test [Hernández et al. (1996)].

- Porosity (ε): The ratio of the volume of pores to the total volume of the membrane, estimated by measuring the weight of a membrane, isopropyl alcohol, and a membrane immersing isopropyl alcohol. Higher porosity has less mass transfer resistance, but the mechanical strength of membrane becomes weaker in general [Smolders and Franken (1989)].

- Tortuosity (τ): The ratio of the shortest pathway of the transport medium through the pores

to the membrane thickness (i.e., the deviation of the pore structure from the cylindrical formation) [Baker (2000)]. This factor describes the mass transfer resistance across the membrane by estimating the travel length across the pores for the transport medium (Fig. 3-1), and thus, a larger value of tortuosity has a lower mass transport performance. Several empirical and analytical works proposed the tortuosity evaluation as inversely proportional to the membrane porosity, as shown in Eq. 3-1 [Alkhudhiri et al. (2012), Ghanbarian et al. (2013)]:

$$\tau = \frac{1}{\varepsilon} \tag{3-1}$$

- Thickness (δ): A factor that gives both the mechanical strength and the mass transfer performance across the membrane. Less membrane thickness also leads to higher mass transfer performance by the reduction in travel distance of molecules across the pore [Smolders and Franken (1989)].

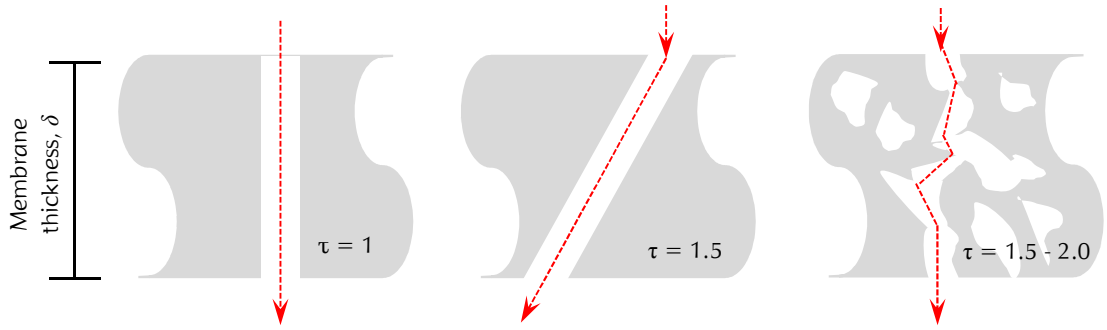

Fig. 3-1. Simplified schematic of microporous membrane describing the path of molecules through pores regarding tortuosity (τ).

3.2. Breakthrough pressure

A critical requirement of the membrane is to confine and control the flow of the LiBr solution. A hydrophobic membrane has a repulsive response to the LiBr solution, which has a larger surface tension than the liquid water. The capillary action in the pores depends on two hostile forces: the liquid adhesion to the solid surface and the cohesive surface tension of the liquid that functions to diminish the liquid-vapor interface. When the LiBr solution flows in direct contact with the hydrophobic membrane surface, curvatures of the liquid-vapor interface are formed at the entrances of the pores due to the large capillary actions (Fig. 3-2).

The several factors affect this wetting phenomenon: pore size, contact angle, and certain pressure difference called as the breakthrough pressure (also called liquid entry pressure). The equation of balance between a force applied to the surface and the surface tension applied to the circumference is achieved, and the Young-Laplace equation [Li and Chen (2005)] gives, such that:

$$\Delta p_b \pi r_p^2 = -2 \pi r_{p,\max} \sigma \cos\theta \tag{3-2}$$

where Δp_b is the breakthrough pressure. σ, θ, and $r_{p,max}$ are the surface tension of the liquid solution, the contact angle between the liquid and membrane surface (Fig. 3-3), and the radius of the largest pore, respectively. Namely, the liquid phase of the LiBr solution cannot seep into the pores as long as the pressure difference across the membrane is kept lower than the breakthrough pressure, which is expressed by

$$\Delta p_b = -\frac{2\sigma\cos\theta}{r_{p,\max}} \tag{3-3}$$

Lower surface energy creates a repulsive force to the LiBr solution which has a high surface tension, and this phenomenon induces the large contact angle. From the theory of the breakthrough pressure, the larger contact angle generates the larger breakthrough pressure that can withstand the higher pressure differential across the membrane layer. As a result, to improve the performance of mass transfer, the contact angle is the most significant physical factor to increase the size of pores within the limits of the breakthrough pressure. Fig. 3-3 presents the method to measure the contact angle between a droplet of the LiBr solution and an HFM used in this study and Fig. 3-4 shows the evaluated breakthrough pressure of the HFM used in this study with the measured values of the contact angle and surface tension of the LiBr solution for several concentrations (surface tension data is obtained from [Taira (2017)]).

3.3. Physical structure of hollow fiber membrane

Fig. 3-5 illustrates the SEM images used to investigate the morphologies of the HFM used in this study, including the following views: (a) cross-sectional, (b) enlarged cross-sectional, (c) an inner surface, and (d) outer surface. Table 3-1 lists the membrane parameters used in the experiments.

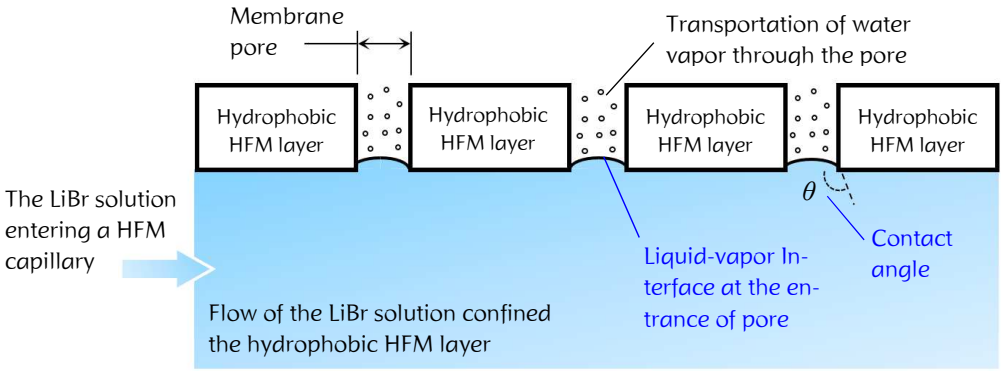

Fig. 3-2. Confined flow of the LiBr solution in direct contact with a hydrophobic membrane surface, describing the contact angle and the liquid-vapor interface at the entrance of pore

Fig. 3-3. Photo measuring the contact angle between 60% LiBr solution and HFM used in this study

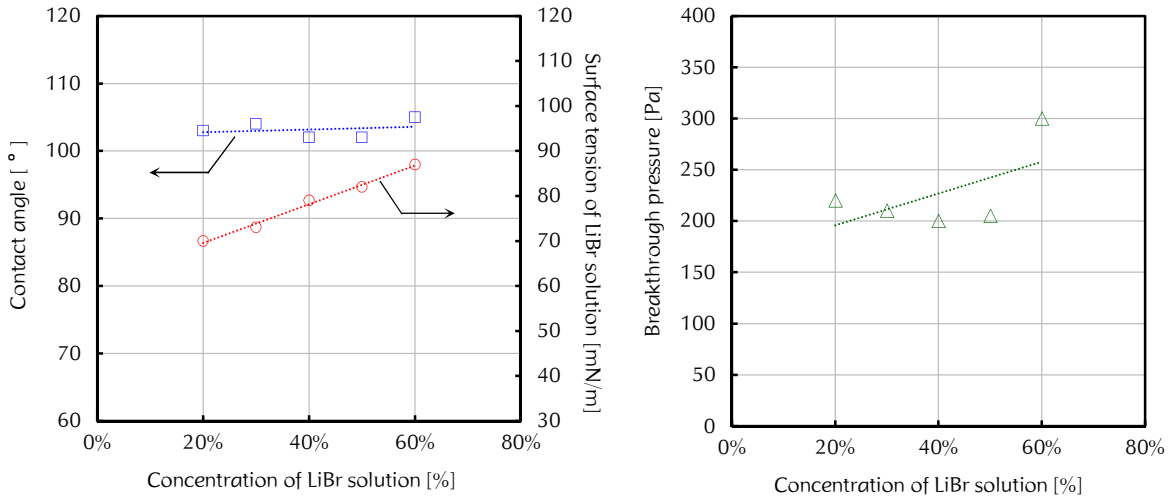

Fig. 3-4. Evaluated breakthrough pressure of the HFM used in the study with the measured values of the contact angle and surface tension of the LiBr solution for several concentrations [Taira (2017)]

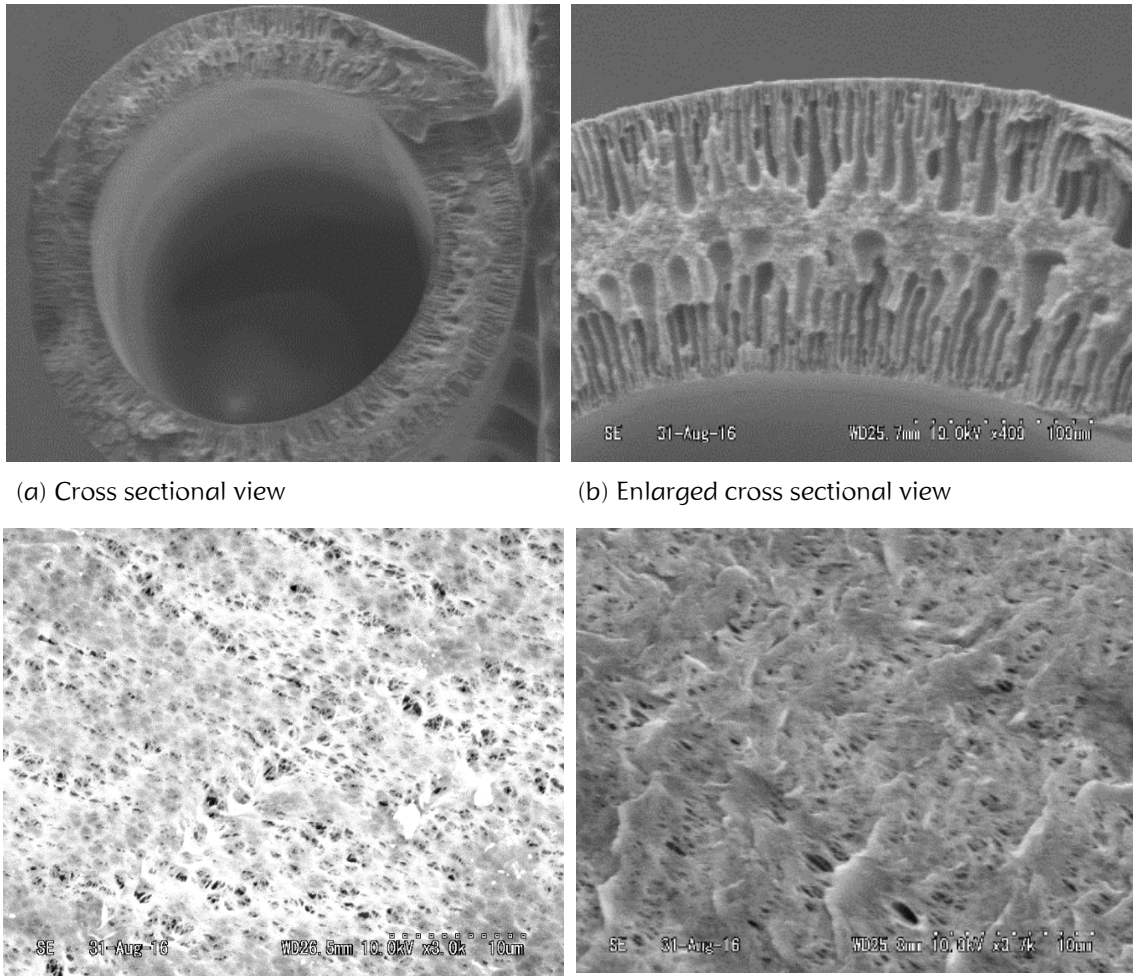

(a) Cross sectional view (b) Enlarged cross sectional view

(c) Inner surface view (d) Outer surface view

Fig. 3-5. SEM images of HFM used in this study, (a) Cross-sectional view, (b) Enlarged cross section, (c) Inner surface view of HFM (Interlaced fibers forming pores), and (d) Outer surface view of HFM

3.4. Gas permeation test

Evaluation of the permeability is essential to identify the mass transfer across the HFM layers. As shown in chapter 3-3, the membrane parameters determine the membrane distillation coefficient, B_m. The fibers are interlaced with each other, forming irregular pore sizes and shapes (Fig. 3-5c, and 3-5d). The nominal membrane pore size is the first approximation for characterizing the mass transport and thus, the determination of the pore size is the first and major requirement for evaluating the mass flux across the membrane. Fig. 3-6 shows a schematic of the experi-

mental setup for the gas permeation test. A commercially used bundle of microporous polypropylene (PP) HFM capillaries was prepared, and an HFM module was made with a transparent acrylic pipe (Φ 3.5 cm × L 35 cm). (Fig. 3-7). Nitrogen gas enters the lumen side of the HFM module's dead-end and is permeated across the HFM layers to the shell side. A pressure regulator adjusts the pressure of the nitrogen gas in the lumen side, and a digital difference manometer (GC62, NAGANO) measures the pressure difference from atmospheric pressure. The permeated nitrogen gas enters a bubble flow meter that is exposed to the atmosphere; as a result, the mass flow rates of the nitrogen are collected under several pressure differences across the HFMs, evaluating the permeability of the HFM, C_m, as:

$$C_m = \dot{m}_{N_2} \frac{\delta}{A} \frac{1}{\Delta p} \tag{3-4}$$

with

$$A = \frac{\pi n l (d_o - d_i)}{\ln (d_o - d_i)} \tag{3-5}$$

where $\dot{m}_{N2}$ is the mass flow rate of nitrogen gas permeated from lumen side of HFMs, and A is the HFM area associated with the thickness, length, and number of HFMs. d_o and d_i are the outer and inner diameter of the HFM, respectively.

The Knudsen diffusion model [Asfand et al. (2016)] was used for the evaluation of the nominal pore size because values of the Knudsen number with the use of submicron pores and nitrogen gas at standard temperature and pressure (STP) are greater than one. The nominal pore size is determined using,

$$d_p = C_m \left(\frac{\varepsilon}{3\tau} \frac{M_{wv}}{RT_m} \sqrt{\frac{8RT_m}{\pi M_{wv}}} \right)^{-1} \tag{3-6}$$

The steady-state gas permeability was evaluated with the pressure difference across the HFM layers. Measuring the flow rate of permeated gas from the lumen side of HFMs for several pressure differences determines the permeable characteristic as shown in Fig. 3-8. The constant permeability was observed for several pressure differences and from this result, the nominal pore size was also estimated as shown in Fig. 3-8.

Table 3-1. Membrane parameters used in the gas permeability experiment

Parameter	Value	Parameter	Value
Membrane material	PP	Effective membrane length [cm]	25
Inner diameter [μm]	390	Outer diameter [μm]	540
Number of membranes in a module	380	Membrane porosity [%]	50

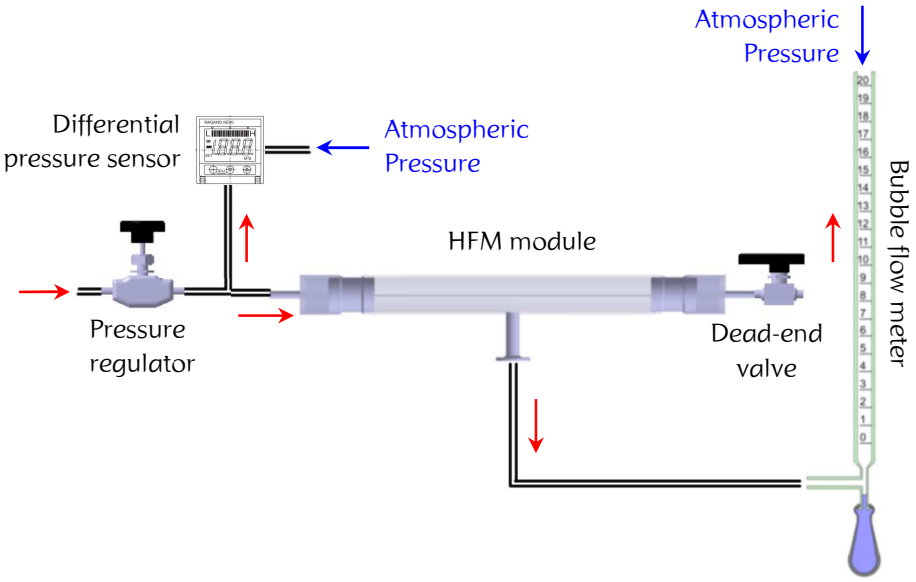

Fig. 3-6. Schematic of experimental setup for gas permeability

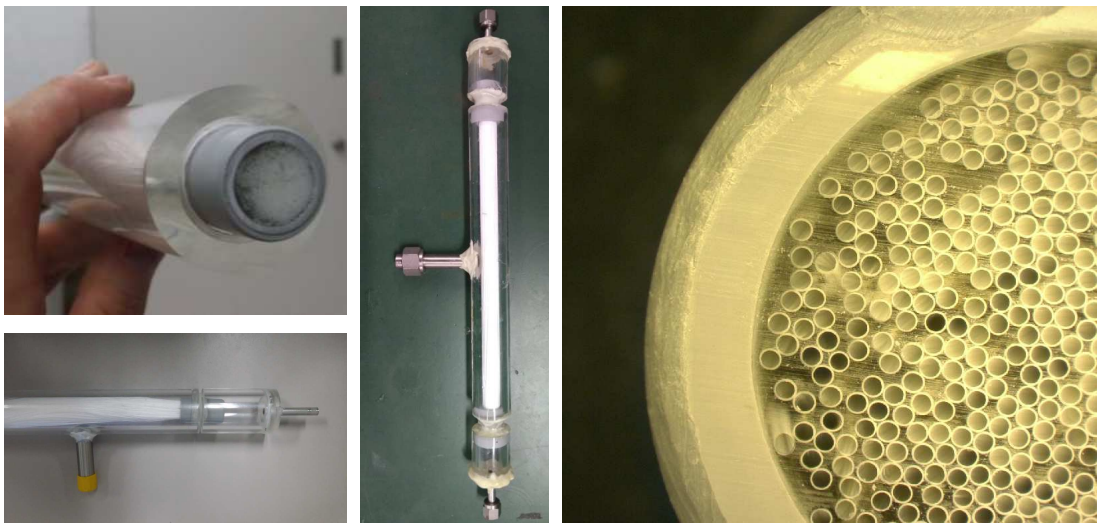

Fig. 3-7. Photos of a bundle of HFMs assembling with a transparent acrylic pipe (Φ 3.5 cm × L 35 cm in total)

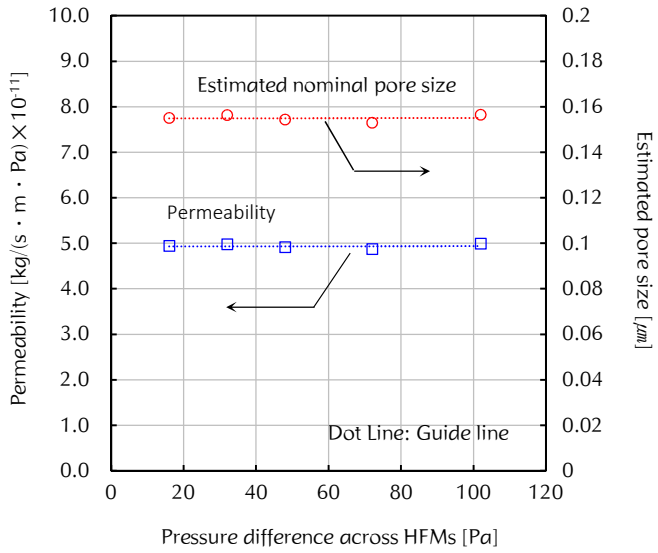

Fig. 3-8. Experimental permeability for the HFM module used in this study, and the estimation of nominal pore size

4

Hollow fiber membrane-based generator

4.1. Theoretical model

Fig. 4-1 shows the configuration of a HFM-based generator (HFM-G). In the proposed configuration, the feed LiBr solution enters the HFM capillaries, and the streams of the aqueous LiBr solution are in direct contact with the inner surface of the HFMs and are also mechanically constrained by the hydrophobic surface. The shell side is filled with water vapor at the static vacuum conditions (i.e., connected with a condenser). The desorption of water vapor takes place across the HFMs when the hot LiBr solution enters the HFMs, i.e., the vapor pressure of the solution is higher than the static equilibrium pressure at the shell side.

4.1.1. Mass transfer

Fig 4-2 depicts a thermal boundary layer of the LiBr solution flowing along an HFM layer when the adiabatic desorption takes place (the shell side is occupied with water vapor, and $p_{v,ms} > p_v$).The volatile component, i.e. water, evaporates at the liquid-vapor interface and permeates through the pores as long as the pressure at the shell side is maintained below the equilibrium vapor pressure at the membrane surface (i.e. liquid-vapor interface at the entrance in the pore). Thus, the driving force of the water vapor mass flux across the HFM layer is the vapor pressure difference between the membrane surface and the shell side. Fig.4-2 also illustrates the profiles

of temperature, concentration, and vapor pressure in the normal direction of the thermal boundary layer when the hot LiBr solution enters a given HFM capillary. Temperature and concentration polarizations between the bulk phase and the membrane surface occur due to simultaneous heat and mass transfer. The hydraulic characteristics in the boundary layer determine the temperature and concentration profiles. The non-volatile component, the LiBr salt, is accumulated near the entrances of pores, which obstructs the movement of the volatile component to the liquid-vapor interface [Alsaadi et al. (2014)]. The mass flux of the water vapor across the HFM layers is evaluated according to Darcy's law as [Peña et al. (1998)]:

$$J_v = B_m \left(p_{v,ms} - p_v\right) \tag{4-1}$$

where $p_{v,ms}$ is the vapor pressure of the solution at the membrane surface, and P_v is the vapor pressure at the shell side. When applying the Antoine equation, the effect of the curvature at the liquid-vapor interface is assumed to have negligible effect as in the case of a flat surface state [Lawson and Douglas (1997)].

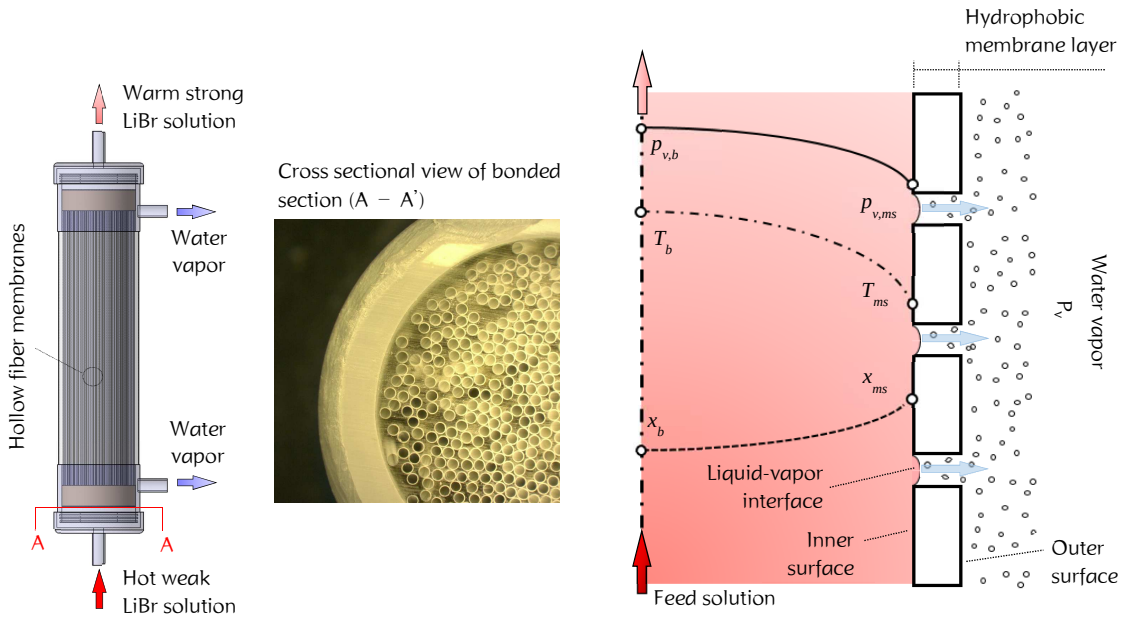

Fig. 4-1. Schematic of the hydrophobic HFM-based generator.

Fig. 4-2. Simplified schematic presenting the heat and mass transfer in a thermal boundary layer of LiBr solution flowing in direct contact with an HFM layer

The empirical numerical fitting evaluates the vapor pressure of the solution using the dew point temperature, considering the temperature and the concentration, as [McNeely, L.A. (1978)]:

$$\log p_v = A_0 + \frac{A_1}{T_d} + \frac{A_2}{T_d^2} \tag{4-2}$$

with

$$T_d = \frac{T - \sum_0^3 C_n x^n}{\sum_0^3 B_n x^n} \tag{4-3}$$

where T_d is the dew point temperature in the range of -15 to 110 in Celsius. T is the temperature of LiBr solution in the range of 5 to 175 in Celsius. x is the concentration of LiBr solution in the range of 45 to 70 %. The constants, A_n, B_n, and C_n are listed in Table 4-1.

The one-dimensional diffusion of gas molecules in the porous media implies the existence of a frictional mass transfer resistance with the pore walls and collisions among molecules. The membrane distillation coefficient across the membrane, B_m, is estimated according to a dominant flow regime. The flow regimes involve the viscous, transitional, and Knudsen flow, depending on the Knudsen (K_n) number described as;

$$K_n = \frac{\lambda}{d_p} \tag{4-4}$$

where K_n is the Knudsen number. λ is the mean free path of working gas in porous media, and d_p is the membrane pore size. The mean free path is expressed as:

$$\lambda = \frac{k_B T}{\sqrt{2}\, p \pi d_g^2} \tag{4-5}$$

where k_B is the Boltzmann constant (1.3807×10^{-23} J/K). T is the temperature of working gas in the pores, and p is the gas pressure. d_g is the molecular diameter of working gas (2.7×10^{-10} m for water vapor).

Table 4-1. Constants for Eq. 4-2 and 4-3

n	A	B	C
0	7.05	- 2.00755	124.937
1	- 1596.49	0.16976	- 7.71649
2	- 104095.5	$- 3.133362 \times 10^{-3}$	0.152286
3		1.97668×10^{-5}	$- 7.95090 \times 10^{-4}$

For $K_n > 1$, the collisions between molecules and pore walls are dominant and the Knudsen diffusion takes place for which the mass transfer coefficient is evaluated as:

$$B_m^{knudsen} = \frac{M_w}{\delta}\left(\frac{D_k}{RT_m}\right) \tag{4-6}$$

where M_w is the molecular weight of water and D_k is the Knudsen diffusion coefficient. T_m is the mean temperature in the pores that is calculated by the average temperature between vapor and liquid-vapor interface at the entrance of pores. The Knudsen diffusion coefficient for porous solid is as below:

$$D_k = \frac{2r_p\varepsilon}{3\tau}\sqrt{\frac{8RT_m}{\pi M_w}} \tag{4-7}$$

where r_p is the radius of membrane pore. ε and τ are the membrane porosity and the tortuosity, respectively. For $K_n < 0.01$, the collisions among the molecules are dominated, and the viscous diffusion occurs, resulting in rapid convective transport [Asfand et al. (2016)].

$$B_m^{viscous} = \frac{M_w}{\delta}\left(\frac{p_m B_o}{RT_m\mu_w}\right) \tag{4-8}$$

where p_m is the mean pressure in pores and B_o is the viscous diffusion coefficient. μ_w is the dynamic viscosity of water vapor. The viscous diffusion coefficient is calculated:

$$B_o = \frac{{d_p}^2\varepsilon}{32\tau} \tag{4-9}$$

For $0.01 < K_n < 1$, the transitional flow regime depends on the Dusty-Gas model and the mass transfer involves both the Knudsen and the viscous diffusion regime.

$$B_m^{transitional} = \frac{M_w}{\delta}\left(\frac{D_k}{RT_m} + \frac{p_m B_0}{RT_m\mu_w}\right) \tag{4-10}$$

The vacuum driven desorption process and sub-micron pore size gives the Knudsen number in the range of the Knudsen diffusion, where the mass transfer coefficient, B_m, is expressed as [Schofield et al. (1987), Martınez et al. (2002), Ramon et al. (2009), Fan and Peng (2012), Lee and Kim (2013), Zuo et al. (2014)],

$$B_m = 1.064 \frac{r_p \varepsilon}{\tau \delta} \sqrt{\frac{M_w}{RT_m}} \tag{4-11}$$

The concentration at the membrane surface increases due to the escape of water vapor from the stream of solution. Thin film theory is widely considered to determine the concentration profile in the thermal boundary layer [Martínez-Díez and Vazquez-Gonzalez (1999), Bui et al. (2010)]:

$$x_{ms} = x_b \exp\left(\frac{J_v}{\rho \alpha}\right) \tag{4-12}$$

where x_{ms} and x_b are the concentration of the LiBr solution at the membrane surface and the bulk, respectively. ρ and α are the density and convective mass transfer coefficient, respectively.

4.1.2. Heat transfer

The water desorption process through the HFMs essentially undergoes an adiabatic process. During the adiabatic water vapor desorption process, no available heat is transferred to the HFM-G. Thus, the LiBr solution temperature decreases along the flowing direction.

$$\dot{Q}_b = G(h_{b,in} - h_{b,out}) \tag{4-13}$$

where $\dot{Q}_b$ is the heat flux by the decrease in temperature along the flowing direction; G is the mass flux of the feed LiBr solution; $h_{b,in}$ and $h_{b,out}$ are the specific enthalpies of the LiBr solution at the inlet and outlet, respectively.

The heat and mass transfer take place simultaneously during the water vapor desorption process via the HFM-G. The heat transfer is mainly explained by two steps: the heat transfer through a thermal boundary layer of the feed LiBr solution, and the heat transfer across the HFM layer, where both values are identical at steady-state. The heat flux across the HFM is directly influenced by the mass flux of the water vapor and the conduction heat transfer, such that:

$$\dot{Q}_{mem} = J_v \Delta H_v + \frac{k_m}{\delta}(T_{ms} - T_{wv}) \tag{4-14}$$

with

$$k_m = \varepsilon k_{wv} + (1-\varepsilon) k_{mt} \tag{4-15}$$

where $\dot{Q}_{mem}$ is the heat flux across the membrane; ΔH_v is the latent heat of vaporization; k_{mem}, k_{wv}, and k_{mt} are the thermal conductivity of HFM, water vapor, and membrane material, respectively. When the downstream area of the water vapor desorption is kept under vacuum conditions and only vapor is present at the vapor side, the conduction term in Eq. 4-12 is negligible [Alsaadi et al (2014), Ramon et al. (2009), Fan et al. (2012), Wang et al. (2011)].

Convective heat transfer across the feed thermal boundary layer developed adjacent to the membrane surface, occurs from the bulk phase to the membrane surface, as:

$$\dot{Q}_f = h_f (T_b - T_{ms}) \tag{4-16}$$

where $\dot{Q}_f$ is the convective heat flux in the thermal boundary layer of the LiBr solution; h_f is the convective heat transfer coefficient; T_b and T_{ms} are the LiBr solution temperatures at the bulk phase and at the membrane surface, respectively.

The convective heat transfer coefficient affects the temperature at the membrane surface, directly influencing the mass desorption transfer. The Nusselt number has commonly been used for evaluating the convective heat transfer coefficient. The empirical heat transfer correlation for a laminar flow regime used in the membrane distillation process is shown as below, [Tomaszewska et al. (2000), Mengual et al. (2004)]:

$$Nu = 4.36 + \frac{0.036\ (Re\, Pr\, D_h / l)}{1 + 0.0011 (Re\, Pr\, D_h / l)^{0.8}} \tag{4-17}$$

where Re is the Reynolds number; Pr is the Prandtl number; D_h is the hydraulic diameter identical to the inner diameter of the HFM; l is the length of the HFM.

The temperature polarization effect leads to diffusive heat transfer resistance in the thermal boundary layer. The value of the temperature polarization coefficient, defined as the ratio of the temperature at the membrane surface to that at the bulk phase, approaching unity stands for an ideally designed HFM module that maximizes mass transfer performance, while a lower value signifies thermal dissipation through the thermal boundary layer. Enhancement in the temperature polarization coefficient is achieved with an increase in the feed flow rate or a decrease in the feed solution temperature.

4.1.3. Pressure drop

Due to the desorption of water vapor, the temperature, and concentration, in combination with the physical properties of the LiBr solution change in flow direction, the local pressure gradient, dp/dx, is expressed by:

$$\frac{dp}{dx} = \frac{f_D}{D_h}\frac{\rho}{2}u^2 \tag{4-18}$$

with

$$f = \frac{64}{\mathrm{Re}} \tag{4-19}$$

where dp is the frictional pressure drop through a single element of the HFM; f_D is the Darcy friction factor for the laminar flow regime for a circular tube; dx is a single element of the HFM; u is the velocity of the solution.

4.1.4. Thermodynamics of vapor absorption refrigeration system with hollow fiber membrane based-generator

Fig. 4-3 illustrates the vapor absorption refrigeration system combined with hollow fiber membrane based-generator (HFM-G based VARs). The HFM-G based VARs has six essential components: the HFM-G, a waste heat-driven heat exchanger, a condenser, an evaporator, an absorber, and a solution heat exchanger. The weak aqueous LiBr solution, which is circulated and pressurized by a solution pump, is heated by the waste heat-driven heat exchanger. As the weak solution enters the HFM-G, there is a significant drop in temperature owing to the consumption of sensible heat for the latent heat of vaporization for the desorption process, and therefore, the vapor partial pressure of the refrigerant also decreases in the flow direction. As long as the partial pressure at the liquid-vapor interface is higher than the condenser pressure, the evaporation continues in the flow direction, and the cooling process in the condenser condenses the evaporated water vapor. After flowing out of the HFM-G, part of the strong solution is recirculated into the HFM-G, while the rest flows back to the absorber via the solution heat exchanger. Recirculation ratio, β, defined as the ratio of $\dot{m}_{8a}$ to $\dot{m}_{8b}$ is controlled by a recirculation pump.

For thermodynamic analysis of the HFM-G based VARs, the conservation of mass follows the mass balance of total mass. The mass flow rate of the solution and refrigerant in each state are given as follows:

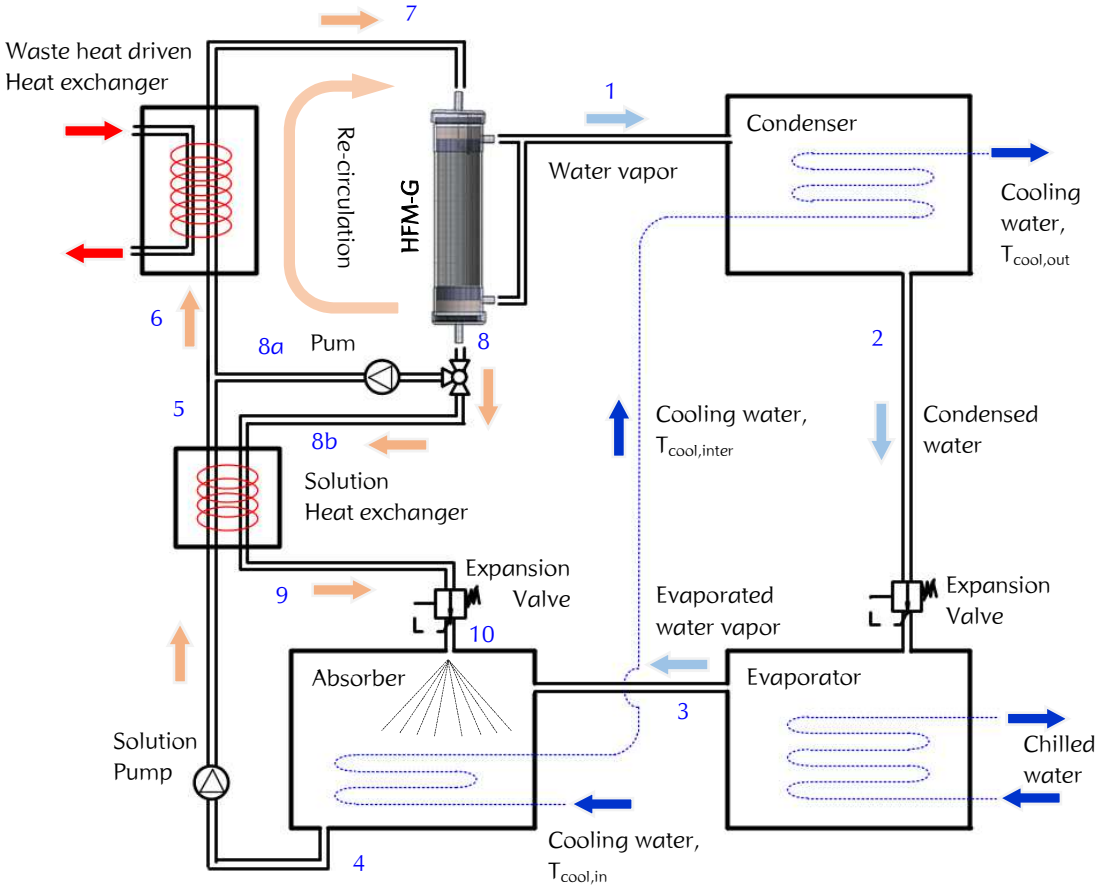

Fig. 4-3. Schematic of vapor absorption refrigeration system combined with hollow fiber membrane based-generator (HFM-G based VARs)

$$\dot{m}_8 = \dot{m}_7 - \dot{m}_{ref} \tag{4-20}$$

$$\dot{m}_6 = \dot{m}_5 + \dot{m}_{8a} \tag{4-21}$$

$$x_6\,\dot{m}_6 = \dot{m}_5\,x_5 + x_8\,\dot{m}_{8a} \tag{4-22}$$

$$\dot{m}_{8a} = \beta\,\dot{m}_{8b} \tag{4-23}$$

where $\dot{m}$ is the mass flow rate; x, the concentration of aqueous LiBr solution; and β, the recirculation factor.

The energy balance equations of each component of the HFM-G based VARs are as follows:

The rate of heat absorption of the evaporator

$$Q_{evap} = \dot{m}_{ref}\,(h_3 - h_2) \tag{4-24}$$

The rate of heat rejection out of the condenser

$$Q_{cond} = \dot{m}_{ref} (h_1 - h_2) \tag{4-25}$$

The rate of heat rejection of the absorber

$$Q_{abs} = \dot{m}_{ref} h_3 + \dot{m}_{10} h_{10} - \dot{m}_4 h_4 \tag{4-26}$$

The rate of heat absorption of the waste-heat driven heat exchanger

$$Q_{WH/HE} = \dot{m}_6 (h_7 - h_6) \tag{4-27}$$

where Q is the heat exchanged, h is the specific enthalpy; and $\dot{m}_{ref}$ is the mass flow rate of the refrigerant (i.e. water). For the analysis, the refrigerant at evaporator and condenser outlet is saturated and the weak solution from the absorber is also saturated.

A solution heat exchanger is used for heat recovery from the strong to weak solution side. The effectiveness of the solution heat exchanger is defined as follows:

$$\varepsilon_{SHE} = \frac{T_{8b} - T_9}{T_{8b} - T_4} \tag{4-28}$$

The overall system performance was evaluated by considering the COP, which is defined as the ratio of the heat extracted from the evaporator to the heat input to the waste-heat exchanger:

$$\mathrm{COP} = \frac{Q_{evap}}{Q_{WH/HE}} \tag{4-29}$$

To determine the amount of heat transferred and the thermodynamic properties of each state, the design parameters (Table 4-2) and the membrane parameters (Table 4-3) are used to simulate the HFM-G based VARs.

4.1.5. Dühring chart

Each state of the HFM-G based VARs is visualized in a p-t-x diagram, Dühring chart (Fig. 4-4).

Table 4-2. Operating conditions used in theoretical simulation of the HFM-G based VARs

Parameter	Value
Generating temperature, T_7 [°C]	80 - 120
Evaporation temperature, T_3 [°C]	6
Absorber temperature, T_4 [°C]	$T_{cool,\ inter} + 3$
Condenser temperature, T_2 [°C]	$T_{cool,\ out} + 3$
Inlet cooling water temperature, $T_{cool,\ in}$ [°C]	25 - 35
Flow rate of weak solution, $\dot{m}_4$ [kg/s]	0.01 - 0.09
Effectiveness of solution heat exchanger, ε	0.80

Table 4-3. Membrane parameters used in cycle simulation of the HFM-G based VARs

Parameter	Value	Parameter	Value
Pore size, d_p [μm]	0.16	Number of membranes, [EA]	80 - 600
Porosity, ε [%]	85	Inner diameter, d_i [μm]	800
Membrane length, l [cm]	20	Outer diameter, d_o [μm]	1100

4.1.6. Simulation procedure

Fig. 4-5 shows a flowchart of the theoretical simulation of the heat and mass transfer of the HFM-G. The simulation begins with longitudinally splitting the HFM into tiny elements, dx. The heat balance (from Eq. 4-14 and 16) enables the evaluation of the mass flux of the water vapor across the HFM for a single element by determining the temperature and concentration at the membrane surface. The thermodynamic properties of the solution at the outlet of a single element of the HFM are then calculated and used as the feed physical properties for the next element. The above process is repeated until the summation of dx reaches the length of the HFM. The performance of the HFM-G based VARs is also conducted with various working conditions. The following assumptions were considered for the simulation.

- The process is a steady-state process.
- The heat and mass transfer process is one-dimensional.
- The mathematical model of one HFM represents the overall performance.
- The membrane surface is in an equilibrium state with respect to the temperature and concentration of the LiBr solution.
- The solution temperature at the outlet of the absorber and refrigerant temperature at the

outlet of condenser decrease to values 3 °C higher than the cooling water temperature at the outlet of each component.

- The solution at the outlet of the absorber is saturated.
- Expansion at the expansion valves is assumed to be adiabatic.
- Heat exchange does not take place with the surroundings.

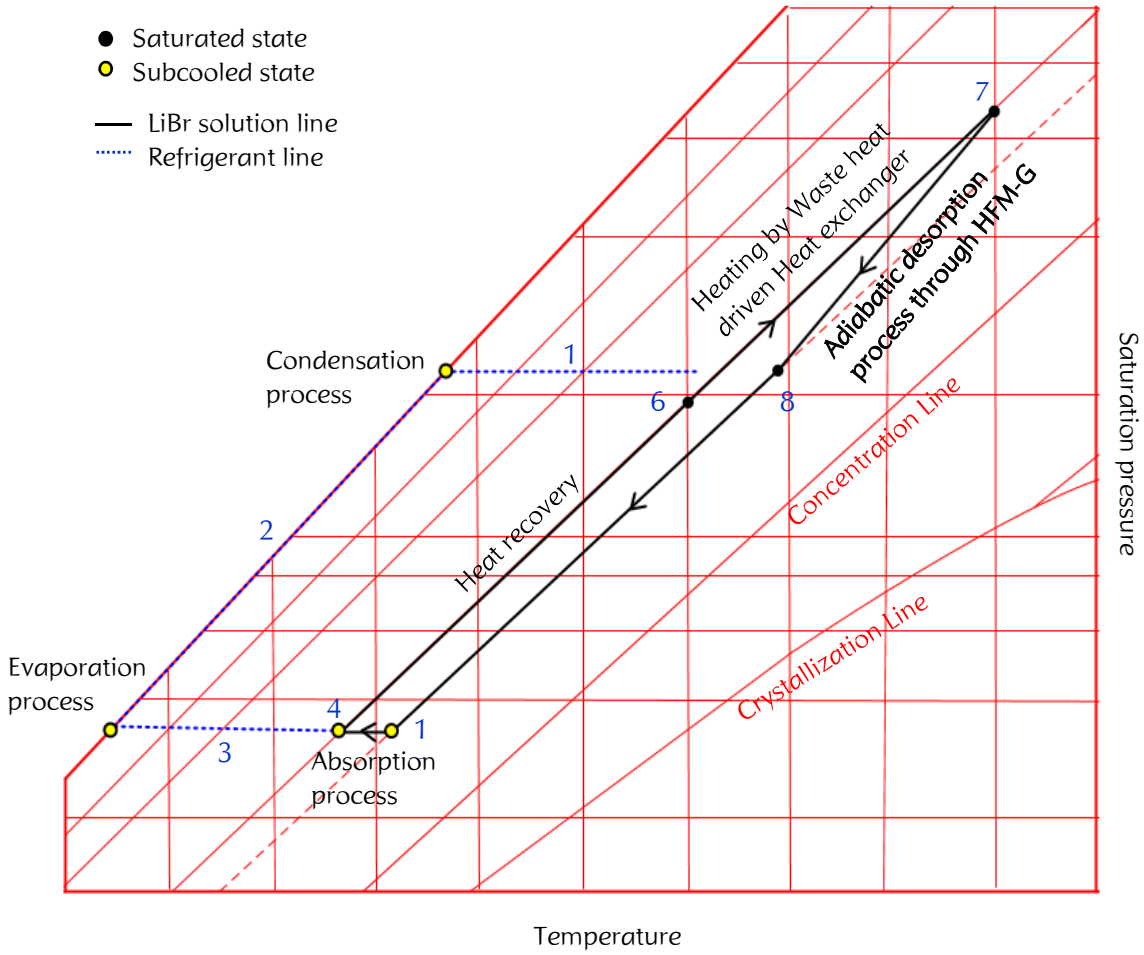

Fig. 4-4. Dühring chart for the HFM-G based VARs

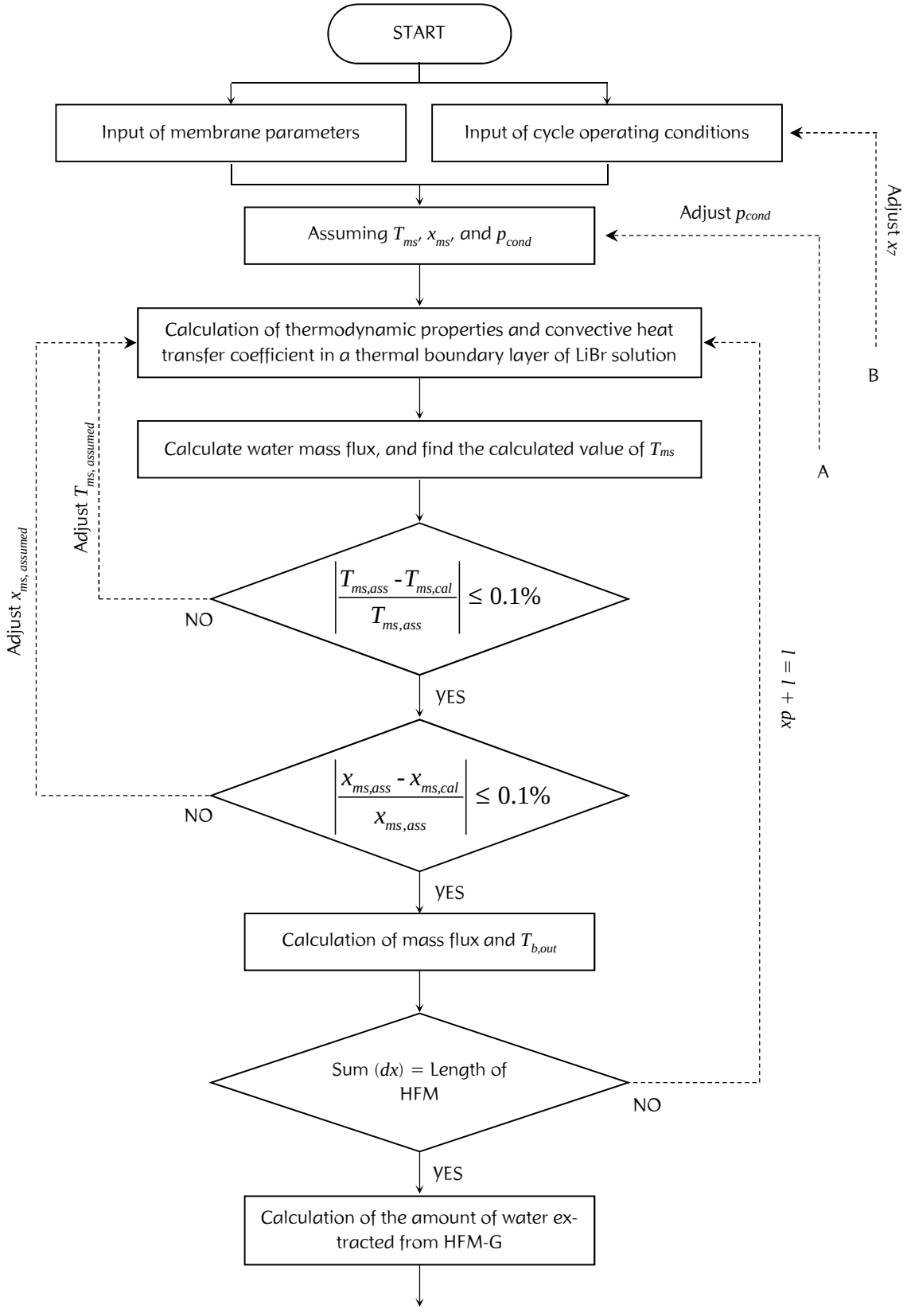
START
Input of membrane parameters
Input of cycle operating conditions
Adjust x_7
Assuming $T_{ms'}$ $x_{ms'}$ and p_{cond}
Adjust p_{cond}
Calculation of thermodynamic properties and convective heat transfer coefficient in a thermal boundary layer of LiBr solution
B
Calculate water mass flux, and find the calculated value of T_{ms}
A
Adjust $T_{ms,\ assumed}$
Adjust $x_{ms,\ assumed}$
$\left|\frac{T_{ms,ass} - T_{ms,cal}}{T_{ms,ass}}\right| \leq 0.1\%$
NO
YES
$xp + l = l$
$\left|\frac{x_{ms,ass} - x_{ms,cal}}{x_{ms,ass}}\right| \leq 0.1\%$
NO
YES
Calculation of mass flux and $T_{b,out}$
Sum (dx) = Length of HFM
NO
YES
Calculation of the amount of water extracted from HFM-G

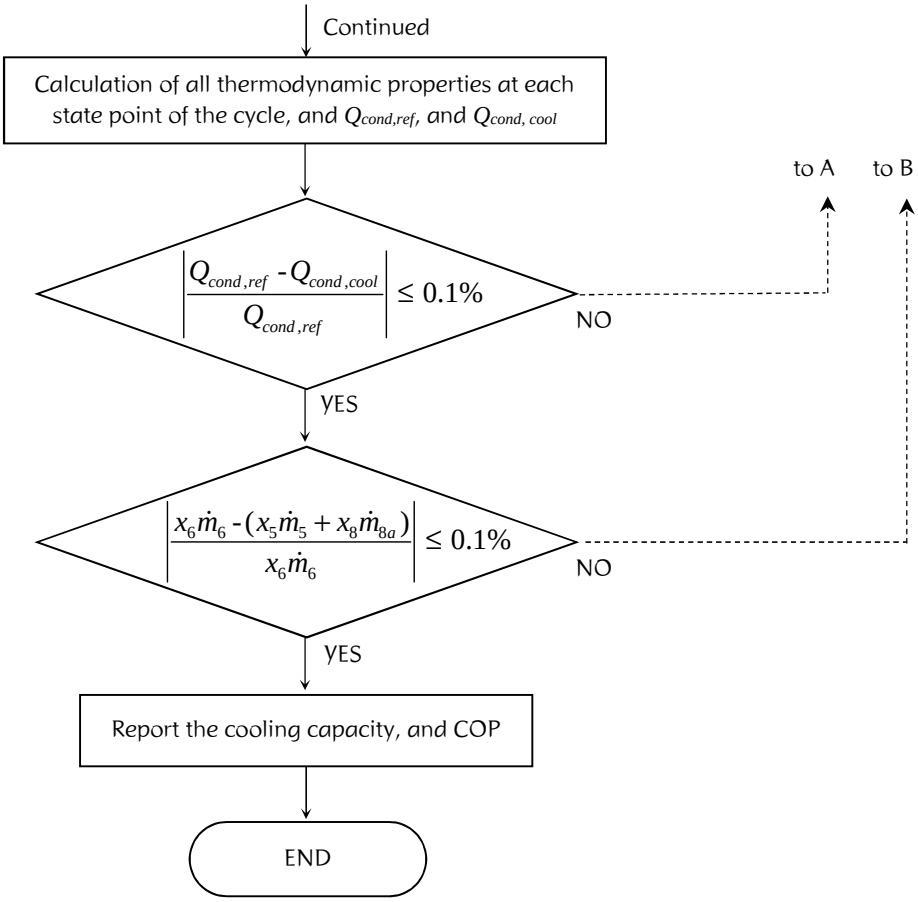

Fig. 4-5. Flowchart of the simulation procedure of the HFM-G based VARs

4.2. Experiment

4.2.1. Apparatus and experimental procedure

Fig. 4-6 shows a schematic of the transient experimental apparatus, which is used to examine the heat and mass transfer characteristics of the HFM adiabatic desorption process. The feed weak LiBr solution is initially contained in a stainless steel-based reservoir and is fed by a solution pump (GB-P25, MICROPUMP). The first Coriolis flow meter (CA003, OVAL) measures the density, temperature, and flow rate of the feed LiBr solution. The feed solution is then heated by a heat exchanger and enters the HFM-G. The shell side of the HFM-G is connected with a condenser so that the pressure downstream of the water vapor desorption is controlled and also maintained by a heat rejection process. The pressure at the condenser is measured by a vacuum pressure transducer (CCMT-100D, ULVAC). The adiabatic desorption process takes place as long as the

vapor pressure at the condenser is lower than the vapor pressure of the solution flowing along the HFMs, while the feed weak solution turns into a strong solution. Two Pt100 sensors (Class A, CHINO) measure the inlet and outlet solution temperatures to evaluate the adiabatic desorption heat transfer. The pressure drop via the HFM-G is measured by a differential pressure transducer (UNIK5000, GE). The density and concentration of the strong solution are measured by another Coriolis flow meter (CA003, OVAL). Prior to the density measurement by the second Coriolis flow meter, the strong solution undergoes a cooling process to prevent density measurement errors, which may occur if a temperature difference exists between the two Coriolis flow meters. As the HFM desorption takes place, the water vapor leaves from the flow path of LiBr solution to the condenser. As a results, the concentration of LiBr solution at the outlet of the HFM-G increases

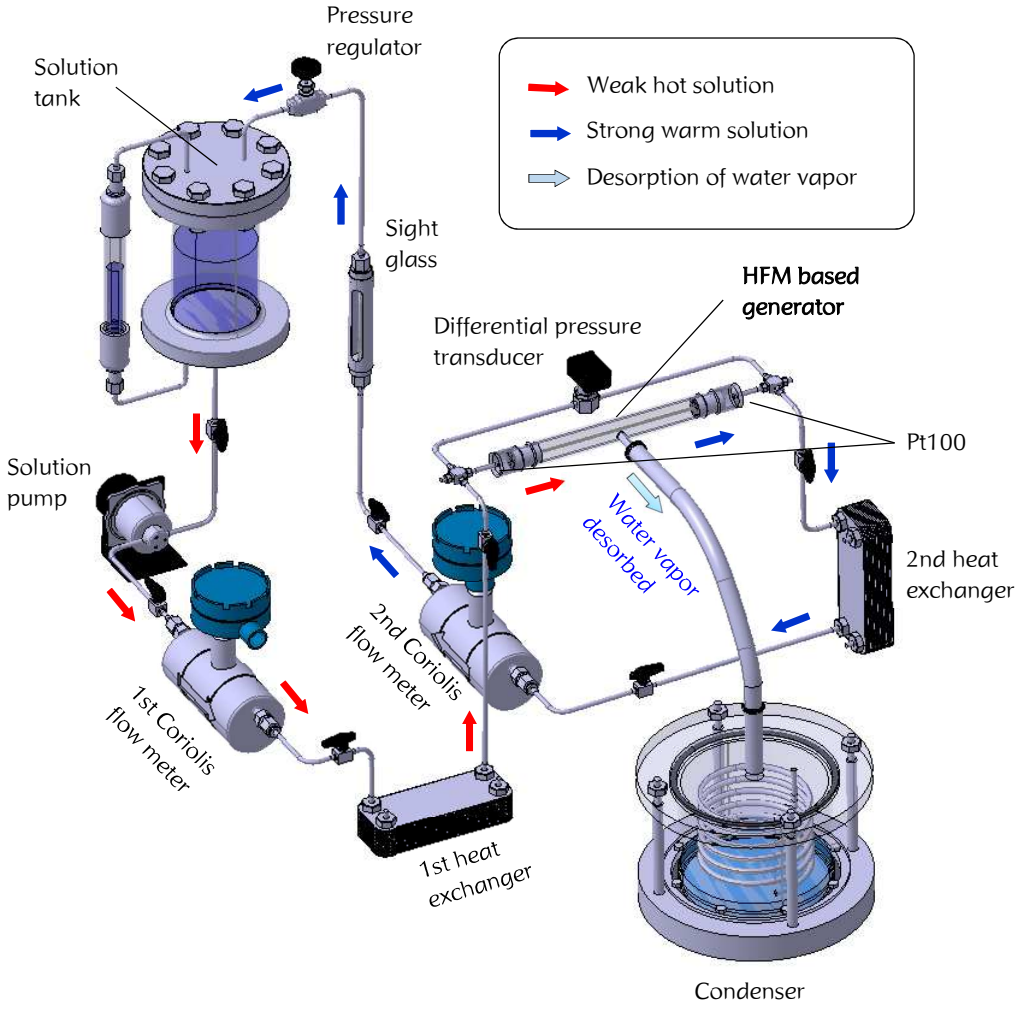

Fig. 4-6. Schematic of experimental apparatus to evaluate the heat and mass transfer of the HFM-G

where the inlet concentration is 'weak' and the outlet is 'strong' solution. The strong solution enters a 2nd Coriolis flow meter (CA003, OVAL) to take the data of solution density and temperature in real time. Meanwhile, before the density measurement process by the 2nd Coriolis flow meter, the strong solution undergoes a cooling process via a 2nd heat exchanger to prevent an error of density measurement which might be occurred by temperature difference between two Coriolis flow meters. As the strong solution returns to the solution tank, the feed solution concentration becomes stronger during a series of experiment; in other words, the 'weak' solution of the inlet HFM-G becomes 'stronger' during a series of experiment. As a result, an initial operating condition (mainly feed solution concentration) changes with experimental time. Note that the established methods [Martınez-Dıez et al. (1998), Martínez-Díez and Vazquez-Gonzalez (1999), Li and Kamalesh (2005), Jin et al. (2008), Wang et al. (2008), Ali and Peter (2009), Wang et al. (2009), Zhu et al. (2013), Chiam and Rosalam (2014)] evaluating the heat and mass transfer of the HFM desorption from a binary mixture generally had the solution circulation process; however, as a binary solution was circulated in the closed path, and the volatile component escaped from the solution, the concentration of the feed kept increasing during a series of experiment. It is, thus, limited to well investigate the performance with respect to the certain feed concentration. Since the concentration of solution is one of major factors to determine the performance of VARs, in this study, a transient experimental method is proposed so that the heat and mass transfer performance are evaluated under the various range of feed solution concentration. All of the experimental data collected during the passage of experimental time was used as initial conditions to serve as a basis for comparison with the theoretical heat and mass transfer. The experimental operating conditions are shown in Table 4-3. Table 4-4 lists the measurement accuracy of the density, mass flow rate, temperature, and pressure.

Table 4-3. Range of experimental operating conditions

Parameter	Value
Temperature of feed LiBr solution [°C]	65 - 83
Concentration of feed LiBr solution [%]	51 - 58
Mass flux of feed LiBr solution [kg/m^{2}s]	157 - 244
Pressure at condenser [kPa]	2.6 - 5.5

Table 4-4. Properties of sensors

Parameter	Measurement Device	Accuracy	Range
Density	CA003, OVAL	± 0.0005 g/ml	0.3 to 2 g/ml
Mass flow rate	CA003, OVAL	± 0.1 % for liquid	0.72 to 72 kg/h
Temperature	Pt sensor, CHINO	± 0.05 °C	- 50 to 100 °C
Temperature	T type, CHINO	± 0.5 °C	- 62 to 125 °C
Pressure at condenser	CCMT-100D, ULVAC	± 0.2 % ± 0.005 % F.S./ °C	1.3 to 13.3 kPa
Pressure at reservoir	CCMT-1000D, ULVAC	± 0.2 % ± 0.005 % F.S./ °C	13 to 133 kPa
Differential pressure	UNIK5000, GE	± 0.04 % F.S.	7 to 70,000 kPa

4.2.2. Data reduction

Two Coriolis flow meters measure both the density and temperature, evaluating the concentrations of LiBr solution both the inlet and outlet of the HFM-G. The concentration of the LiBr solution is evaluated by:

$$\rho_{sol} = D_0 + D_1 x + D_2 x^2 - T(D_3 + D_4 x) \quad (4\text{-}30)$$

where ρ_{sol} is the density of LiBr solution. x and T is the concentration and temperature of the LiBr solution, respectively. Constants, D_0 = 1145.36, D_1 = 470.84, D_2 = 1374.79, D_3 = 0.333393, D_4 = 0.571749. All the thermos-physical properties of LiBr solution is calculated from the established numerical fittings data from thermos-physical property charts [McNeeley (1978), Patterson and Perez-Blanco (1988), Florides et al. (2003), Samanta (2003)], such that: the density, viscosity, specific heat, and thermal conductivity of LiBr solution.

In order to evaluate the HFM desorption mass transfer, the assumption of mass conservation was first built. Mass of LiBr, non-volatile, in the binary mixture is conserved in a whole flow path of LiBr solution, and is thus estimated by measuring both the solution flow rate and the concentration at the inlet of the HFM-G:

$$\dot{m}_{LiBr} = \dot{m}_{sol,in}\, x_{in} \quad (4\text{-}31)$$

where $\dot{m}_{LiBr}$ and $\dot{m}_{sol,in}$ is the mass flow rate of LiBr and inlet weak solution, respectively. x_{in} is the concentration of solution at the inlet, defined as $\dot{m}_{LiBr} / (\dot{m}_{LiBr} + \dot{m}_{water,in})$. The amount of desorbed water vapor is estimated by the difference between the measured value of inlet solution flow rate and the calculated outlet solution flow rate calculated by outlet concentration as:

$$\dot{m}_{vapor} = \dot{m}_{sol,in} - \frac{\dot{m}_{LiBr}}{x_{out}} \tag{4-32}$$

where $\dot{m}_{vapor}$ is the mass flow rate of desorbed water vapor, and x_{out} is the concentration of solution at outlet, defined as $\dot{m}_{LiBr} / (\dot{m}_{LiBr} + \dot{m}_{water,out})$. Thus, the mass flux of water vapor across the HFMs is determined as function of the total interfacial area for evaporation of water vapor,

$$J_v = \frac{\dot{m}_{vapor}}{A_{mem}} \tag{4-33}$$

where J_v is the mass flux of water vapor across hollow fiber membrane, and A_{mem} is the total contact area of the HFMs.

4.2.3. Validation of concentration measurement

Two Coriolis flow meters measure the density and temperature of the strong and weak solution, respectively, without the desorption process. Fig. 4-7 shows the validation of concentration measurement between two Coriolis flow meters, evaluated by Eq. 4-30. The deviation in the concentrations is less than 0.03%.

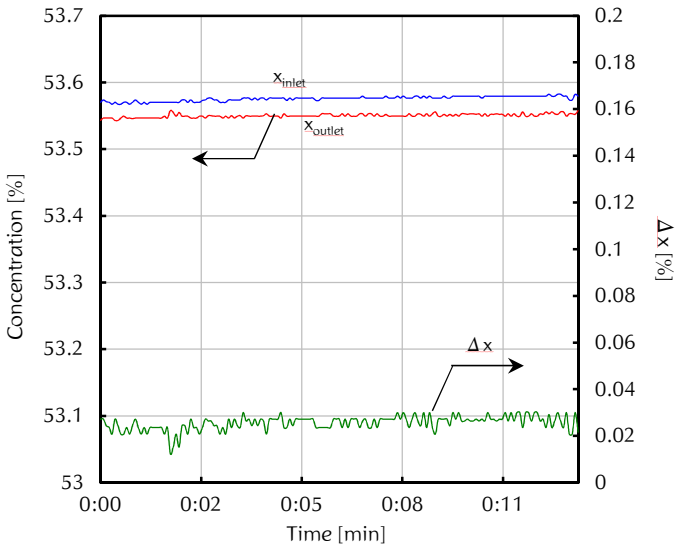

Fig. 4-7. Concentration measurement between two Coriolis flow meters without desorption process.

4.3. Results and discussion

4.3.1. Theoretical simulation results

4.3.1.1. Characteristics of adiabatic desorption mass transfer

Fig. 4-8 shows the axial variation in the solution bulk temperature and the membrane surface temperature in the flow direction. The evaporation of the refrigerant vapor at the liquid-vapor interface leads to a reduction in the solution temperature and an increase in the solution concentration simultaneously. In the flow direction, the rates of the reduction in solution temperature and of the increase in solution concentration decrease in the flow direction as the amount of heat needed for the vaporization decreases. In conjunction with the membrane surface temperature, the rate of variations in the vapor partial pressure decreases, and the driving force of mass transfer, represented by $P_{p,ms} - P_{cond}$, also decreases. Therefore, the performance of the HFM desorption worsens in the flow direction. The desorption hardly occurs when the partial pressure of water vapor at the membrane surface is close to the pressure at the permeate side. Fig. 4-9 shows the bulk temperature variation in the flow direction in an HFM for different feed mass flow rates. The plot shows that the temperature curve for a solution flow rate of 0.01 kg/s is almo st flat and hardly varies near the outlet of the membrane. As the solution

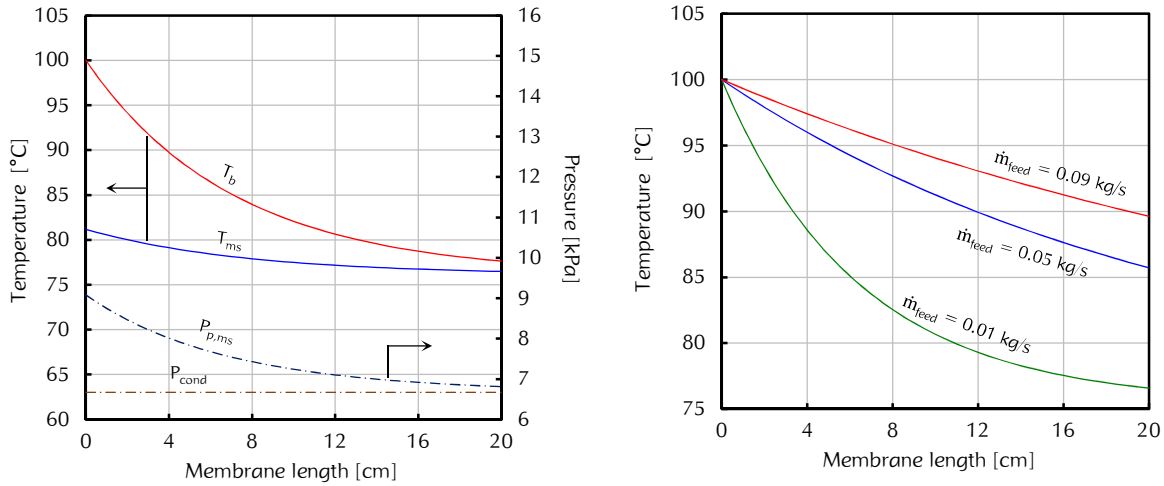

Fig. 4-8. Comparison of temperature variations between the bulk phase (T_b) and membrane surface (T_{ms}), and driving force variations ($P_{p,ms}$ - P_{cond}) in the flow direction (T_{gen} = 100 °C, $\dot{m}_{feed}$ = 0.01 kg/s, x_{feed} = 56.41 %, and P_{cond} = 6.67 kPa, EA = 200, β = 0)

Fig. 4-9. Bulk temperature variation in the flow direction in a HFM for different mass flow rates of the feed solution (T_{gen} = 100 °C, x_{feed} = 56.41 %, and P_{cond} = 6.67 kPa, EA = 200, β = 0)

flow rate increases the temperature drop between the inlet and outlet of the HFM-G decreases because for certain membrane parameters, an increase in solution flow rate (i.e., increase in input energy) is not exactly proportional to the amount of refrigerant evaporated.

Fig. 4-10 shows the variation in solution concentrations in the bulk phase and at the membrane surface. As the water vapor is transported through the membrane pores, the solution concentration at the membrane surface is higher than that at the bulk phase. This phenomenon is termed concentration polarization. It results in resistance to mass transport during membrane distillation; it is expected that the smaller the inner diameter of the HFM, the lesser is the concentration polarization effect, as described in chapter 4.1.2.

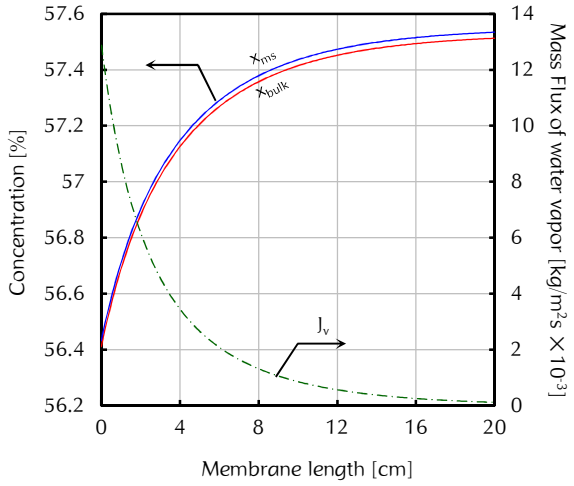

Fig. 4-10. Variation in concentrations at the bulk and at the membrane surface, and in mass flux of water vapor in the flow direction (T_{gen} = 100 °C, x_{feed} = 56.41 %, and P_{cond} = 6.67 kPa, EA = 200, β = 0)

4.3.1.2. Effect of generating temperature on system performance

As shown in Fig. 4-11, a generating temperature directly influences the concentration difference between the inlet and outlet of the HFM-G. At higher generating temperature and lower feed solution flow rate, the solution concentration at the outlet of the HFM-G becomes stronger because the membrane distillation performance depends dominantly on the feed temperature. Therefore, the circulation ratio, which is defined as $\dot{m}_{weak} / (\dot{m}_{weak} - \dot{m}_{strong})$, is extremely high at the low generating temperature; however, it tends to decrease drastically with an increase in the generating temperature. The circulation ratio is a significant design and optimizing factor as it

directly influences the size and cost of VARs. As shown in Fig. 4-12, the cooling capacity is enhanced with an increase in the generating temperature and the flow rate of the feed solution. Further, note that the higher flow rate of the weak solution which enters the HFM-G leads to higher cooling capacity by diminishing the rate of a temperature drop (i.e., driving force drop), as shown in Fig. 4-12. The COP drastically increases with the increase in the generating temperature and the decrease in the feed flow rate, but then the rate of change of COP tends to decrease. In other words, the COP does not increase beyond a certain value despite an increase in the generating temperature at a given flow rate.

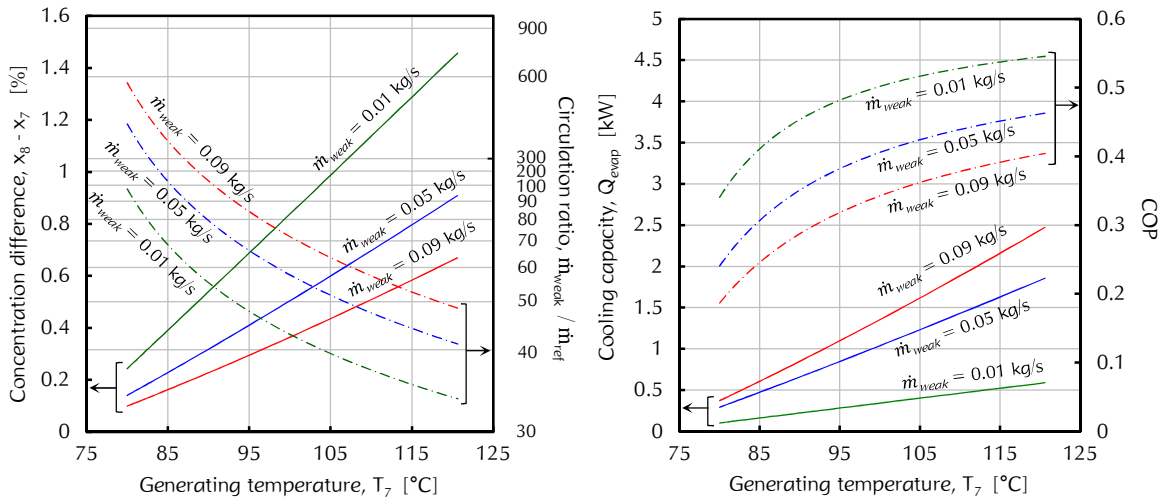

Fig. 4-11. Effect of generating temperature, T_7, on the concentration difference between the inlet and outlet of the HFM-G, and the circulation ratio for different mass flow rates with feed solution temperature (x_{weak} = 56.41 %, $T_{cool,in}$ = 30 °C, EA = 200, β = 0)

Fig. 4-12. Effect of generating temperature, T_7, on the cooling capacity and COP for different mass flow rate with feed solution temperature (x_{weak} = 56.41 %, $T_{cool,in}$ = 30 °C, EA = 200, β = 0)

4.3.1.3. Effect of mass flow rate of weak solution on system performance

Fig. 4-13 and 14 present the effect of variation in solution flow rate on the system. The cooling capacity is enhanced with increases in generating temperature and the flow rate, as described earlier, but the circulation ratio also drastically increases at higher mass flow rates of the feed solution. This is because for given membrane parameters, all the sensible input energy (i.e., larger feed flow rate) is hardly used for the adiabatic desorption process. Note that pressure drop is directly influenced by velocity and viscosity of the solution, which depends on the flow rate and

temperature. Fig. 4-14 also shows that the increase in weak solution flow rate leads to the decrease in the COP. This is also because the membrane distillation efficiency, namely, the ratio of the desorbed water vapor and the energy input (i.e., the increase in the flow rate), decreases for the given membrane parameters.

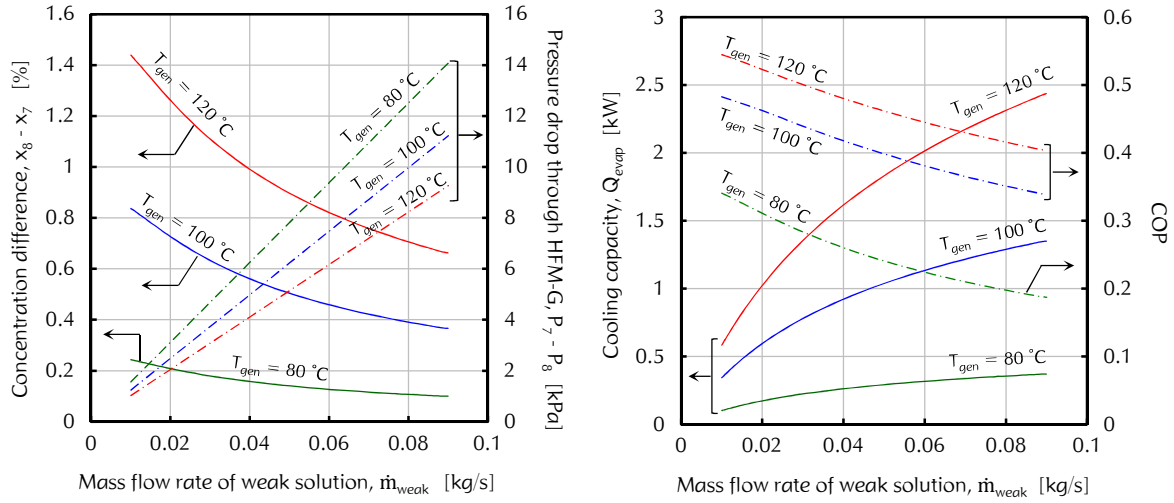

Fig. 4-13. Effect of mass flow rate of weak solution, $\dot{m}_7$, on concentration difference of the HFM-G and pressure drop for different generating temperature (x_{weak} = 56.41 %, $T_{cool,in}$ = 30 °C, EA = 200, β = 0)

Fig. 4-14. Effect of mass flow rate of weak solution, $\dot{m}_7$, on the cooling capacity and COP for different generating temperature (x_{weak} = 56.41 %, $T_{cool,in}$ = 30 °C, EA = 200, β = 0)

4.3.1.4. Effect of cooling water temperature on system performance

The effect of cooling water temperature on the condenser pressure and the circulation ratio is shown in Fig. 4-15. The circulation ratio is sensitive to cooling water temperature for lower feed temperature, and as a result, the system becomes very large under conditions of at lower generating temperature and higher cooling water temperature. The cooling water temperature also directly influences the condenser pressure that affects the driving force of the HFM desorption. Thus, as the cooling water temperature increases, the amount of water vapor desorbed from the HFM-G decreases because of the increase in condenser pressure (i.e., the reduction of desorption driving force). Thus, both the cooling capacity and COP decrease as the heat rejection rate decreases with higher cooling water temperature, as shown in Fig. 4-16. In case of 80 °C generating temperature, the COP drastically decreases with the increase in the cooling water temperature, and a further increase in the cooling water temperature does not result in the desorption process

where the COP could not be evaluated.

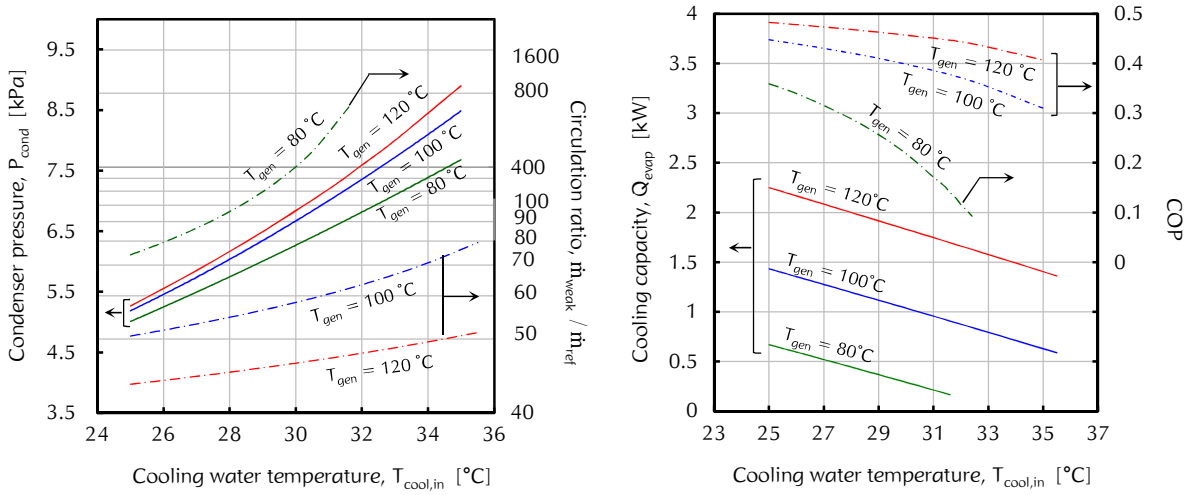

Fig. 4-15. Effect of cooling water temperature, $T_{cool,in}$, on condenser pressure, P_{cond}, and circulation ratio for different generating temperatures ($\dot{m}_{weak}$ = 0.05 kg/s, EA = 200, β = 0)

Fig. 4-16. Effect of cooling water temperature, $T_{cool,in}$, on the cooling capacity and COP for different generating temperatures ($\dot{m}_{weak}$ = 0.05 kg/s, EA = 200, β = 0)

4.3.1.5. Effect of the number of hollow fiber membranes on system performance

One of the great advantages of the HFM-G is that, by changing the number of HFMs for a given volume of the HFM module, the contact area for the desorption of water vapor can be easily adjusted to control its performance. As shown in Fig. 4-17, the circulation ratio and pressure drop through the HFM-G decreases as the number of membranes increases for the given operation. For given flow rate of the feed solution, the number of the HFMs directly influences the solution velocity through the HFM-G. Thus, with the increase in the number of the HFMs (i.e., the decrease in the solution velocity), the sensible input energy is relatively easily used up, resulting in the increase in the amount of desorption water vapor. This decreases the circulation ratio, and the lower solution velocity leads to the lower pressure drop. Fig. 4-18 shows the effect of the number of HFMs in a module on the cooling effect and COP. The cooling capacity and COP, both are improved with an increase in the number of HFMs (i.e., an increase in the contact area for the vapor desorption). Note that sensible heat at the inlet of the HFM-G provides the energy for the HFM desorption. Thus, regardless of the number of membranes, the improvement in the distillation performance is limited because the performance depends completely on the given inlet conditions of the membrane, as shown in Fig. 4-18.

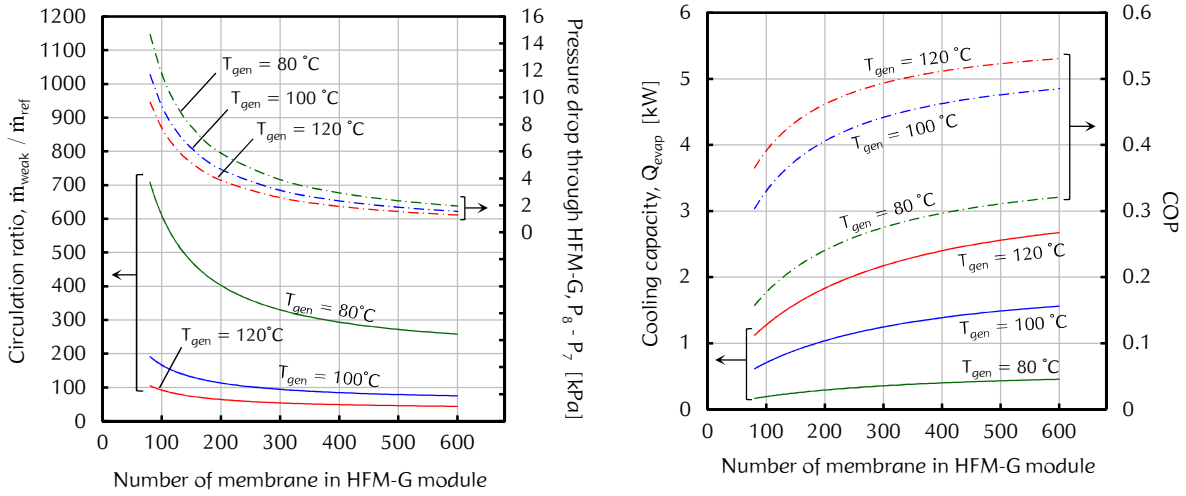

Fig. 4-17. Effect of the number of membranes on the circulation ratio and pressure drop through the HFM-G for different generating temperatures ($\dot{m}_{weak}$ = 0.05 kg/s, x_{weak} = 56.41 %, $T_{cool,in}$ = 30 °C, β = 0)

Fig. 4-18. Effect of the number of membranes on the cooling capacity and COP for different generating temperatures ($\dot{m}_{weak}$ = 0.05 kg/s, x_{weak} = 56.41 %, $T_{cool,in}$ = 30 °C, β = 0)

4.3.1.6. Effect of recirculation ratio on system performance

Fig. 4-19 and 20 show how the recirculation ratio affects the system performance. The recirculation ratio is basically used due to two aspects: (a) the re-utilization of feed solution which still has a potential to be evaporated, and (b) the increase in feed solution flow rate to maximize the sensible energy for the adiabatic desorption process. Thus, as shown in Fig. 4-19, the difference in solution concentration increases as the recirculation ratio increases, and therefore, the absorber capacity increases because the amount of water vapor being absorbed increases. At the higher generating temperature, the rate of change of the concentration difference increases. For instance, the concentration difference at a recirculation ratio of 9.0 at a generating temperature of 120 °C is approximately thrice that when the system operates without recirculation. The recirculation enables to achieve a certain decrease in the generating temperature for the given rate of heat load in the waste-heat heat exchanger. This is because a large amount of strong solution, which is at a much higher temperature than the weak solution from the absorber, is directly mixed with the weak solution. The COP of the HFM-G based VARs reaches that of the conventional cycle by the recirculation process of strong solution emerged from the HFM-G, as shown in Fig. 4-20. The strong solution from the HFM-G was directly recirculated into the waste-heat heat exchanger by the recirculation pump. The recirculated strong solution, which did not

pass the solution heat exchanger, was at a sufficiently high temperature to diminish the heating load to attain the required generating temperature. Hence, the required heat input becomes less. Thus, by increasing the recirculation ratio, both the cooling capacity and the COP increases to values as high as those in the case of the conventional cycle as shown in Table 4-5.

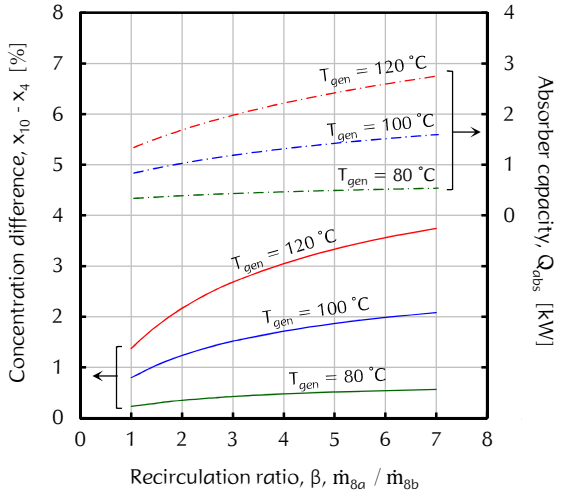

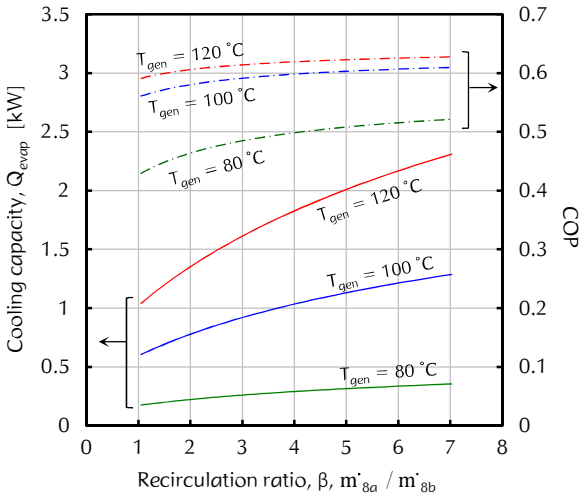

Fig. 4-19. Effect of recirculation ratio on the concentration difference of the absorber and absorber capacity for different generating temperatures ($\dot{m}_{weak}$ = 0.01 kg/s, $T_{cool,in}$ = 30 °C, EA = 200)

Fig. 4-20. Effect of recirculation ratio on the cooling capacity and COP for different generating temperatures ($\dot{m}_{weak}$ = 0.01 kg/s, $T_{cool,in}$ = 30 °C, EA = 200)

4.3.1.7. Effect of variation in both feed temperature and mass flow rate on adiabatic desorption heat and mass transfer

Fig. 4-21 and 22 give the influence of simultaneous changes in both the feed solution temperature and mass flow rate on the HFM desorption heat and mass transfer characteristics. As depicted Fig. 4-13, the concentration difference between the inlet and outlet of the HFM-G decreases with the increase in mass flow rate of the feed since the sensible energy associated with the feed flow rate is not entirely used for the given membrane parameter; however, the total desorption mass flux (i.e., the rate of mass flow rate per unit area) increases due to the larger sensible energy input. The feed solution temperature exponentially accelerates the HFM desorption mass flux as well, leading to the fact that the feed temperature is highly dominant on the adiabatic HFM desorption process. As shown in Fig. 4-22, the temperature difference between the inlet and outlet increases with the increase in the feed solution since the desorption mass transfer increases (i.e., much more sensible heat is used for the latent heat of vaporization). A

lower mass flow rate of the feed causes a higher temperature drop through the adiabatic desorption process because the lower energy input tends to be easily used up during the process.

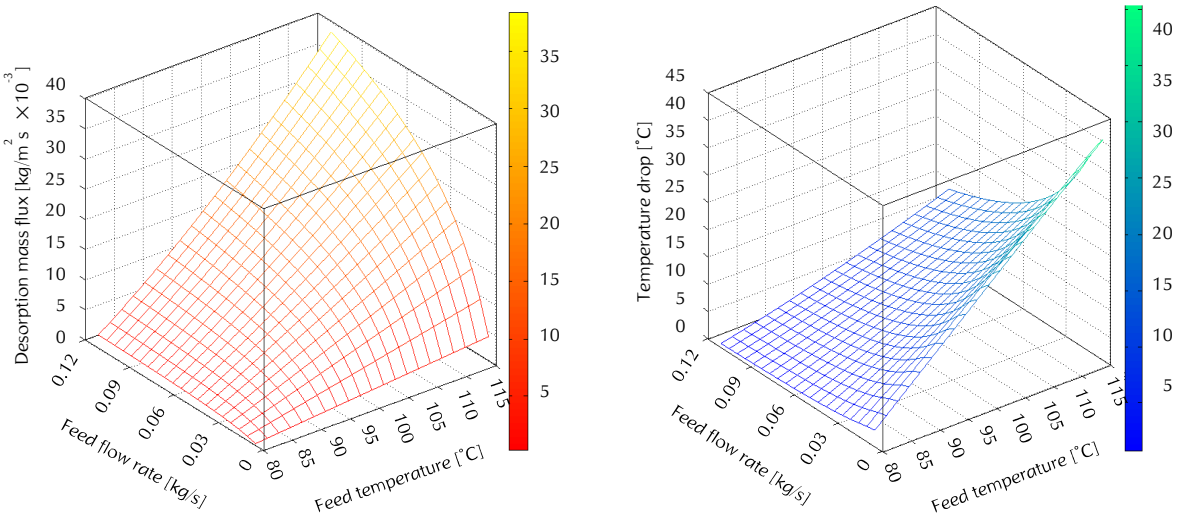

Fig. 4-21. Mass flux via HFM adiabatic desorption with respect to both the temperature and the mass flow rate of feed LiBr solution

Fig. 4-22. Temperature drop via HFM adiabatic desorption with respect to both the temperature and the mass flow rate of feed LiBr solution

4.3.1.8. Effect of variation in both length and number of hollow fiber membranes on adiabatic desorption heat and mass transfer

Fig. 4-23, 24 and 25 present the effect of concurrent variations in the dimension of the HFM-G (i.e., the length and number of the HFMs) on the HFM desorption heat and mass transfer performance. As shown in Fig. 4-23, the increases in both the number and length of the HFMs enhance the concentration difference; however, the rate of increase in concentration difference becomes almost flat and hardly increases. The change in the number of the HFMs is associated with the solution velocity, and the change in length of the HFMs is directly related to the decrease in the driving force in the flowing direction. That is, with larger dimension of the HFM-G, the driving force of mass transport drastically decreases in the flowing direction as the solution temperature relatively easily decreases by the adiabatic desorption process; as a result, a certain HFM could have a certain maximum concentration difference no matter how the dimension of the HFM-G keeps increasing. The desorption mass flux across HFMs decreases with the increases in both the number and length of the HFMs, as shown in Fig. 4-24. Note that the sensible heat

input to the HFM-G provides the energy for the adiabatic desorption process. The sensible heat is used up by the adiabatic desorption process in the capillaries of HFMs as the dimension of the HFM-G increases, which means that the desorption process no longer occurs at a certain point in the HFMs due to the extremely low driving force. As a result, the efficiency of mass flux across the HFMs decreases with the larger dimension of the HFM-G. The solution temperature drop by the HFM desorption in terms of the dimension of the HFM-G has a similar variation trend with the case of the concentration difference, associated with the velocity of the feed solution (Fig 4-25). The increases in dimensions of the HFMs tend to have more potential for the desorption for the given operating conditions and therefore, the input sensible energy tends to be used more for the adiabatic desorption process, leading to the larger temperature drop. The simulation results of the thermodynamic properties at each state point of the cycle are listed in Table 4-6.

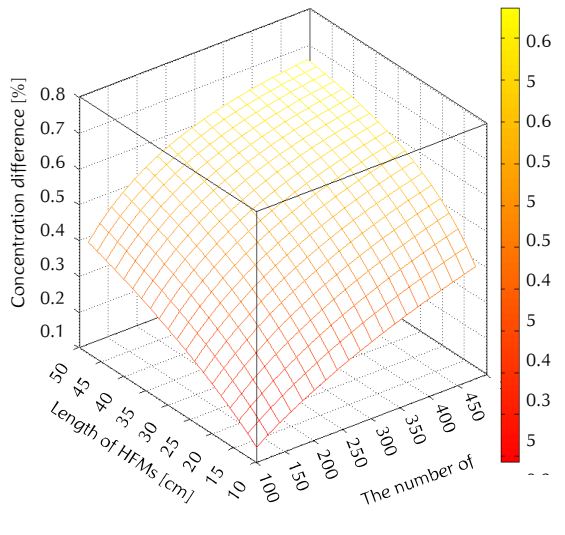

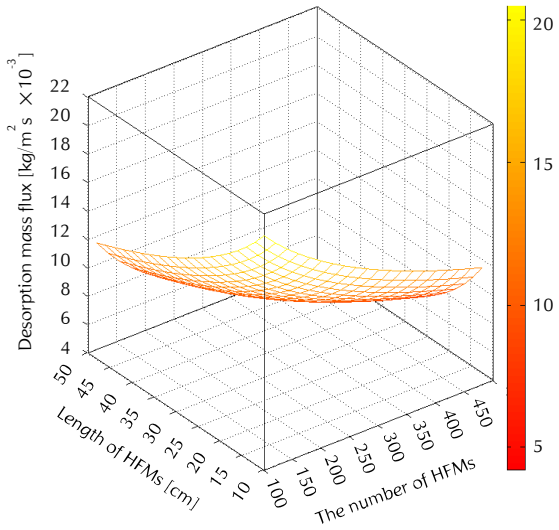

Fig. 4-23. Concentration difference between the inlet and outlet of HFM-G with respect to both the length and the number of HFMs

Fig. 4-24. Mass flux via HFM adiabatic desorption with respect to both the length and the number of HFMs

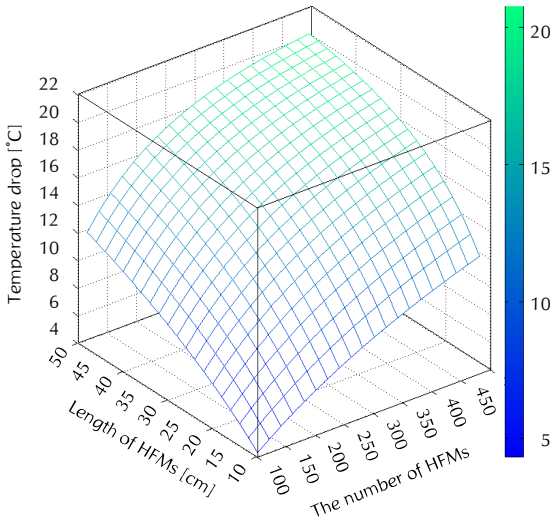

Fig. 4-25. Temperature drop via HFM adiabatic desorption with respect to both the length and the number of HFMs

Table 4-5. COP comparison data for the conventional LiBr-water singly-effect VARs and the HFM-G based VARs

Reference	Generating Temperature [°C]	Evaporation Temperature [°C]	Cooling Capacity [kW]	Effectiveness of Solution H/E	COP	Study
Horuz (1998)	55 - 110	10	N/A	N/A	0.75 - 0.80	Numerical
Joudi et al. (2001)	75 - 95	8	N/A	0.85	0.52 - 0.68	Numerical
Kilic et al. (2007)	85 - 103	8	10.0	0.70	0.62 - 0.76	Numerical
Kaynakli et al. (2007)	66 - 86	6	N/A	0.80	0.55 - 0.74	Numerical
Gomri (2009)	75 - 110	10	300.0	0.70	0.63 - 0.78	Numerical
Karamangil et al. (2010)	76 - 100	5	N/A	0.80	0.42 - 0.79	Numerical
Florides et al. (2003)	65 - 15	6	10	N/A	0.62 - 0.83	Experimental
Aphornratana et al. (2007)	65 - 85	5	up to 1.344	N/A	0.33 -0.52	Experimental
Gordon and Kim (1995)	75 - 90	11.4	up to 3.58	N/A	0.38 - 0.60	Experimental
HFM-G based VARs	75 - 120	6	up to 2.88	0.80	0.25 - 0.63	Numerical

Table 4-6. Thermodynamic state of the cycle (T_{gen} = 120 °C, T_{evap} = 6 °C, $T_{cool,in}$ = 30 °C, $\dot{m}_{weak}$ = 0.05 kg/s, β = 0)

State	T [°C]	P [kPa]	h [kJ/kg]	$\dot{m}$ [kg/s]	x [%]
1	39.6	7.196	2572.1	0.0002304	
2	39.6	7.196	175.3	0.0002304	
3	6.0	0.965	2511.2	0.0002304	
4	38.0	0.965	95.8	0.010	56.4071
5	38.0	adjustable	95.8	0.010	56.4071
6	70.5	adjustable	161.2	0.010	56.4071
7	120.0	adjustable	261.6	0.010	56.4071
8	80.2	adjustable	184.7	0.009796	57.7375
9	46.4	adjustable	117.7	0.009796	57.7375
10	46.4	0.965	117.7	0.009796	57.7
$T_{cool,\ inter}$	35.0	N/A	146.5	0.037	
$T_{cool,\ out}$	39.5	N/A	162.8	0.037	

4.3.2. Transient experimental results

4.3.2.1. Effect of feed solution temperature on heat and mass transfer

Fig. 4-26 presents the experimental desorption mass flux of the water vapor regarding the feed solution temperature for several feed concentrations. An increase in the feed solution temperature led to an increase in the mass flux due to the exponential increase in the vapor pressure, which is dependent on temperature, i.e., the Antoine equation [Thomson (1946)]. For example, the desorption mass flux was enhanced by approximately 2.7, 3.2, 3.9, and 5.8 times for the solution concentrations of 51, 52, 53, and 54 %, respectively, as the solution temperature was increased from approximately 65 to 82 ºC. The lower feed concentration also caused a higher desorption mass flux due to the lower vapor pressure of the solution. For example, in the case with a solution temperature of 82 ºC, the mass flux increased by approximately 2.3 times, while the solution concentration varied from 57 to 51 %. This is because the vapor pressure of the solution increases from approximately 8.1 to 13.8 kPa under the above case, and as a result, the difference in the driving force of the mass transport results in approximately 2.6 times the designated condenser pressure. Fig. 4.27 depicts the temperature drops through the adiabatic desorption process for several conditions. The sensible heat is supplied as latent heat to evaporate the water vapor at the liquid-vapor interface, and thus, a significant temperature drop takes place in the flow direction. Because the higher feed temperature and the lower feed concentration gave rise to a higher mass flux, the temperature drops became larger over the entire concentration range. This is due to the use of more sensible energy for the latent heat of vaporization for higher feed temperatures and lower concentrations. It was observed that for a concentration of 51 %, the feed solution temperature increased from approximately 65 to 82 ºC, as the temperature drop was varied from 7.8 to 22.4 ºC.

4.3.2.2. Effect of feed solution mass flux on heat and mass transfer

As shown in Fig. 4-28, the desorption mass flux is enhanced by a larger mass flux of the feed solution. A higher feed solution mass flux generates a higher value for the temperature polarization coefficient, for which the temperature difference between the bulk and membrane surface (i.e., the heat transfer resistance in the thermal boundary layer) becomes smaller. Note that the rate of increase in the mass flux was reduced with an increase in the feed solution flux.

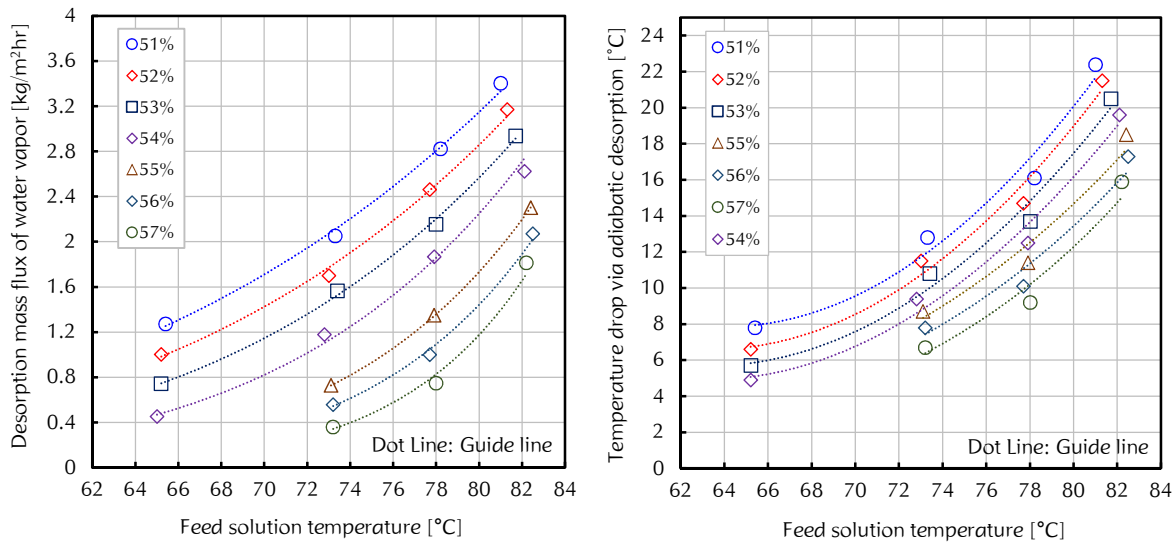

Fig. 4-26. Experimental HFM desorption mass flux of water vapor with feed solution temperature for several feed concentrations ($\dot{m}_{feed}$ = 152.9 kg/m^{2}s, P_{cond} = 4.7 ±0.3 kPa)

Fig. 4-27. Experimental temperature drop by the HFM adiabatic desorption with feed solution temperature for several feed concentrations ($\dot{m}_{feed}$ = 152.9 kg/m^{2}s, P_{cond} = 4.7 ±0.3 kPa)

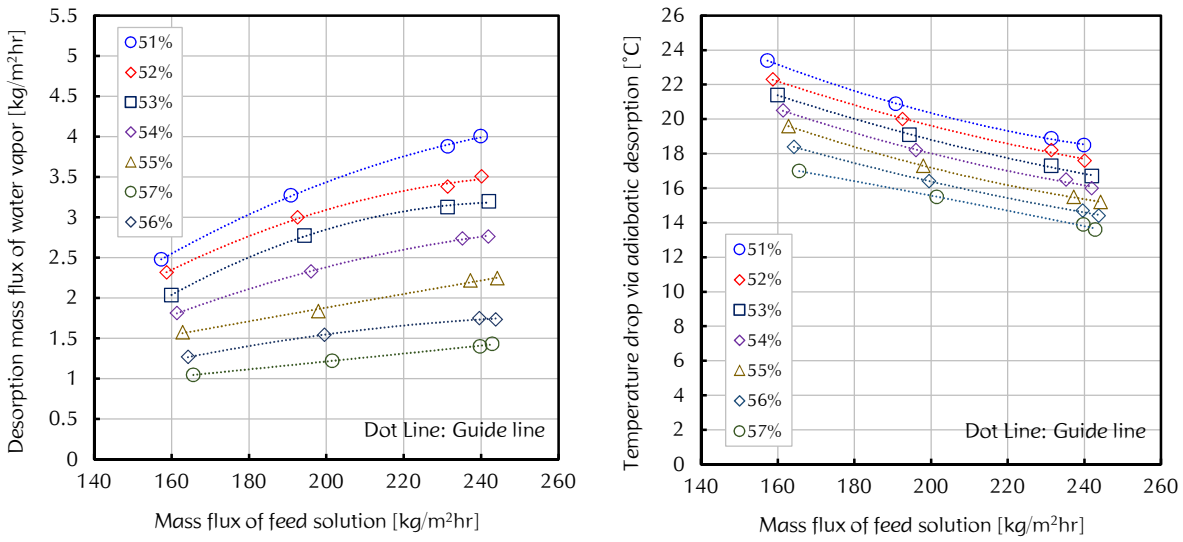

Fig. 4-28. Experimental HFM desorption mass flux of water vapor with mass flux of feed solution for several feed concentrations (T_{feed} = 80 °C, P_{cond} = 4.7 ±0.3 kPa)

Fig. 4-29. Experimental temperature drop by the HFM adiabatic desorption with mass flux of feed solution for several feed concentrations (T_{feed} = 80 °C, P_{cond} = 4.7 ±0.3 kPa)

This means that the enhancement of input energy is not exactly proportional to the mass flux performance because the larger sensible energy is not entirely used in the adiabatic desorption process for given membrane parameters. The desorption mass flux was enhanced from approximately 2.5 to 4 kg/ m^2h as the mass flux of the feed solution increases from 157.3 to 239.8 kg/m^2 s for a 51 % concentration of the feed solution. As shown in Fig. 4-29, the temperature drop via the desorption process decreases with an increase in the mass flux of feed solution. The explanation for this is that not all of the sensible input energy was used for the evaporation of the water vapor as the feed solution flux increased. For the solution concentration of 51 %, for instance, the solution temperature dropped by 23.4 ºC for a feed mass flux of 157.3 kg/m^2s, and a temperature drop of 18.5 ºC was found for a feed mass flux of 239.8 kg/m^2s.

4.3.2.3. Effect of condenser pressure on heat and mass transfer

The cooling water temperature is one of the significant factor influencing the cooling capacity and COP as shown in Fig. 4-16. Especially in summer, the cooling water temperature in the vehicle tends to be high, resulting in the higher condenser pressure. The effect of the condenser pressure on the mass flux performance is shown in Fig. 4-30. The condenser pressure is directly related to the driving force of the desorption mass flux, and as a result, the enhancement of desorption was found with a decrease in the condenser pressure. The feed solution concentration also inversely influences the mass flux. The temperature drop decreases with higher condenser pressures due to the lower mass flux performance, as shown in Fig. 4-31.

4.3.2.4. Pressure drop via hollow fiber membrane-based generator

The pressure drop of the LiBr solution via the HFM-G used in this study is shown in Fig. 4-32. It was found that the pressure drop linearly increases with an increase in the solution velocity. The solution concentration also influences the solution pressure drop through the HFMs mainly due to the change in density and viscosity of the solution. The calculation values by the Darcy friction pressure drop, considering the change of the thermodynamic properties in the flow direction, is also shown in Fig. 4-32. It is noteworthy that the pressure drop resists the flow of the solution through the HFMs, and thus, a larger solution pressure is mandatory against the larger pressure drop; however, the HFM is wet (i.e., the liquid phase of the solution is permeated into the pores) if the solution pressure becomes higher than the breakthrough pressure. Furthermore,

to prevent the significant pressure drop by the phase change of the solution during the preheating process, the solution pressure must be larger than the static equilibrium pressure. As a result, considering the breakthrough pressure and phase change, the pressure drop is an essential factor to avoid malfunction during the desorption process in the HFM-G.

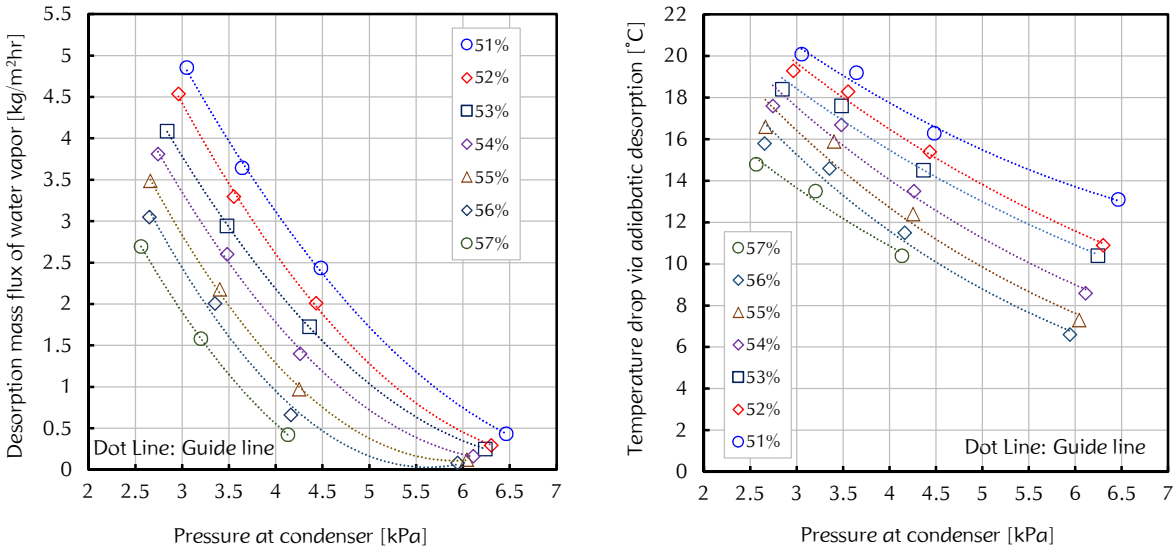

Fig. 4-30. Experimental HFM desorption mass flux of water vapor with pressure at the condenser for several feed concentrations (T_{feed} = 80 °C, $\dot{m}_{feed}$ = 183.6 kg/m^{2}s)

Fig. 4-31. Experimental temperature drop by the HFM adiabatic desorption with pressure at the condenser for several feed concentrations (T_{feed} = 80 °C, $\dot{m}_{feed}$ = 183.6 kg/m^{2}s)

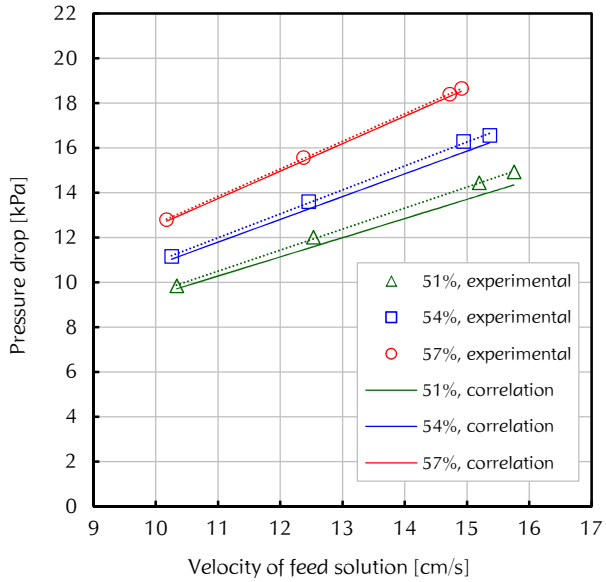

Fig. 4-32. Pressure drop of solution via HFM with solution velocity in hollow fiber membrane (T_{feed} = 80 °C, P_{cond} = 2.4 kPa)

4.3.2.5. Comparison of experimental heat and mass transfer with theoretical results

All of the initial experimental conditions influencing the heat and mass transfer, such as feed solution temperature, concentration, mass flow rate, and condenser pressure, were collected during the series of experiments. The obtained data were used as initial operating conditions to conduct the theoretical simulation process, as introduced in the preliminary work. The theoretical heat and mass transfer model using the estimated nominal pore size showed relatively high accuracy when compared with the experimental desorption mass flux under high feed solution temperature conditions; however, the error became more significant with increasing the feed solution concentration, as shown in Fig. 4-33. Under relatively low feed solution temperatures, the model successfully effectively predicted the mass transfer performance, though the error became more severe as the feed concentration increased. This is due to experimental uncertainty causing data reduction errors under meager driving forces, i.e., both low feed solution temperature and high solution concentration. The experimental temperature drop via the adiabatic desorption process was also compared with the simulated results, as shown in Fig. 4-34.

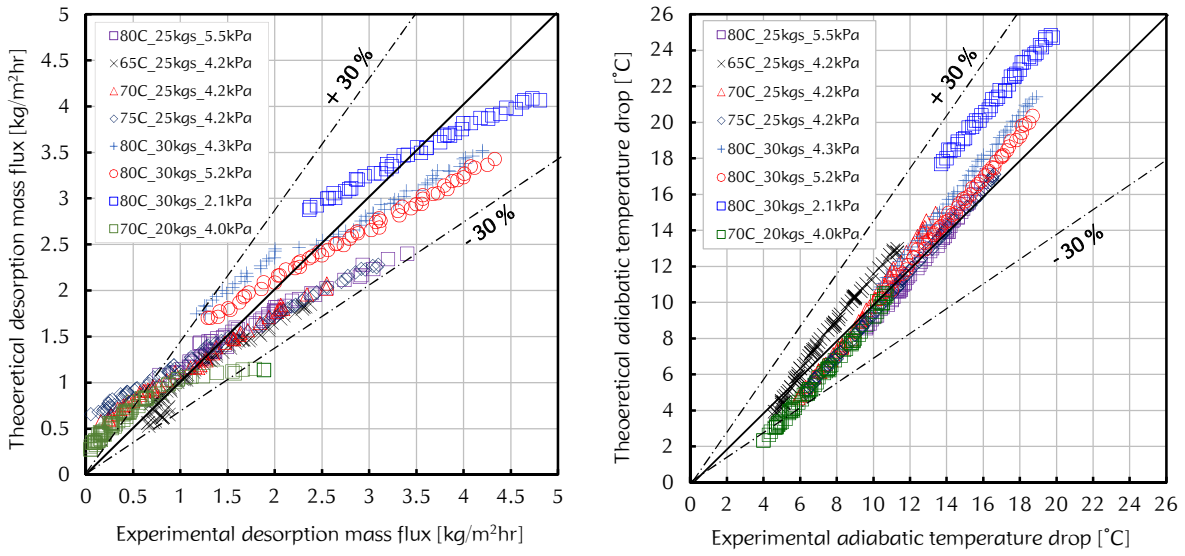

Fig. 4-33. Comparison of experimental mass flux of water vapor desorption with theoretical simulation results (x_{feed} = 51 to 58 %)

Fig. 4-34. Comparison of experimental temperature drop via adiabatic desorption process with theoretical simulation results (x_{feed} = 51 to 58 %)

5

Hollow fiber membrane-based solution mass exchanger

This chapter 5 presents two types of hollow fiber membrane-based solution mass exchangers (HFM-SME). Mass recovery process is emphasized by understanding the simultaneous heat and mass transfer. The characteristics of the mass recovery process, which is a form of the traditional HFM module (named "traditional HFM-SME"), are clarified regarding the flow direction of the solutions. The improved type of the HFM-SME (named "new type of HFM-SME) is also suggested with the theoretical analysis as an alternative to the traditional HFM-SME to achieve maximized mass recovery performance.

Not available due to patent pending

6

Conclusion, and future work

Chapter 6 is finalized with the conclusion by summarizing research contribution and discussion of the perspective work directions. The iso-thermal type of HFM-based heat and mass exchangers are designed for the future works. It is expected that the proposed iso-thermal types make up for shortcomings that the adiabatic HFM-based heat and mass exchangers have shown.

Not available due to patent pending

INDEX

Nomenclature

A	area [m^2]
B_m	membrane distillation coefficient [kg m^{-2} s^{-1} Pa^{-1}]
C_m	permeability coefficient of membrane [kg m^{-1} s^{-1} Pa^{-1}]
D_h	hydraulic diameter [m]
D_k	Knudsen diffusion coefficient [m^2 s^{-1}]
d	diameter of hollow fiber membrane [m]
dp	pressure drop [Pa]
d_p	membrane pore size [m]
d_{wv}	molecular size of water vapor
dx	single element of HFM
ΔH_v	latent heat of vaporization [J kg^{-1}]
Δp_b	breakthrough pressure [Pa]
$\Delta\pi$	osmosis pressure [Pa]
EA	number of hollow fiber membranes
f_D	Darcy friction factor
G	mass flux [kg m^{-2} s^{-1}]
h	specific enthalpy [J kg^{-1}]
h_f	convective heat transfer coefficient of feed solution [W m^{-2}]
h_l	convective heat transfer coefficient of lumen side [W m^{-2}]
h_s	convective heat transfer coefficient of lumen side [W m^{-2}]
HFM	hollow fiber membrane
J_v	mass flux across the membrane [kg m^{-2} s^{-1}]
k_B	Boltzmann constant [J K^{-1}]
k	thermal conductivity [W m^{-1}]
K_n	Knudsen number
l	length of hollow fiber membrane [m]
M	molecular weight [kg mol^{-1}]
M_c	molar concentration [mol $liter^{-1}$]
$\dot{m}$	mass flow rate [kg s^{-1}]
n	number of hollow fiber membranes
Nu	Nusselt number

p	pressure [Pa]
Pr	Prandtl number
p_v	vapor pressure [Pa]
$\dot{Q}$	heat flux [W m^{-2}]
R	gas constant [m^3 Pa K^{-1} mol^{-1}]
Re	Reynolds number
r_p	radius of membrane pore [m]
T	Temperature [K]
u	velocity [m/s]
U	overall heat transfer coefficient [W $m^{-2}K^{-1}$]
x	concentration of LiBr solution [%]

Greek symbols

α	convective mass transfer coefficient [m s^{-1}]
β	recirculation ratio
τ	membrane tortuosity
δ	membrane thickness [m]
ρ	Density [kg m^{-3}]
ε	membrane porosity
σ	surface tension [N m^{-1}]
θ	contact angle [°]
λ	mean free path

Subscripts

ass	assumed
abs	absorption
b	bulk
cal	calculated
cond	condenser
cool	cooling water
d	dew point
des	desorption
f	feed
flux	flux

g	gas
h	hot
LiBr	lithium bromide solution
lumen	lumen side
i	inner
in	inlet
m	membrane, or mean
ms	membrane surface
mt	material
N_2	nitrogen gas
o	outer
out	outlet
p	pore, or permeate
sol	solution
strong	strong solution
v	vapor
weak	weak solution
w	water, or warm
wv	water vapor

REFERENCE

Abbasgholipourghadim, MOHAMMAD, and M. Malilah. "Porosity and pore area determination of hollow fiber membrane incorporating digital image processing." Recent Advances in Mechanics and Mechanical Engineering (2015): 118-123.

Alkhudhiri, Abdullah, Naif Darwish, and Nidal Hilal. "Membrane distillation: a comprehensive review." Desalination 287 (2012): 2-18.

Ali, Ahmed Hamza H., and Peter Schwerdt. "Characteristics of the membrane utilized in a compact absorber for lithium bromide–water absorption chillers." International journal of refrigeration 32.8 (2009): 1886-1896.

Alsaadi, Ahmad S., et al. "Experimental and theoretical analyses of temperature polarization effect in vacuum membrane distillation." Journal of Membrane Science 471 (2014): 138-148.

Aphornratana S. and Sriveerakul T. "Experimental studies of a single-effect absorption refrigerator using aqueous lithium–bromide: effect of operating condition to system performance." Experimental Thermal and Fluid Science 32.2 (2007): 658-669.

Asfand, F., & Bourouis, M. (2015). A review of membrane contactors applied in absorption refrigeration systems. Renewable and Sustainable Energy Reviews, 45, 173-191.

Asfand, Faisal, Youssef Stiriba, and Mahmoud Bourouis. "Impact of the solution channel thickness while investigating the effect of membrane characteristics and operating conditions on the performance of water-LiBr membrane-based absorbers." Applied Thermal Engineering 108 (2016): 866-877.

Baker, Richard W. Membrane technology. John Wiley & Sons, Inc., 2000.

Banat, Fawzi A., et al. "Modeling of desalination using tubular direct contact membrane distillation modules." Separation science and technology 34.11 (1999): 2191-2206.

Banat, Fawzi A., and Jana Simandl. "Removal of benzene traces from contaminated water by vacuum membrane distillation." Chemical Engineering Science 51.8 (1996): 1257-1265.

Bandini, Serena, C. Gostoli, and G. C. Sarti. "Separation efficiency in vacuum membrane distillation." Journal of Membrane Science 73.2-3 (1992): 217-229.

Benzeguir, Bachir, Frederick Setterwall, and H. Uddholm. "Use of a wave model to evaluate falling film absorber efficiency." International journal of refrigeration 14.5 (1991): 292-296.

Brown, Philip S., and Bharat Bhushan. "Durable, superoleophobic polymer–nanoparticle composite surfaces with re-entrant geometry via solvent-induced phase transformation." Scientific reports 6 (2016): 21048.

Bui, V. A., Lin TT Vu, and Minh H. Nguyen. "Modelling the simultaneous heat and mass transfer of direct contact membrane distillation in hollow fibre modules." Journal of Membrane Science353.1 (2010): 85-93.

Busch, Jan, Andreas Cruse, and Wolfgang Marquardt. "Modeling submerged hollow-fiber membrane filtration for wastewater treatment." Journal of Membrane Science 288.1 (2007): 94-111.

Calabro, Vincenza, Enrico Drioli, and Filippo Matera. "Membrane distillation in the textile wastewater treatment." Desalination 83.1-3 (1991): 209-224.

Chakrabarty, B., A. K. Ghoshal, and M. K. Purkait. "SEM analysis and gas permeability test to characterize polysulfone membrane prepared with polyethylene glycol as additive." Journal of colloid and interface science 320.1 (2008): 245-253.

Ghanbarian, Behzad, et al. "Tortuosity in porous media: a critical review." Soil science society of America journal 77.5 (2013): 1461-1477.

Chen, Junghui, Hsuan Chang, and Siang-Ru Chen. "Simulation study of a hybrid absorber–heat exchanger using hollow fiber membrane module for the ammonia–water absorption cycle." International journal of refrigeration 29.6 (2006):

1043-1052.

Chiam, Chel-Ken, and Rosalam Sarbatly. "Heat transfer in the rectangular cross-flow flat-sheet membrane module for vacuum membrane distillation." Chemical Engineering and Processing: Process Intensification 79 (2014): 23-33.

Gordon, J. M., and Kim Choon Ng. "A general thermodynamic model for absorption chillers: theory and experiment." Heat Recovery Systems and CHP 15.1 (1995): 73-83.

Criscuoli, A., M. C. Carnevale, and E. Drioli. "Modeling the performance of flat and capillary membrane modules in vacuum membrane distillation." Journal of membrane science 447 (2013): 369-375.

Daiguji, H., E. Hihara, and T. Saito. "Mechanism of absorption enhancement by surfactant." International journal of heat and mass transfer 40.8 (1997): 1743-1752.

De Barros, S. T. D., et al. "Study of fouling mechanism in pineapple juice clarification by ultrafiltration." Journal of Membrane Science 215.1 (2003): 213-224.

Determan, Matthew D., and Srinivas Garimella. "Ammonia–water desorption heat and mass transfer in microchannel devices." international journal of refrigeration 34.5 (2011): 1197-1208.

DiGuilio, R. M., et al. "Properties of lithium bromide–water solutions at high temperatures and concentrations–I. Thermal conductivity." ASHRAE Trans 96.1 (1990): 702-708.

Dullien, Francis AL. Porous media: fluid transport and pore structure. Academic press, 2012.

Fan, Hongwei, and Yuelian Peng. "Application of PVDF membranes in desalination and comparison of the VMD and DCMD processes." Chemical engineering science 79 (2012): 94-102.

Florides, G. A. et al. "Design and construction of a LiBr–water absorption machine." Energy Conversion and Management 44.15 (2003): 2483-2508.

Garimella, S. "Miniaturized heat and mass transfer technology for absorption heat pumps." Proceedings of the International Sorption Heat Pump Conference, Munich, Germany. 1999.

Garimella, S et al. "Microchannel component technology for system-wide application in ammonia/water absorption heat pumps." international journal of refrigeration 34.5 (2011): 1184-1196.

Glebov, Dmitrey, and Fredrik Setterwall. "Experimental study of heat transfer additive influence on the absorption chiller performance." International journal of refrigeration 25.5 (2002): 538-545.

Goel, Nitin, and D. Yogi Goswami. "A compact falling film absorber." Journal of Heat Transfer 127.9 (2005): 957-965.

Goel, Nitin, and D. Yogi Goswami. "Experimental Verification of a New Heat and Mass Transfer Enhancement Concept in a Microchannel Falling Film Absorber." Journal of Heat Transfer 129.2 (2007): 154-161.

Gomri, Rabah. "Second law comparison of single effect and double effect vapour absorption refrigeration systems." Energy Conversion and Management 50.5 (2009): 1279-1287.

Gomri, Rabah. "Investigation of the potential of application of single effect and multiple effect absorption cooling systems." Energy Conversion and Management 51.8 (2010): 1629-1636.

Hernández, A. C. J. I., et al. "Pore size distributions in microporous membranes. A critical analysis of the bubble point extended method." Journal of Membrane Science 112.1 (1996): 1-12.

Hihara, Eiji, and Takamoto Saito. "Effect of surfactant on falling film absorption." International journal of refrigeration 16.5 (1993): 339-346.

Hong, Sung Joo, Eiji Hihara, and Chaobin Dang. "Novel absorption refrigeration system with a hollow fiber membrane-based generator." International Journal of Refrigeration 67 (2016): 418-432.

Hong, Sung Joo, Eiji Hihara, and Chaobin Dang. "Simulation and optimization on hollow fiber membrane based solution heat exchanger in vapor absorption refrigeration system." Proceedings of the 8th Asian Conference on Refrigeration and Air Conditioning (2016)

Horuz, I. "A comparison between ammonia-water

and water-lithium bromide solutions in vapor absorption refrigeration systems." International communications in heat and mass transfer25.5 (1998): 711-721.

Horuz, I. "Vapor absorption refrigeration in road transport vehicles." Journal of Energy Engineering 125.2 (1999): 48-58.

Hozawa, Mitsunori, et al. "Marangoni convection during steam absorption into aqueous LiBr solution with surfactant." Journal of chemical engineering of Japan 24.2 (1991): 209-214.

Isfahani, Rasool Nasr, and Saeed Moghaddam. "Absorption characteristics of lithium bromide (LiBr) solution constrained by superhydrophobic nanofibrous structures." International Journal of Heat and Mass Transfer 63 (2013): 82-90.

Isfahani, Rasool Nasr, et al. "Physics of lithium bromide (LiBr) solution dewatering through vapor venting membranes." International Journal of Multiphase Flow 58 (2014): 27-38.

Ishida, Kenji, and Yasuhiko H. Mori. "Surface tension of aqueous lithium bromide solutions containing 1-octanol as a "heat-transfer additive"." International communications in heat and mass transfer 23.7 (1996): 907-915.Z.

Jeter, S. M., J. P. Moran, and A. S. Teja. "Properties of Lithium Bromide-Water solutions at High Temperatures and Concentrations–III: Specific Heat." ASHRAE Transactions 98 (1992).

Jin, Zhao, Shou Hai Zhang, and Xi Gao Jian. "Hydrophobic modification of poly (phthalazinone ether sulfone ketone) hollow fiber membrane for vacuum membrane distillation." Journal of Membrane Science 310.1 (2008): 20-27.

Joudi, Khalid A., and Ali H. Lafta. "Simulation of a simple absorption refrigeration system." Energy conversion and Management 42.13 (2001): 1575-1605.

Kaita, Y. "Thermodynamic properties of lithium bromide–water solutions at high temperatures." International Journal of Refrigeration 24.5 (2001): 374-390.

Karamangil, M. I., et al. "A simulation study of performance evaluation of single-stage absorption refrigeration system using conventional working fluids and alternatives." Renewable and Sustainable Energy Reviews 14.7 (2010): 1969-1978.

Kashiwagi, T., Y. Kurosaki, and H. Shishido. "Enhancement of vapor absorption into a solution using the Marangoni effect." Trans. JSME 51.463B (1985): 1002.

Kaushik, S. C., and Akhilesh Arora. "Energy and exergy analysis of single effect and series flow double effect water–lithium bromide absorption refrigeration systems." International journal of Refrigeration 32.6 (2009): 1247-1258.

Kaynakli, Omer, and Muhsin Kilic. "Theoretical study on the effect of operating conditions on performance of absorption refrigeration system." Energy Conversion and Management 48.2 (2007): 599-607.

Kazuo Yamamoto, Masami Hiasa, Talat Mahmood, Tomonori Matsuo, "Direct solid-liquid separation using hollow fiber membrane in an activated sludge aeration tank", Water Pollution Research and Control Brighton (1989) 43-54

Khayet, M., M. P. Godino, and J. I. Mengual. "Study of asymmetric polarization in direct contact membrane distillation." Separation science and technology 39.1 (2005): 125-147.

Khayet, Mohamed. "Membranes and theoretical modeling of membrane distillation: a review." Advances in colloid and interface science 164.1 (2011): 56-88.

Killion, J. D., & Garimella, S. (2004). Simulation of pendant droplets and falling films in horizontal tube absorbers. Transactions of the ASME-C-Journal of Heat Transfer, 126(6), 1003-1013.

Kilic, Muhsin, and Omer Kaynakli. "Second law-based thermodynamic analysis of water-lithium bromide absorption refrigeration system." Energy 32.8 (2007): 1505-1512.

Kim, D. S., and CA Infante Ferreira. "Analytic modelling of steady state single-effect absorption cycles." International Journal of Refrigeration 31.6 (2008): 1012-1020.

Kim, Jin-Kyeong, Chan Woo Park, and Yong Tae Kang. "The effect of micro-scale surface treatment on heat and mass transfer performance

for a falling film H 2 O/LiBr absorber." International journal of refrigeration 26.5 (2003): 575-585.

Kim, K. J., and V. P. Janule. "Dynamic surface tension of aqueous lithium bromide with 2-ethyl-1-hexanol." International communications in heat and mass transfer 21.6 (1994): 839-848.

Kim, Kwang J., Neil S. Berman, and Byard D. Wood. "Surface tension of aqueous lithium bromide+ 2-ethyl-1-hexanol." Journal of Chemical and Engineering Data 39.1 (1994): 122-124.

Kim, Yoon Jo, Yogendra K. Joshi, and Andrei G. Fedorov. "An absorption based miniature heat pump system for electronics cooling." International Journal of Refrigeration 31.1 (2008): 23-33.

Kimura, Shoji, Shin-Ichi Nakao, and Shun-Ichi Shimatani. "Transport phenomena in membrane distillation." Journal of Membrane Science 33.3 (1987): 285-298.

Kirk, D. E., M. W. Montgomery, and M. G. Kortekaas. "Clarification of pear juice by hollow fiber ultrafiltration." Journal of food science48.6 (1983): 1663-1667.

Koehler, J., et al. "Absorption refrigeration system for mobile applications utilizing exhaust gases." Heat and Mass Transfer 32.5 (1997): 333-340.

Kren, Ch, H. M. Hellmann, and F. Ziegler. "Dynamic surface tension of LiBr-solutions with higher alcohols as heat-transfer-additives." International Sorption Heat Pump Conference. 1999.

Kulankara, S., and K. E. Herold. "Surface tension of aqueous lithium bromide with heat/mass transfer enhancement additives: the effect of additive vapor transport." International journal of refrigeration 25.3 (2002): 383-389.

Laganà, Fortunato, Giuseppe Barbieri, and Enrico Drioli. "Direct contact membrane distillation: modelling and concentration experiments." Journal of Membrane Science 166.1 (2000): 1-11.

Lawson, Kevin W., and Douglas R. Lloyd. "Membrane distillation. I. Module design and performance evaluation using vacuum membrane distillation." Journal of membrane science 120.1 (1996): 111-121.

Lawson, Kevin W., and Douglas R. Lloyd. "Membrane distillation." Journal of membrane Science 124.1 (1997): 1-25.

Lee, Hanyong, et al. "Desalination with a cascade of cross-flow hollow fiber membrane distillation devices integrated with a heat exchanger." AIChE Journal 57.7 (2011): 1780-1795.

Lee, Jung-Gil, and Woo-Seung Kim. "Numerical modeling of the vacuum membrane distillation process." Desalination 331 (2013): 46-55.

Lee, Kuan-Chun, and Bruce E. Rittmann. "Applying a novel autohydrogenotrophic hollow-fiber membrane biofilm reactor for denitrification of drinking water." Water Research 36.8 (2002): 2040-2052.

Lee, R. J., et al. "Properties of lithium bromide-water solutions at high temperatures and concentrations-II: Density and Viscosity." ASHRAE Trans 96.1 (1990): 709-728.

Lenard, J. L. Y. et al. "Properties of lithium bromide-water solutions at high temperatures and concentrations-part IV: vapor pressure." ASHRAE Trans 98.1 (1992): 167-172.

Li, Baoan, and Kamalesh K. Sirkar. "Novel membrane and device for vacuum membrane distillation-based desalination process." Journal of Membrane Science 257.1 (2005): 60-75.

Li, Jian-Mei, et al. "Microporous polypropylene and polyethylene hollow fiber membranes. Part 3. Experimental studies on membrane distillation for desalination." Desalination 155.2 (2003): 153-156.

Li, Jing-Liang and Bing-Hung Chen. "Review of CO2 absorption using chemical solvents in hollow fiber membrane contactors." Separation and Purification Technology. 41.2 (2005): 109-122.

Lovineh, Shirin Gh, Morteza Asghari, and Bita Rajaei. "Numerical simulation and theoretical study on simultaneous effects of operating pa-

rameters in vacuum membrane distillation." Desalination 314 (2013): 59-66.

Manzela, André Aleixo, et al. "Using engine exhaust gas as energy source for an absorption refrigeration system." Applied energy 87.4 (2010): 1141-1148.

Martınez-Dıez, L., M. I. Vazquez-Gonzalez, and F. J. Florido-Dıaz. "Study of membrane distillation using channel spacers." Journal of Membrane Science 144.1 (1998): 45-56.

Martínez-Díez, L., and Mi I. Vazquez-Gonzalez. "Temperature and concentration polarization in membrane distillation of aqueous salt solutions." Journal of membrane science 156.2 (1999): 265-273.

Martınez, L., et al. "Characterisation of three hydrophobic porous membranes used in membrane distillation: modelling and evaluation of their water vapour permeabilities." Journal of membrane science 203.1 (2002): 15-27.

Maskell, W. C. "Tortuosity Factor in Non-Homogeneous Membranes." Berichte der Bunsengesellschaft für physikalische Chemie 97.5 (1993): 680-683.

Matyka, Maciej, Arzhang Khalili, and Zbigniew Koza. "Tortuosity-porosity relation in porous media flow." Physical Review E 78.2 (2008): 026306.

McNeely, L.A. "Thermodynamic properties of aqueous-solutions of lithium bromide." ASHRAE JOURNAL-AMERICAN SOCIETY OF HEATING REFRIGERATING AND AIR-CONDITIONING ENGINEERS. Vol. 20. No. 12. 1791 TULLIE CIRCLE NE, ATLANTA, GA 30329: AMER SOC HEAT REFRIG AIR-CONDITIONING ENG INC, 1978.

Meacham, J. M., and S. Garimella. "Ammonia-Water Absorption Heat and Mass Transfer in Microchannel Absorbers with Visual Confirmation." ASHRAE Transactions 110.1 (2004).

Meacham, J. M., and S. Garimella. "Experimental demonstration of a prototype microchannel absorber for space-conditioning systems." International Sorption Heat Pump Conference, Shanghai, China. 2002.

Meacham, J. M., and S. Garimella. "Modeling of local measured heat and mass transfer variations in a microchannel ammonia-water absorber." TRANSACTIONS-AMERICAN SOCIETY OF HEATING REFRIGERATING AND AIR CONDITIONING ENGINEERS 109.1 (2003): 412-422.

Mengual, J. I., M. Khayet, and M. P. Godino. "Heat and mass transfer in vacuum membrane distillation." International Journal of Heat and Mass Transfer 47.4 (2004): 865-875.

Mohamed Bentrcia, Mohamed Alshatewi and Hanafy Omar, 'Developments of vapor-compression systems for vehicle air-conditioning: A review', Advances in Mechanical Engineering 9(8) (2017) 1-15

Naidu G. et al., "Experiments and modeling of a vacuum membrane distillation for high saline water", Journal of Industrial and Engineering Chemistry 20 (2014) 2174–2183

Nakatsuka, Shuji, Ichiro Nakate, and Tadaaki Miyano. "Drinking water treatment by using ultrafiltration hollow fiber membranes." Desalination 106.1-3 (1996): 55-61.

Oleinik, S. V., Yu I. Kuznetsov, and A. R. Vartapetyan. "Corrosion inhibition of steel in lithium bromide brines." Protection of metals 39.1 (2003): 12-18.

Park, Chan Woo, Hyun Churl Cho, and Yong Tae Kang. "The effect of heat transfer additive and surface roughness of micro-scale hatched tubes on absorption performance." International journal of refrigeration 27.3 (2004): 264-270.

Patnaik, Vikas, H. Perez-Blanco, and W. A. Miller. An empirical methodology for the design of vertical-tube absorbers. No. CONF-9406105--. American Society of Heating, Refrigerating and Air-Conditioning Engineers, Inc., Atlanta, GA (United States), 1994.

Patterson, M. R., and H. Perez-Blanco. Numerical fits of the properties of lithium-bromide water solutions. No. CONF-880627-2. Oak Ridge National Lab., TN (USA), 1988.

Peña, Luis, M. Paz Godino, and Juan I. Mengual. "A method to evaluate the net membrane distillation coefficient." Journal of membrane science 143.1 (1998): 219-233.

Pongtorn kulpanich, A., et al. "Experience with fully

operational solar-driven 10-ton LiBr/H 2 O single-effect absorption cooling system in Thailand." Renewable Energy 33.5 (2008): 943-949.

Ramon, Guy, Yehuda Agnon, and Carlos Dosoretz. "Heat transfer in vacuum membrane distillation: Effect of velocity slip." Journal of Membrane Science 331.1 (2009): 117-125.

Riffat, S. B., S. Wu, and B. Bol. "Pervaporation membrane process for vapour absorption system." International journal of refrigeration 27.6 (2004): 604-611.

Rivera, W., and J. Cerezo. "Experimental study of the use of additives in the performance of a single-stage heat transformer operating with water–lithium bromide." International journal of energy research 29.2 (2005): 121-130.

Samanta, Indraneel. "JAVA software for LiBr-water absorption refrigeration system evaluation." (2003).

Sarti, G. C., C. Gostoli, and S. Bandini. "Extraction of organic components from aqueous streams by vacuum membrane distillation." Journal of Membrane Science 80.1 (1993): 21-33.

Schofield, R. W., A. G. Fane, and C. J. D. Fell. "Heat and mass transfer in membrane distillation." Journal of Membrane Science33.3 (1987): 299-313.

Schroeder, J. J., W. Sander-Beuermann, and P. Fast. "Optimization of heat transfer on vertically finned falling film evaporator surfaces." PROCEEDINGS OF THE 7 th INTERNATIONAL SYMPOSIUM ON FRESHWATER FROM THE SEA, 1980,. Vol. 1. 1980.

Şencan Arzu et al. "Exergy analysis of lithium bromide/water absorption systems." Renewable energy 30.5 (2005): 645-657.

Schaal, F., et al. "Membrane contactors for absorption refrigeration." Tenth Aachen Membrane Colloquium, Mar. 2005.

Sharlene A. McEvoy, 'A brave new world: The environmental and economic impact of autonomous cars', Modern Environmental Science and Engineering 1 (2015) 1-7

Shimizu, Yasutoshi, et al. "Filtration characteristics of hollow fiber microfiltration membranes used in membrane bioreactor for domestic wastewater treatment." Water Research 30.10 (1996): 2385-2392.

Smolders, K., and A. C. M. Franken. "Terminology for membrane distillation." Desalination 72.3 (1989): 249-262.

Taira, Naoki "疎水性膜を用いた小型吸収式冷凍機の研究" Master's thesis (2018) Department of Human and Engineered Environmental studies, The University of Tokyo

Talom, Hugues L., and Asfaw Beyene. "Heat recovery from automotive engine." Applied Thermal Engineering 29.2 (2009): 439-444.

Tomaszewska, M., M. Gryta, and A. W. Morawski. "Mass transfer of HCl and H 2 O across the hydrophobic membrane during membrane distillation." Journal of Membrane Science 166.2 (2000): 149-157.

Thomas, David G. "Enhancement of film condensation heat transfer rates on vertical tubes by vertical wires." Industrial & Engineering Chemistry Fundamentals 6.1 (1967): 97-103.

Thorud, Jonathan D., James A. Liburdy, and Deborah V. Pence. "Microchannel membrane separation applied to confined thin film desorption." Experimental thermal and fluid science 30.8 (2006): 713-723.

Urtiaga, A. M., et al. "Parallelism and differences of pervaporation and vacuum membrane distillation in the removal of VOCs from aqueous streams." Separation and Purification Technology 22 (2001): 327-337.

Venegas, M., et al. "A simple model to predict the performance of a H 2 O–LiBr absorber operating with a microporous membrane." Energy 96 (2016): 383-393.

Wang, Hongtao, et al. "Permeate flux curve characteristics analysis of cross-flow vacuum membrane distillation." Industrial & Engineering Chemistry Research 51.1 (2011): 487-494.

Wang, Kai Yu, Tai-Shung Chung, and Marek Gryta. "Hydrophobic PVDF hollow fiber membranes with narrow pore size distribution and ultra-thin skin for the fresh water production

through membrane distillation." Chemical Engineering Science 63.9 (2008): 2587-2594.

Wang, Peng, May May Teoh, and Tai-Shung Chung. "Morphological architecture of dual-layer hollow fiber for membrane distillation with higher desalination performance." Water research 45.17 (2011): 5489-5500.

Wang, Rong, et al. "Characterization of novel forward osmosis hollow fiber membranes." Journal of membrane science 355.1 (2010): 158-167.

Wang, Xuyun, et al. "Feasibility research of potable water production via solar-heated hollow fiber membrane distillation system." Desalination 247.1-3 (2009): 403-411.

Wang, Zanshe, et al. "Application of vacuum membrane distillation to lithium bromide absorption refrigeration system." international journal of refrigeration 32.7 (2009): 1587-1596.

Wu, Yonglie, et al. "An experimental study on membrane distillation-crystallization for treating waste water in taurine production." Desalination 80.2-3 (1991): 235-242.

Yang, Ru, and Derming Jou. "Heat and mass transfer of absorption process for the falling film flow inside a porous medium." International journal of heat and mass transfer 38.6 (1995): 1121-1126.

Yang, Qian, Kai Yu Wang, and Tai-Shung Chung. "Dual-layer hollow fibers with enhanced flux as novel forward osmosis membranes for water production." Environmental science & technology 43.8 (2009): 2800-2805.

Yao, Wen, Henrik Bjurstroem, and Fredrik Setterwall. "Surface tension of lithium bromide solutions with heat-transfer additives." Journal of chemical and engineering data 36.1 (1991): 96-98.

Yasuda, H., and J. T. Tsai. "Pore size of microporous polymer membranes." Journal of Applied Polymer Science 18.3 (1974): 805-819.